Ministero dell'Istruzione,
dell'Università
e della Ricerca

Università degli Studi
di Palermo

Facoltà di
"Scienze MM. FF. NN"
Dipartimento di Fisica

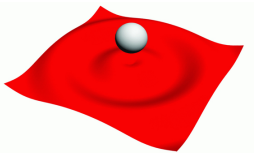

PhD in Physics

XXIII Cycle, 2009–2011

"Protein-Sugar-Water Systems Far From Thermodynamic Ideality"

S.S.D.: FIS/07

Dr. Massimo Panzica

Tutor
Prof. Antonio Emanuele

Coordinator
Prof. Antonio Cupane

PhD in Physics

XXIII Cycle, 2009–2011

"Protein-Sugar-Water Systems Far From Thermodynamic Ideality"

S.S.D.: FIS/07

Dr. Massimo Panzica

Tutor
Prof. Antonio Emanuele

Coordinator
Prof. Antonio Cupane

Università degli Studi di Messina
Dipartimento di Fisica
Università di Messina

Prof. Salvatore Magazù
Dipartimento di Fisica
Università di Messina
Viale D'Alcontres 31, 98166 Messina
tel: 090 6765025, fax: 090 395004
e-mail: smagazu@unime.it

Messina, 15 Gennaio 2012

To whom it might concern:

I am hereby writing an evaluation of the PhD thesis, entitled *Protein-sugar-water systems far from thermodynamic ideality*, of Dr. Massimo Panzica who has performed his doctorate at the Department of Physics of University of Palermo.
I have read with great interest and pleasure the thesis, as well as the research papers authored by Dr. Panzica and by his tutor Prof. Antonio Emanuele. The thesis contains a detailed account of the research work carried out during the years of the PhD program. It is mainly addressed to the experimental investigation of the structural and dynamical properties of some confined and crowded biophysical systems, such as those constituted by protein-sugar-water mixtures. The main focus of the thesis is to clarify how the external matrix influences the protein properties in conditions close to those occurring in living organisms. Such conditions are mimicked in vitro by studying the behavior of proteins in saccharide matrices.
The thesis is well written and clearly structured. It is divided into four chapters, the first one providing a general introduction concerning the scientific background, the second chapter describing the employed experimental techniques, i.e. small-angle X-ray scattering, light scattering, electronic absorption spectroscopy and circular dichroism, together with a description of the formal relations and of the data analysis protocols; the third and the fourth chapters represent the core of the thesis, since they describe the original results obtained by Dr. Panzica. It follows a chapter containing a summary of the obtained results and the conclusive considerations.
As already mentioned, with chapters 3 and 4 we reach the focal point of the thesis and its motivation. Here, the literature regarding the investigated systems and the results obtained by Dr. Panzica are reported. These latter contain a sizeable amount of new and original information, that already provided material for some publications appeared in well recognized international journals.
In more detail, in the third chapter small-angle X-ray scattering findings obtained in myoglobin embedded in low hydrated saccharide matrices are reported. On purpose, two types of myoglobin (metmyoglobin and carboxymyoglobin) and four homologous disaccharides (trehalose, sucrose, maltose and lactose) have been taken into account.

Finally the fourth chapter reports the findings of a study on thermal aggregation of BSA in trehalose and sucrose solutions by static and dynamic light scattering; here the effects of the two disaccharides, on the first steps of the thermal aggregation, at two protein concentrations at increasing sugar/water ratio are taken into account.
Particularly noteworthy are the SAXS results obtained on samples of myoglobin embedded in low hydrated amorphous matrices of disaccharide, where the best protective effect of trehalose against protein damaging is confirmed.
A further first magnitude result comes out from the analyses of the scattered intensity and of the hydrodynamic radius of protein aggregates as a function of temperature which show that such curves are shifted towards higher temperatures when sugar content is increased; such shifts are shown to depend on disaccharide; furthermore it is also shown that the growth mechanisms of the aggregates are not affected by the presence of sugar. These results allow to ascertain that effects of the addition of sugar occur only via global changes of the solvent. Interestingly, the results on protein aggregation have been put in a unifying view by noting that the observed temperature shifts depend mainly on the configurations of the solvent matrix and its interactions with proteins.
In my opinion, in his thesis, Dr. Panzica has carried out a substantial amount of work both in terms of experiments as well as in terms of data analysis and theoretical thinking. The presented scientific case is compelling and timely. The candidate appears to be a careful experimentalist, able to elaborate original ideas. The conclusions reached are important and they will have impact and recognition in the field. Both the scientific relevance of the new results reported in the thesis, and the quality of the presentation, fully conforms to the standards required to obtain a PhD title from major European universities. The quality of the research and the writing of the thesis are very high. I am confident that Dr. Panzica's thesis will receive a positive evaluation during the coming PhD examination and I wish to Dr. Panzica a successful career as a biophysics researcher.

Sincerely yours,

Prof. Salvatore Magazù

CONTENTS

Introduction

Biomolecules are molecules produced and used by living organisms, which play fundamental roles in all the biological processes. In particular, proteins, nucleic acids and sugars are of key importance in this context. Proteins perform a variety of functions, from structural ones to those of catalysis (enzymes), while nucleic acids (DNA and RNA) constitute the genetic heritage that a mother cell transmits to the daughter cells and keep all the information necessary for the cell development and life. Finally, sugars have both energy reserve functions and structural functions. Hence it is clear how much scientific interest is devoted to the study of biomolecules. As a result, small and large scale mechanisms that regulate life cannot be completely understood without taking into account their **molecular aspects**, on which they are grounded. However, it is worth noticing the intrinsic impossibility of explaining how a biological system works just on the basis of a molecular point of view, because even a simple biological function is not the sum of individual molecular results. In fact, in all biological systems, which are highly crowded, the simultaneous presence of several particles in a limited space is responsible for large interference contributions to the mechanisms, which regulate the whole global system and are not easily to predict or analyze. A well established knowledge is that biomolecules work in aqueous solvent. However, because of the difficulties to study complex biological systems, the first studies on the function of proteins were performed on **ideal solutions** (*Lehninger et al., 2008*). These systems were diluted so much, to obtain a linear dependence of the properties of interest on the concentration of the solutes. Furthermore, some studies showed how the perturbation by cosolvents sizably affects the conformational equilibria of proteins (*Von Hippel and Wong, 1965; Tanford, 1968; Herskovits and Solli, 1975*), while others focused on the effect of organic cosolvents (monohydric alcohols and amides) on protein functionality (*Cordone et al., 1979; Cordone et al., 1989; Bulone et al., 1992; Bulone et al., 1993*). Nevertheless, such systems are far apart from the actual conditions of biological processes, since the **macromolecular crowding** cannot be neglected. However, in-vivo systems are often hard to study at a molecular level, because of their complexity. As a consequence, it has been afterwards thought to study crowded and confined biological systems. In particular, in order to understand the way, in which the external medium influences the structure, dynamics and interactions among the biological molecules in confined and crowded systems as those in vivo, the behaviour of proteins has been studied in **saccharide matrices**, which do not realize the conditions of thermodynamical ideality. On one hand, living organisms are very rich in saccharides, especially in the extra-cellular medium (*Karp, 2004*); on the other hand, sugars have been of large interest in the last decades, because of their bioprotective properties (*Crowe and Clegg, 1973; Crowe et al., 1984*). Among all the saccharides, trehalose, a non-reducing disaccharide composed of two linked

units of glucose, has proved to be the best stabilizer of biostructures against thermal denaturation (*Crowe, 2007; Jain et al., 2008*). Recent experimental (*Librizzi et al., 2002; Cordone et al., 2005; Giuffrida et al., 2006; Francia et al., 2008*) and simulative (*Cottone et al., 2001; Cottone, 2007*) studies have shown that a hydrogen bond network couples the protein surface to the external matrix in dry amorphous systems of protein embedded in saccharide matrices. Moreover, its rigidity increases when the residual water reduces. This coupling is stronger in trehalose than in other saccharides, such as sucrose, maltose and raffinose (*Giuffrida et al., 2006; Francia et al., 2008*).
In addition to this, biological systems can be regarded as non-ideal systems also because of their thermodynamic **instability**, which can be responsible for misfolding, phase separations or aggregation, including micelles, oligomers and fibers formation, even of pathological relevance. This additional aspect has also been studied in the last few years by Palma and coworkers (*Bulone et al., 1999; Manno et al., 2004; Vaiana et al., 2004; Vaiana et al., 2005; Pullara et al., 2008*). In particular, it has been shown that nucleation and aggregation processes of proteins are strictly connected to the universal scaling properties of concentration fluctuations, occurring in proximity of phase transitions.

The work presented in this thesis has been focused to the study of biological confined and crowded systems, which cannot therefore be considered as ideal thermodynamic systems. The study has been done at the Department of Physics of University of Palermo, in line with previous studies carried out at the Department. In particular, structural and dynamic properties of protein-sugar-water systems have been considered, for the reasons previously discussed. Such systems, however, are composed by objects of different size (water molecules, sugars, proteins), so that dynamics at different temporal scales are simultaneously present. On one hand, structural properties of amorphous systems have been studied, where the confinement induced by the glass formation reduces the faster motions (picoseconds), thus allowing to study the systems in a slower time scale. On the other hand, protein aggregation has been studied in crowded saccharide solutions, where the solvent effects on the protein are thought to be averaged up to the protein time scale (from nanoseconds to microseconds). In both cases, the present work is aimed to understand the mechanisms, according to which the external matrix influences the protein structure and dynamics in conditions similar to those in which biological events occur in living organisms.
The first chapter of this thesis ("*Basic Concepts*") provides the reader with the proper scientific background, on which the present work is grounded. Preliminarily, proteins and sugars are introduced as some of the most important biological macromolecules, then their interaction is reviewed, with particular emphasis on the biopreservation by sugars.
In the second chapter ("*Experimental Techniques*") the physical phenomena, which are the basis of each technique used, and the main mathematical relations used for the data analysis are shown. In particular, the chapter deals with small-angle X-ray

scattering, light scattering, electronic absorption spectroscopy and circular dichroism.

Finally, in the last two chapters the experimental results and their discussion are reported. In each chapter, the main current literature regarding the studied systems is reviewed. The third chapter ("*Myoglobin Embedded in Amorphous Saccharide Matrices*") reports small-angle X-ray scattering measurements performed on samples of myoglobin embedded in low hydrated saccharide matrices. The study has been carried out on two types of myoglobin, namely metmyoglobin and carboxymyoglobin, and four different sugars: trehalose, sucrose, maltose and lactose. Previous studies (*Longo et al., 2010*) on carboxymyoglobin embedded in amorphous saccharide matrices suggested that, at low hydration level, the protein influences the structural properties of trehalose matrices, but it has a limited effect in sucrose matrices. Furthermore, Longo et al. reported on the mechanism for trehalose bioprotection based on water-buffering action, confirming some previous results (*Cesàro et al., 2006; Kilburn et al., 2006*). In this work, the study has been extended to metmyoglobin and to maltose and lactose matrices, in order to investigate whether the observed behaviour is a peculiarity of trehalose or a common phenomenon in presence of sugar matrices.

The fourth chapter ("*Thermal Aggregation of Bovine Serum Albumin in Sugar Solutions*") deals with thermal aggregation of bovine serum albumin (BSA) in trehalose and sucrose solutions. Static and dynamic light scattering measurements have been performed in order to study the effects of the two disaccharides on the first steps of the thermal aggregation of BSA in aqueous solutions at two protein concentrations (1 mg/ml and 30 mg/ml) at increasing sugar/water ratio. The purpose of the study was to separate the direct sugar action from effects of sugar-water networks on BSA aggregation and to explore the correlation between thermodynamic properties of protein aggregation and the glass transition temperature of the water-sugar solvent.

The last chapter ("*Conclusions*") summarizes the results obtained and the main conclusions, put together in a unifying view.

1 – Basic Concepts

In this chapter the basic concepts, which are the grounds of the present work, are presented. Preliminarily, proteins and sugars are introduced as some of the most important biological macromolecules, then their interaction is reviewed.

1.1 – The Biomolecules

The biomolecules are molecules that naturally play special roles in living beings (*Lodish et al., 2009*). They consist mainly of carbon and hydrogen, which are often associated with nitrogen, oxygen, phosphorus and sulphur.
There are two main types of biomolecules: some **small organic compounds**, absorbed or synthesised by living systems, and **biological macromolecules**, which are essentially polymers consisting of a number of fundamental units called monomers.
Among the small molecules there are:

- **simple sugars and disaccharides:** the first ones consisting of an aldehydic group or a chetonic group that in solution often close into a ring, whereas the second ones are composed of two linked simple sugars;
- **lipids:** molecules with heterogeneous chemical structures, hydrophobic or amphipathic, among which there are fatty acids, amphipathic and consisting of non-branching hydrocarbon chains, triglycerides, hydrophobic and consisting of one molecule of glycerol linked to three fatty acids, and phospholipids, amphipathic and obtained by replacing a fatty acid with a phosphate group in a triglyceride;
- **vitamins:** classified according to their water solubility and liposolubility, and not on the basis of their structure, which is quite heterogeneous.

The main polymeric biomolecules are instead:

- **proteins:** polymers formed by different amino acids;
- **nucleic acids:** such as DNA and RNA, which are polymers formed by different nucleotides;
- **polysaccharides:** polymers formed by condensation of simple sugars.

Polymers may have informational functions, composed by the specific sequence of its monomers (genetic information in DNA, 3D structure in protein), deposit and transport functions, such as energy reserve polysaccharides, or structural functions.

The bonds between a monomer and the adjacent ones are covalent bonds, obtained by *condensation reactions* and with *intrinsic directionality*.

The forces that play a role in the structure determination of the biological macromolecules are essentially those listed in table 1.1. In addition to these forces, there are the so-called hydrophobic interactions, which includes macromolecule-solvent and solvent-mediated macromolecule-macromolecule interactions. Due to their intrinsic collective character, these interactions are generally described by using the Gibbs's thermodynamic potential.

Table 1.1 –Main forces that determine the structure of biological macromolecules, with orders of magnitude of the relative energies. The energy k_BT at 300 K is reported for comparison.

	$E \sim$
covalent bond	100 kcal/mol
hydrogen bond	10 kcal/mol
van der Waals interactions	1 kcal/mol
k_BT at 300 K	0.6 kcal/mol

1.1.1 – Functional Groups

Functional groups are particular parts of the structure of a given molecule, which have specific elements and structure and give the molecule a peculiar reactivity, similar to that of other molecules containing the same group. The main functional groups that can be found in biomolecules can be divided into three categories:

(a) negative charged groups: carboxylic group $-CO_2^-$, phosphoric group $-PO_3^{2-}$;

(b) positive charged groups: aminic group $-NH_3^+$;

(c) neutral, polar groups: hydroxyl group $-OH$, sulphydryl group $-SH$, carbonyl groups $-CO$, aldeidic group $-COH$.

The figure below shows the structure of the groups just listed.

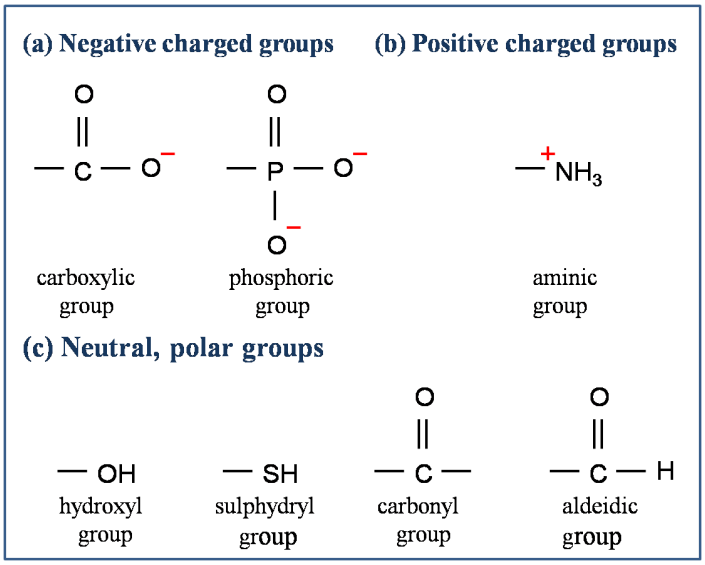

Figure 1.1 – Structure of the main functional groups present in biomolecules.

1.2 – Proteins

Proteins are organic molecules composed of amino acids, interconnected through a **covalent bond,** called **peptide bond**. Amino acids[1] are organic molecules composed of a central carbon atom, which is tetravalent, bound to a hydrogen atom H, to a carboxylic group $-COOH$ (which is acid) , to an amino group $-NH_2$ (which is basic) and to a side chain R consisting of a single atom or a chain of more atoms, as shown in the figure that follows[2] (*Karp*, 2004).

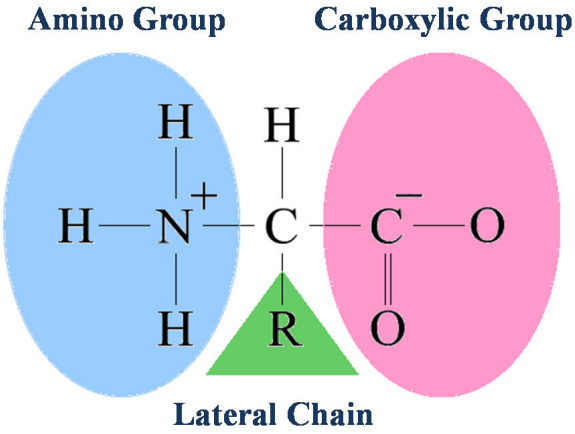

Figure 1.2 – Chemical formula of a generic amino acid.

Between the amino group of a given amino acid and the carboxylic group of the following amino acid a covalent bond is formed for condensation and, thus, *polypeptide chains* are built.

1.2.1 – Functions and Structure of Proteins

Proteins can perform different functions:

- they constitute the structural material for tissues;
- they store and carry small molecules (hemoglobin carries oxygen in the blood, while myoglobin stores it in muscles);
- they constitute the immune defense of living organisms (antibodies);
- they regulate biological reactions (enzymes);
- they can play the role of molecular messengers (hormone proteins).

[1] In nature there are 20 different amino acids.

[2] In a neutral aqueous solution, the carboxylic group loses its proton and so it is negatively charged ($-COO^-$), while the amino group acquires a proton and gets positively charged ($-NH_3^+$).

As regards their structure, it can be summarised as follows:

- ◊ **PRIMARY STRUCTURE:** it is the specific sequence of amino acids in the protein. It contributes to the three dimensional aspect of the molecule and determines the function and the type of interaction with other substances.
- ◊ **SECONDARY STRUCTURE:** it is the local arrangement of the chain, favoured by different types of bonds among the amino acids in the polypeptide chain. It may be an **alpha helix** if the polypeptide chain is wrapped on itself to form an helix, a **beta sheet** if the chain has a laminar arrangement or is "leaflet folded" or, in addition to this, it may be formed of **random coils**, that are sections of chain that do not assume an ordered structure.
- ◊ **TERTIARY STRUCTURE:** it is caused by the interaction of side chains R with other groups R or with molecules of water that determine the final three-dimensional shape of the protein.
- ◊ **QUATERNARY STRUCTURE:** it is caused by the interaction of several polypeptide chains, which may take a globule or fibrous shape or other shapes. Proteins with a single polypeptide chain do not possess a quaternary structure.

The different levels of protein structure are shown in figure 1.3.

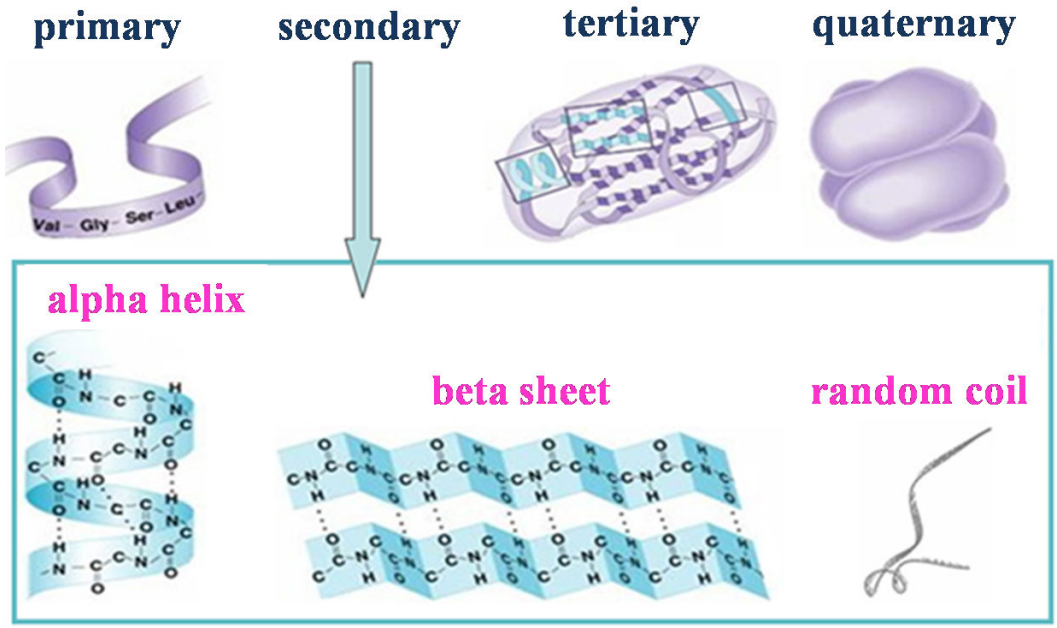

Figure 1.3 – Levels of protein structure.

1.2.2 – Protein Folding and Configurational Landscape

Proteins are assembled from amino acids using information encoded in genes, which specify the protein amino acid sequence by the nucleotide sequence. In particular, a specific amino acid is designated by a specific set of three nucleotides, called codon. Genes encoded in DNA are first **transcribed** by RNA-polymerase enzyme into messenger RNA (mRNA), which is then used as a template for protein synthesis by ribosomes: this process is known as **translation**.

When translated from a sequence of mRNA to a linear chain of amino acids, each protein lacks any three-dimensional structure and this prevents it from being functional (*Lodish et al., 2009*). However, the amino acids in the protein interact with each other to fold the protein in a well-defined three-dimensional structure, known as the **native state**. The native protein structure is determined by the amino acid sequence in order to minimize the free energy of the system (*Anfinsen, 1972*).

The **folding process** is a current open issue (*Borgia et al., 2008*), since it is not yet clear how the amino acid sequence specifies the 3D protein structure and how proteins avoid misfolding. In addition to this, there is still a question of kinetics regarding the way in which a protein can reach its native state from a random coil in a biologically relevant timescale. With regard to the latter question, Levinthal observed (*Levinthal, 1968*) that, if a protein were to fold by sequentially sampling all the possible conformations, it would take an astronomical amount of time to do so, even if the conformations were sampled at a picosecond scale. Taking into account that proteins fold much faster than this, he then proposed that a random conformational search does not occur, and the protein must, therefore, fold through a series of meta-stable intermediate states. Some years later it was experimentally shown that a protein can reach its native state very quickly, often reversibly and following different and independent pathways (*Anfinsen, 1972*). Dill and Chan overcame Levinthal's paradox (*Dill and Chan, 1997*) by making use of the **configurational landscape**, that represents the free internal energy of a protein, obtained by mediating the potential energy of the protein-solvent system on the fast variables of the solvent (*Vaiana et al., 2001*), as a function of its freedom degrees or configurational coordinates. So the free internal energy contains enthalpic terms, due to the interaction between the amino acids, and thermodynamically mediated terms, both enthalpic and entropic, linked to the interaction between the amino acids and the molecules of the solvent. In order for the protein to properly reach its native state (N) in a quick way, corresponding to the minimum of free energy, the configurational landscape must have a **funnel shape**, as shown in figure 1.4.

The presence of secondary minima and maxima in the peripheral area of the funnel, smaller than the minimum central, justifies the existence of independent,

but equivalent, pathways. Moreover, the secondary minima show the existence of **kinetic traps**, which lead the protein to assume stable, but non-functional, configurations: this is called **misfolding**.

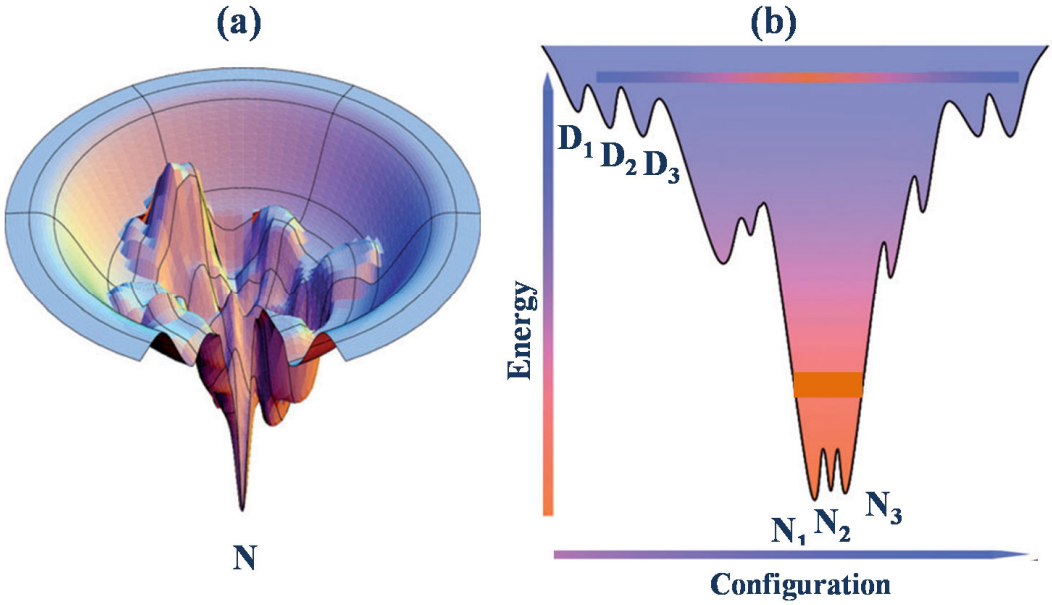

Figure 1.4 – Funnel-shaped configurational energy landscape for a protein folding process, with secondary minima, responsible for the native state (*N*) and the denaturated state (*D*). (a) 3D-view (function of two configurational variables) and (b) projection on one configurational variable.

Although the folding process is not yet fully understood, it is known (*Cantor and Schimmel, 2001; Van den Berg et al., 2000*) that this process depends on different environment factors, such as the solvent molecules, the temperature and the pH of the solvent and the concentration of salts. Two driving forces contribute to the protein stability: the **minimization of the number of hydrophobic side-chains exposed to water** (*Pace et al., 1996; Rose et al., 2006*), with the formation of a hydrophobic core and a charged or polar side chain at the solvent-exposed surface, and the **maximization of the number of intramolecular hydrogen bonds**, both the ones enveloped in a hydrophobic core and those exposed to the aqueous environment.

The following figure shows how the hydrophobic amino acids (black spheres) are in general shielded from the solvent after the protein folding.

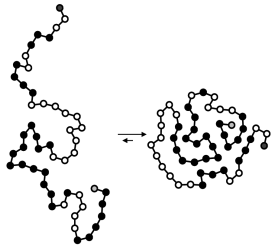

Figure 1.5 – After the protein folding, the hydrophobic amino acids (black spheres) are in general shielded from the solvent.

1.2.3 – Solvent Induced Forces

For a system of proteins in solution, solute-solvent interactions strictly depend on the local macroscopic context and cannot be predicted on the basis of the chemical-physical properties of the single residues. In fact, in addition to Coulomb's and van der Waals's interactions, **solvent induced forces**, that are solute-solvent and solvent-mediated solute-solute interactions, are not negligible. These forces make the system hard to study, because of their **non-additivity** (*San Biagio et al., 1998*).

In the simple case of two non-interacting solute molecules (*S*) in water (*W*), the solute changes the energy landscape of water, and so the free energy of the system, of an amount ΔG_{SW}. This quantity depends on the distance and orientation of the two solute molecules, since the displacement of one of them modifies the water energy landscape near the other one. In this way, the solvent is responsible for the interaction between the two solute molecules. As a consequence, a generalized **solvent induced force** can be introduced as:

$$F_{solvent,induced} = -\mathrm{grad}\left(\Delta G_{SW}\right) \tag{1.1}$$

where the gradient is calculated over the translational and rotational coordinates of the solutes. Such force is caused by structural configuration rearrangements of the solvent around the solute molecules until the free energy of hydration is minimized.

If three or more solute molecules are present in solution, the total free energy is not simply the sum of the contributes $\Delta G_{SW}(i)$ of single particles taken alone, but it must be written as:

$$\Delta G_{SW}(1,\ldots,n) = \sum_i \Delta G_{SW}^{(1)}(i) + \sum_{i,j} \Delta G_{SW}^{(2)}(i,j) + \sum_{i,j,k} \Delta G_{SW}^{(3)}(i,j,k) + \ldots \tag{1.2}$$

taking into account the interaction among *n*-particles.

Since each term depends on the distance and orientation among the molecules, the three-body terms and the higher ones are not expressible as sum of two body terms, as in the case of additive forces.

The non-additivity of the solvent induced forces are pointed out by molecular dynamics simulations (*San Biagio et al., 1998*), as shown in figure 1.6.

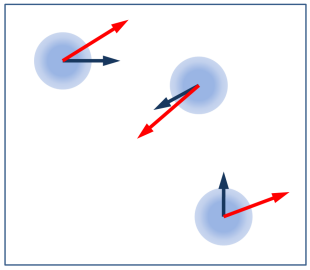

Figure 1.6 – Non-additivity of the solvent induced forces are pointed out by molecular dynamics simulations. The blue forces, in the additivity approximation, are compared to the red forces, calculated from simulations, which consider the simultaneous presence of the three particles (*San Biagio et al., 1998*).

1.2.4 – Protein Denaturation and Aggregation

When a protein is heated to temperatures generally higher than 60 °C or when it interacts with some chemical substances (such as acids, strong bases, salts in high concentration) a **denaturation process** can occur, which consists in the break of the weak bonds that maintain the protein in its native state: the protein changes its three-dimensional shape and loses its functionality. This process could sometimes be irreversible, depending on the type of bonds, which are broken.

Very often proteins in partially folded or misfolded states tend to **aggregate** in a concentration-dependent way. This is due to the fact that these forms typically expose to the solvent hydrophobic amino acid residues and regions of unstructured polypeptide backbone, which were previously buried in the native state (*Eichner et al., 2011*). Like intramolecular folding, aggregation is largely driven by hydrophobic interactions and primarily results in amorphous structures. The aggregates are characterized by strong bonds and low solubility. Alternatively, fibrillar aggregates called **amyloid** may form, defined by β-strands that run perpendicular to the long fibril axis.

In addition to hydrophobic interactions, electrostatic interactions also play a fundamental role in denaturation and aggregation processes, as it is suggested by their strong dependence on pH and on salt concentration. These forces can be either long-range or short-range. The former are directionless and non-specific and exert their influence over several nanometres, while the latter are well-oriented and can affect the protein stability through salt bridges (*Akke and Forsén, 1990; Dill, 1990; Grimsley et al., 1999*). The protein charge contributes to the modulation of the rates and the forms of aggregation. In fact, far from the isoelectric point the partially unfolded protein molecules are highly charged, thus resulting in long-range repulsion and slow aggregation (*Militello et al., 2004; Bromley et al., 2005; Vetri et al., 2006*). As a consequence, the screening of electrostatic repulsions is a prerequisite for aggregation, as indicated by several experiments (*Picotti et al., 2007*), because it favours protein-protein association processes. The protein charge can be easily regulated by varying the pH of the solution, since many of the amino acids composing the polypeptide chain are either strong acids or bases, or contain polar groups that may be partially dissociated.

Lastly, the aggregation process can be regarded in terms of the energy landscape previously introduced. When several molecules fold simultaneously in the same volume, the free-energy surface of folding may overlap with that of intermolecular aggregation, resulting in the formation of amorphous aggregates, which may be toxic oligomers or ordered amyloid fibrils (red), as it is shown in figure 1.7.

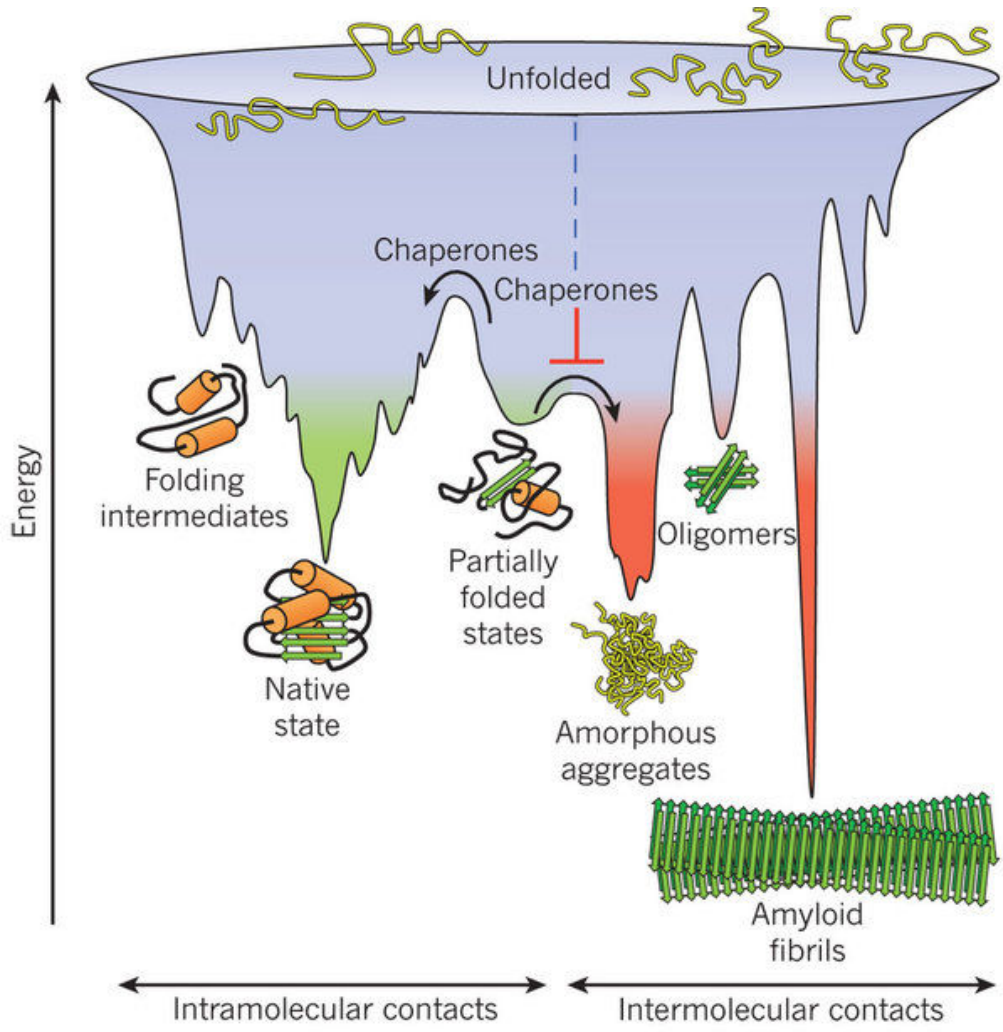

Figure 1.7 – Funnel-shaped energy landscape for protein folding and aggregation processes.

The study of denaturation and the consequent aggregation of the protein is very important in many fields, spanning from food technologies and polymer science to the study of **neurodegenerative diseases** (*Vaiana et al., 2001; Chiti and Dobson, 2006*), such as Alzheimer's disease, Parkinson's disease and multiple sclerosis, characterized by deposits of denatured and aggregated proteins in the brain.

1.3 – Saccharides or Carbohydrates

Saccharides or carbohydrates are the main molecules of the energy reserve for the majority of living beings and are, in addition, the main structural components of cells (*Lodish et al., 2009; Karp, 2004*). They are composed of carbon (*carbo-*), hydrogen and oxygen (*-hydrate*). There are three main types of saccharides, classified according to the number of molecules:

- ◊ **MONOSACCHARIDES OR SIMPLE SUGARS:** they consist of a single molecule and can be, therefore, the monomers of more complex saccharides;
- ◊ **DISACCHARIDES:** they consist of two monosaccharides, connected by a covalent bond;
- ◊ **POLYSACCHARIDES:** they are polymers consisting of long chains of monosaccharides joined together by glycosidic bonds.

1.3.1 – Monosaccharides or Simple Sugars

The *empirical formula* of monosaccharides or simple sugars is:

$$C_n\left(H_2O\right)_n,$$

where n can be as small as 3 or as great as 8.

All monosaccharides contain **hydroxyl groups** ($O-H$), so they may be considered as they were polyvalent alcohol. In addition, they contain an **aldeidic group** or a **chetonic group**, shown in figure 1.8.

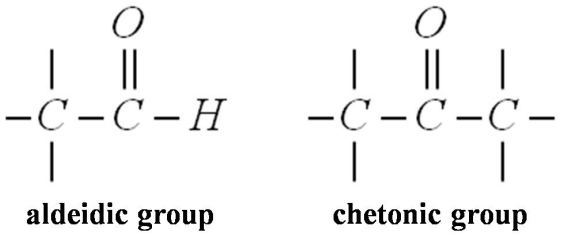

Figure 1.8 – Aldeidic group and chetonic group that can be present in saccharides.

Glucose or **dextrose**, **fructose** and **galactose** are monosaccharides with 6 carbon atoms and have, therefore, the following empirical formula:

$$C_6H_{12}O_6.$$

Glucose is represented in the following figure.

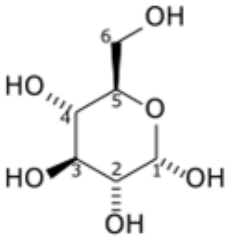

Figure 1.9 – Structure of glucose.

In general, saccharides with 6 carbon atoms are called **hexoses** and may exist in 3 forms:

- a linear structure with an open chain;
- a 5 atom ring, called **furanose**.
- a 6 atom ring, called **pyranose**.

In biological systems glucose prevails in the *pyranose form*.

1.3.2 – Disaccharides

Disaccharides consist of the union of two monosaccharides by means of a $C-O-C$ bond, called **glicosidic bond**.
Glycosidic bonds form by **condensation** reaction: the carbon atom 1 of a molecule of sugar reacts with a hydroxyl group ($O-H$) of another molecule of sugar and a molecule of water is eliminated. When, instead, a disaccharide is splitted in the two monosaccharides that constitute it, for example when it has to be used to produce energy, it is added a molecule of water: this process is called **hydrolysis**.

Examples of disaccharides are **sucrose**, **trehalose**, **maltose** and **lactose**.
Sucrose is formed by the union of glucose and fructose, while trehalose and maltose are composed of two glucose units. These last two ones differ in the type of bond: in trehalose the bond is $(1\rightarrow1)$[3], while in maltose it is $(1\rightarrow4)$, as shown in figure 1.10 . At last lactose is formed from galactose and glucose.

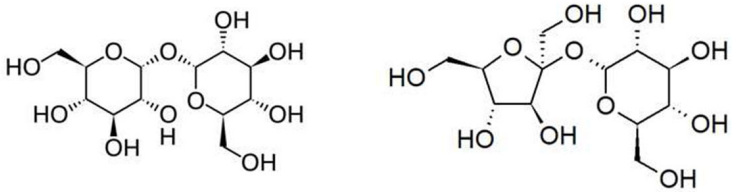

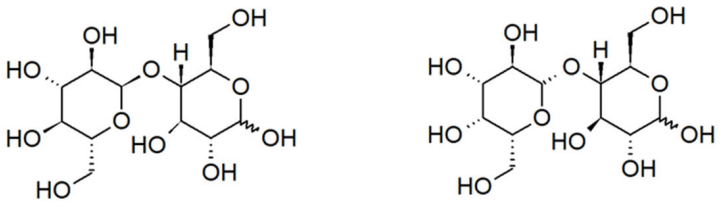

Figure 1.10 – Structure of some disaccharides.

[3] The number after the arrow indicates the carbon atom of the second glucose which is bound to the first carbon atom of the first glucose.

1.3.3 – Polysaccharides

Polysaccharides are formed by monosaccharides bound in long chains. Some of them are the reserve forms of simple sugars, such as **starch** in plants and **glycogen** in animals and fungi. Others, on the other hand, play structural roles, such as **cellulose** in plants and **chitin** in animals and fungi. Sometimes, in order to be used, polysaccharides must first be hydrolysed in monosaccharides or disaccharides. Another relevant polysaccharide is **agarose**, generally extracted from seaweed and very soluble in water, thanks to the high number of hydroxyl groups ($O-H$). If dissolved in solution, agarose tends to form an aqueous gel, that is an elastic solid, colloidal material, consisting of a liquid dispersed and incorporated in a solid phase. The latter uses the surface tension of the hosted liquid in order not to collapse.

1.3.4 – Maillard's Reaction

Maillard's reaction is a chemical reaction between an amino acid and a reducing sugar, promoted by high temperatures and alkaline conditions (*Maillard, 1912*). In particular, the reactive carbonyl group of the sugar can react with the amino group of the amino acid, thus forming an ultimately complex mixture of poorly characterized molecules. In the process, hundreds of different compounds might be created, which in turn can further break down to form more species. This reaction is responsible for changes in colour, flavour and nutritive properties of food. Although it can improve some food features, such as the pleasant smell of bread and coffee, it has at the same time negative effects from a nutritional point of view, since it is responsible for the inhibition of the intestinal absorption of essential amino acids and the decreased digestibility of the involved proteins, due to the loss of lysine as a result of the reaction (*Cappelli and Vannucchi, 1998*).
Maillard's reaction occurs in three main steps. Initially, the carbonyl group of the sugar reacts with the amino group of the amino acid, leading to glycosylamine and water through an iminic intermediate, as shown in figure 1.11.

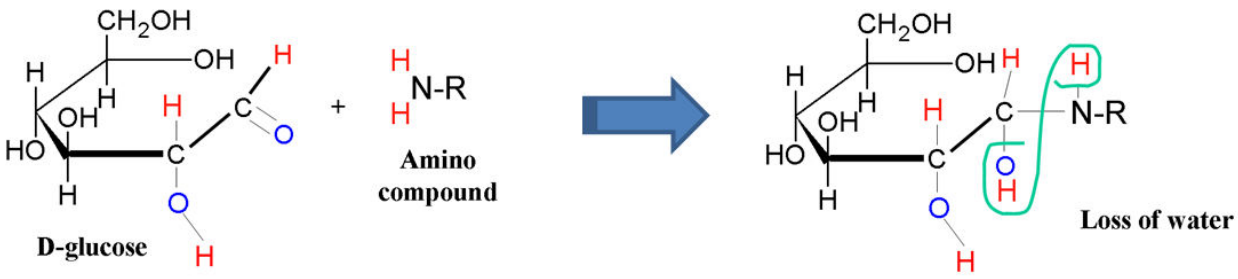

Figure 1.11 – First step of Maillard's reaction. The carbonyl group of the sugar reacts with the amino group of the amino acid, leading to glycosylamine and water through an iminic intermediate.

Secondly, the glycosilamine undergoes Amadori's rearrangement (*Amadori, 1931*), which is an organic reaction that produces a compound called ketosamine, through the formation and isomerisation of an immonium ion, as it is shown in the following figure. All the reactions involved in the first two steps of Maillard's reaction are reversible and their products are colourless.

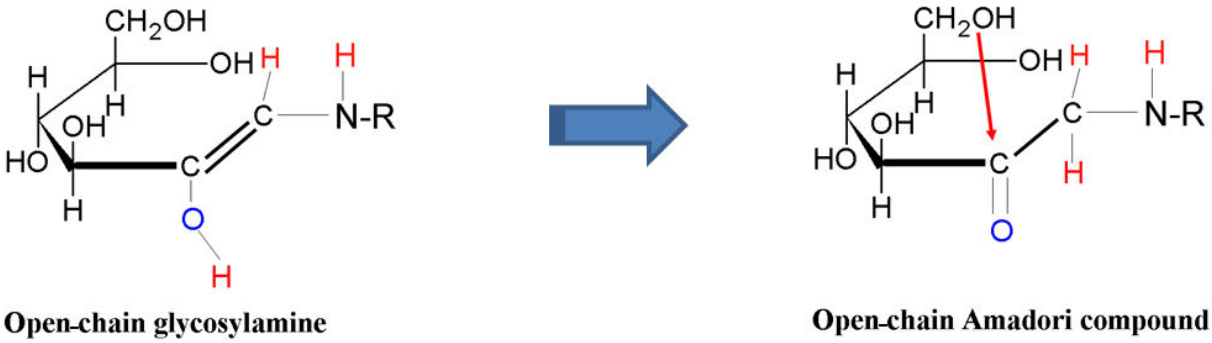

Figure 1.12 – The glycosilamine undergoes Amadori's rearrangement, thus forming ketosamine.

Lastly, depending on the condition at which the reaction occurs, several compounds can be produced from ketosamine, such as brown nitrogenous polymers, diacetyl, aspirin, pyruvaldehyde and other short-chain hydrolytic fission products. Generally, intensive molecular cross-bridging might happen, with strong alterations of the thermodynamic properties of the whole system.

Maillard's reaction occurs also *in vivo*, and contributes to the ageing of organism. In fact, the brown terminal products of the reaction accumulate in tissues and modify their physiology, mainly the elasticity, because of the cross-linking among the proteins, in particular collagen.

1.3.5 – The Main Saccharides

Table 1.2 provides an overview of the main saccharides.

Table 1.2 – Overview of the main saccharides.

Monosaccharides	Disaccharides	Polysaccharides
Glucose or Dextrose: 6 atom ring sugar, especially present in sugary fruit. It is the main product of chlorophyll photosynthesis and is used as a fuel in cellular breathing to extract energy.	**Sucrose:** sugar from kitchen, present in sap of plants, formed by condensation of a molecule of glucose with a molecule of fructose.	**Starch:** Reserve saccharide present in plants. It is formed at day in chloroplasts of green parts of plants from the glucose produced as a result of the chlorophyll photosynthesis
Fructose: the sweetest among the sugars and isomer of glucose, to which is easily converted by the liver and the intestine. It is a 5 atom ring and is present in many sugary fruits and in honey.	**Trehalose:** present in plants, in the blood of insects and in fungi. It consists of two molecules of glucose. It is thought to play a role of biopreserving better than other sugars.	**Glycogen:** reserve saccharide present in animals and in fungi. It is found mainly in the liver and muscles.
Galactose: isomer of glucose, it is used for the synthesis of complex polymers and for the production of energy, after conversion to glucose.	**Maltose:** present in some plants and in honey, it is the intermediate product of the degradation of the starch. It consists of two molecules of glucose.	**Cellulose:** structure saccharide present in plants and is the product of the condensation of a very large number of molecules of glucose.
	Lactose: it is found most notably in milk and is formed from galactose and glucose.	**Chitin:** structure saccharide very resistant to chemical agents and present in animals and fungi, especially in the external skeletons of arthropods (invertebrate animals).

1.4 – Biopreservation by Sugars

In addition to their classical roles of energy reserve and structural material, saccharides, and in particular disaccharides, can protect the biological material. Although it is known for a long time that sugars can preserve food, as is the case for example of jam, the interest in this subject increased in the last few tens of years because of the discovery of some organisms, both plants and animals, that can survive to adverse environmental conditions thanks to the protective action of sugars (*Crowe et al., 1984; Bianchi et al., 1991*).

More specifically these organisms can enter into a particular ametabolic state of life called **cryptobiosis** (*Keilin, 1959; Crowe and Clegg, 1973; Tomos, 1992*), where all metabolic procedures stop, preventing reproduction, development and repair. An organism in a cryptobiotic state can essentially live indefinitely until environmental conditions return to being hospitable. When this occurs, the organism returns to its metabolic state of life as it was prior to the cryptobiosis.

There are five types of cryptobiosis, depending on the environmental stress.

- **Anhydrobiosis**: it is the most intensely studied type of cryptobiosis and occurs in situations of extreme desiccation. The term "anhydrobiosis" derives from the Greek and means "life without water": it is most commonly used for the desiccation tolerance observed in certain plants, like the "resurrection plant" *Craterostigma plantagineum*, and invertebrate animals, such as bdelloid rotifers, tardigrades, brine shrimp and nematodes. Invertebrates undergoing anhydrobiosis turn into a contracted form called "tun", where their body water content is reduced from about 80% in the active state to 1-3% in the anhydrobiotic state.
- **Cryobiosis**: it takes place in reaction to very low temperatures, stopping molecule mobility when the water surrounding the organism's cells has been frozen. Organisms capable of enduring these conditions typically feature molecules that facilitate freezing of water in preferential locations, preventing the growth of large ice crystals that could otherwise damage cells.
- **Chemobiosis**: it is the cryptobiotic response to high levels of environmental toxins.
- **Anoxybiosis**: it occurs in situations of lack of oxygen. In this case, the organism absorbs water and becomes turgid and immobile.
- **Osmobiosis**: it is the least studied of all types of cryptobiosis and occurs in response to increased small solute concentration in the solution where the organism lives.

The following image summarizes the different types of cryptobiosis just listed.

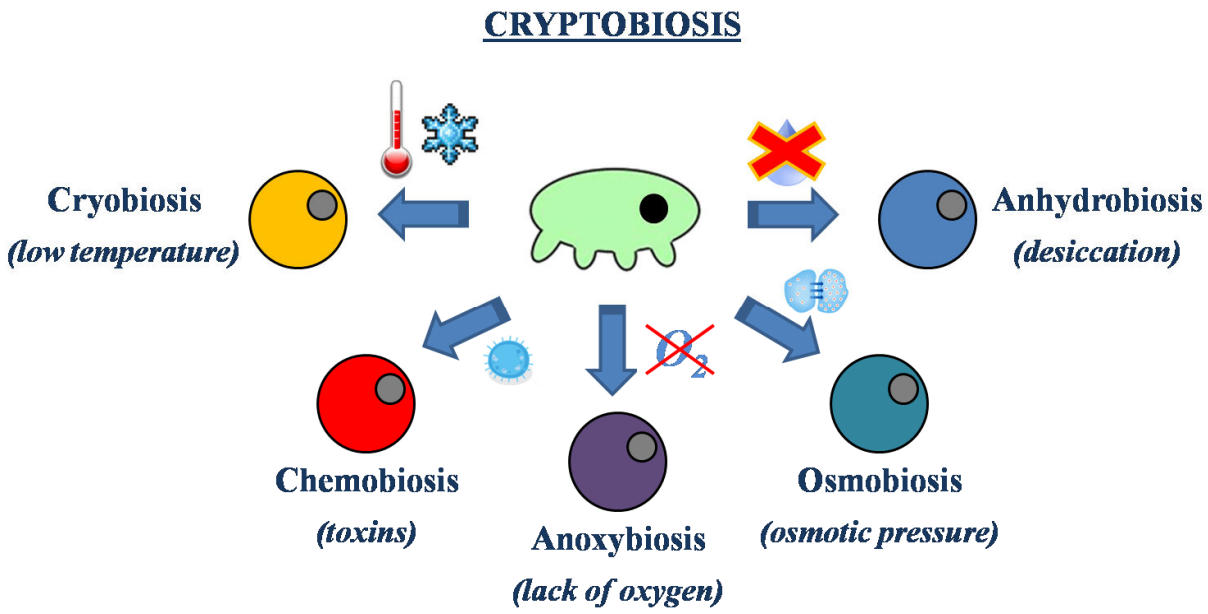

Figure 1.13 – Different types of cryptobiosis.

The *tardigrade*, or *water bear*, is a widely studied and notable example of invertebrate animal undergoing cryptobiosis, partially because it can undergo all five types of cryptobiosis (*Crowe and Madin, 1975; Wright, 2001; Horikawa et al., 2008*).

Figure 1.14 shows anhydrobiosis for (a) a tardigrade and (b) the "resurrection plant" *Craterostigma Plantagineum*: these organisms, that were first dehydrated, return to their previous metabolic state of life when hydrated, without reporting any damage.

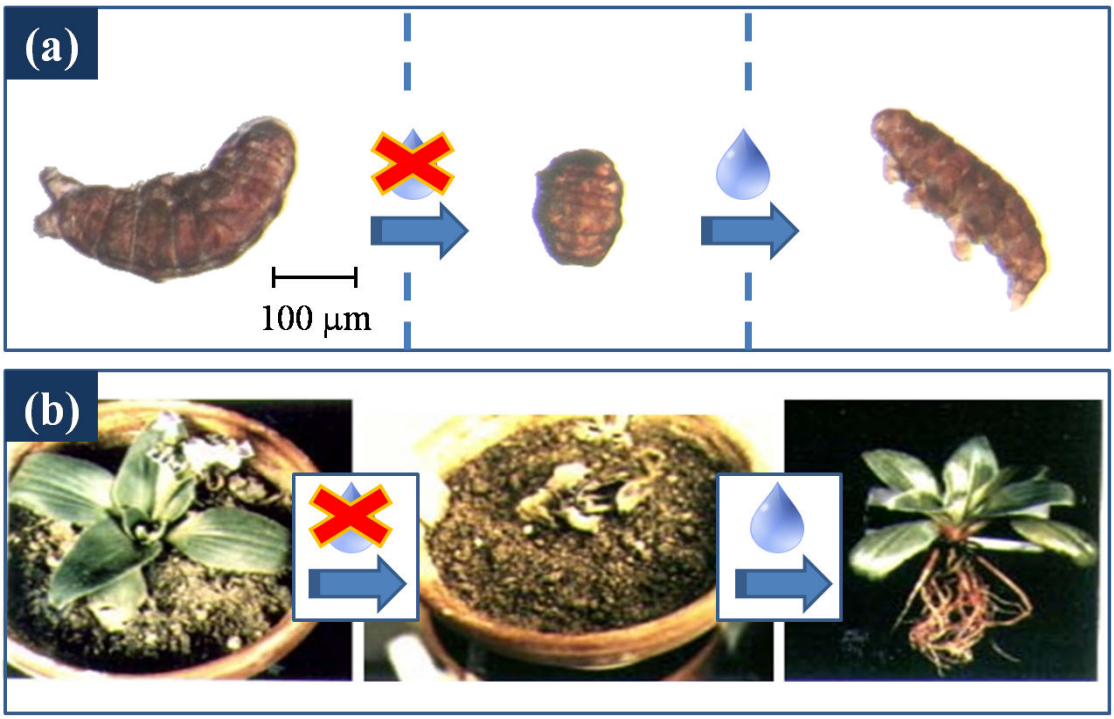

Figure 1.14 – Anhydrobiosis for (a) a tardigrade and (b) the "resurrection plant" *Craterostigma plantagineum*. These organisms, that were first dehydrated, return to their previous metabolic state of life when hydrated, without reporting any damage.

All the organisms that have such a resistance to extreme conditions contain sugars at great concentrations, usually trehalose for animals (Clegg, 1967; *Crowe and Madin, 1975*) and sucrose for plants (*Bianchi, 1993*). For this reason sugars are considered necessary to the establishment of anhydrobiosis, in spite of the fact that the underlying mechanisms are still not fully understood.
Understanding the mechanism of saccharide-based biopreservation, both in vivo and in vitro, is nowadays a relevant topic for its **technologic implications** in food industry, pharmaceutics and medicine.

1.4.1 – The Peculiar Effect of Trehalose

Among saccharides, **trehalose** resulted **the best bioprotecting agent** (*Crowe, 2007; Jain et al., 2008*). From a structural point of view, trehalose is a symmetric molecule with respect to the glycosidic bond, characterized by the absence, in the crystalline state, of direct hydrogen bonds between the two monomers. The more stable crystalline form TRE_h is dihydrate, where two water molecules form H-bonds with the $-OH$ groups of the two sugar subunits (*Brown et al., 1972*), as shown in the following figure.

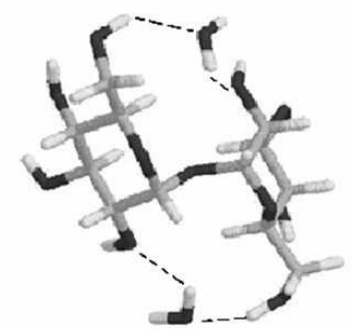

Figure 1.15 – Dihydrate crystalline form of trehalose (TRE_h).

Water molecules are strongly bound to the trehalose, thus it is very difficult to remove them. As a consequence, trehalose crystals develop in wetter environments than other sugars and the storage in a dry atmosphere is required for keeping it amorphous. Furthermore, the two sugar subunits don't perform H-bonds with each other, but only via the water molecules (*Batta and Kövér, 1999*).
In addition to the dehydrate form, other different crystalline forms have been found, such as two anhydrous forms: TRE_β, where all the $-OH$ constitute a H-bond network without water molecules, and TRE_α, which can be formed by gently removing the water molecules under vacuum. The crystal structure of TRE_α is still unknown, but this form is however thought to be more easily hydratable than TRE_β and, therefore, readily convertible to TRE_h (*Cesàro et al., 2008*).
Although the mechanism behind trehalose bioprotective effectiveness is not fully understood, as well as for the other sugars, several hypotheses have been proposed to explain the origin of its peculiarity. These hypotheses, which are listed below, are not mutually exclusive.

- **Water Replacement Hypothesis**: in the dry state trehalose molecules replace the water molecules in the first hydration shell of the protein (*Carpenter and Crowe, 1989*), so that the stabilization of the biostructure is due to the formation of hydrogen bonds between the disaccharide and the biostructure. The water replacement hypothesis has been proposed to explain the trehalose bioprotective effect on membranes (*Sum et al., 2003; Pereira et al., 2004*).
- **Water Entrapment or Preferential Hydration Hypothesis**: trehalose is preferentially excluded from the protein domain (*Timasheff, 1998; Timasheff, 2002*), rather than direct binding the biomolecule as according the water replacement hypothesis, and entraps the residual water at the interface by glass formation, thus preserving the native solvation. Different cosolvents in solution are classified on a scale from the most preferentially bound to the most preferentially excluded (*Timasheff, 2002*), the latter better stabilizing the protein structure. Disaccharides are among the most excluded cosolvents, in a scale in which trehalose is at the top.
- **High Viscosity Hypothesis**: trehalose reduces the large-scale internal protein motions that lead to the loss of structure and to denaturation (*Sampedro and Uribe, 2004*).
- **Water Network Perturbation Hypothesis**: each saccharide perturbs the hydrogen bond water network surrounding the protein in a different way, and trehalose is the best destructurant among them (*Magazù et al., 2004; Lerbret et al., 2005*). The disruption and reordering of the tetrahedral water network would avoid ice formation when temperature decreases. Furthermore, when strong, extended hydrogen bond network is formed, as in amorphous saccharide systems, the protein surface is connected to the water–sugar medium by a hydrogen bond network, which couples the internal degrees of freedom of the protein to the degrees of freedom of the external matrix (*Francia et al., 2008*).
- **Trehalose Polymorphism**: trehalose peculiarity is due to its polymorphism (*Sussich et al., 1998; Cesàro, 2006*), namely its capability to switch between TRE_{α} form and TRE_{h} form. As a result, a gentle, reversible dehydration-hydration mechanism can occur at the time scale of the main degradation processes, with a water-buffering action against abrupt moisture variations.

As mentioned before, the above hypotheses are not mutually exclusive and the way trehalose protects biostructures probably depends on the particular biological system. For what concerns the work presented in this thesis, two or more of the previous hypotheses are necessary to explain the experimental results. The data on

amorphous systems (*chapter 3*) could be interpreted by taking into account both the perturbation of the water network and the water replacement hypothesis, since it seems that the concentration of water at the surface of the protein is lower than elsewhere. Conversely, as regard to the data on the *aggregation of proteins in saccharide solutions* (*chapter 4*), there is of course an effect of viscosity by the sugar on the protein denaturation and aggregation kinetics, but it is not enough to explain the greater stability of protein, because this effect is slightly different changing sugar and cannot, therefore, be explained only by assuming a non-specific hypothesis. In this context, the water perturbation hypothesis will be taken into consideration.

2 – Experimental Techniques

The techniques used in this thesis work are discussed in this section. In particular, the physical phenomenon that is the basis of each technique and the main mathematical relations used for data analysis are reported.

2.1 – Small-Angle X-Ray Scattering

When the X-rays, which are electromagnetic waves with wavelength in the range of $(0.1 \div 100\ \text{Å})$, penetrate the matter, the electrons of its atoms are induced to oscillate at the frequency of the incident wave, thus emitting secondary waves. The **Small-Angle X-Ray Scattering (SAXS)** is based on the analysis of the interference of the secondary waves at small angles, namely up to about 10°. This technique, which usually makes use of X-rays with wavelength in the range of $(0.5 \div 2.5\ \text{Å})$, allows to derive parameters of **size** and **shape** and to study the **structure** of colloidal objects, which have a size of tens or hundreds of Å, such as molecules, polymers, metal clusters and proteins.
All the phenomena of scattering are governed, through the *Fourier transform theory*, by laws of reciprocity: at fixed wavelength the greater the size of the object of study, the less the scattering angle. Figure 2.1 shows the relation of reciprocity between the scattering object and its scattering image.

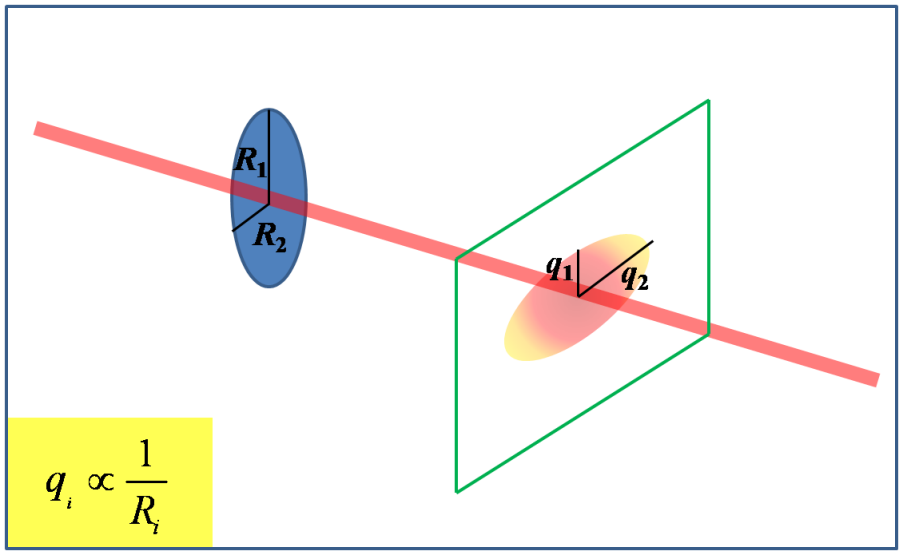

Figure 2.1 – The figure of scattering is linked to the scattering object by a law of reciprocity.

For a fixed wavelength of the incident radiation, the explored size at a certain angle θ (expressed in radians) is approximately equal, for small value of θ, to $\lambda/2\theta$ (*Warren, 1969*). For example, if $\lambda = 1$ Å the explored size is about 290 Å at 0,1°, while it is about 29 Å at 1°.

The electromagnetic radiation interacts with electrons, thus the variation in the electronic density of the irradiated matter is what causes small-angle X-ray scattering. The simplest case is that of an object of constant electronic density in a medium with different constant electronic density, called matrix. The difference in electronic density between the object and the matrix is called **contrast**. Systems with small contrast diffuse not much the incident beam.
Scattering phenomena are generated not only by both amorphous structures and crystalline structures, but also by pores, bubbles and cracks: in fact, as gaps in materials otherwise homogeneous, they produce a contrast of electronic density, detectable by scattering measurements .

2.1.1 – Scattering by a Free Electron

If a free electron is accelerated by an electromagnetic wave linearly polarized of amplitude E_0, it will emit a secondary wave of amplitude $E(\theta)$ and same wavelength, as shown in the following figure, where θ is the angle between the direction of polarization of the incident wave and the direction of propagation of the scattered wave.

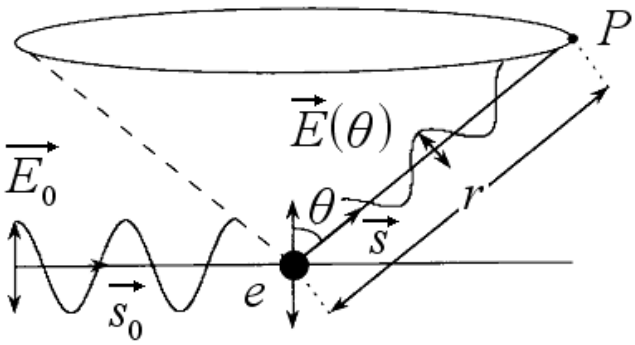

Figure 2.2 – When a free electron is accelerated by an electromagnetic wave, a secondary wave is produces. The incident and scattered waves have the same wavelength.

According to general physics (*Focardi et al., 2005*), the amplitude of the wave emitted by an accelerated charge e is given, at great distance r, by :

$$E_{em} = \frac{1}{4\pi\varepsilon_0}\frac{a_\perp}{c^2}\frac{e}{r} \tag{2.1}$$

where $a_\perp$ is the acceleration perpendicular to $\vec{r}$ and c is the speed of light.

In the present case, $a_\perp = a\sin\theta$ and $a = \frac{F}{m_e} = \frac{eE_0}{m_e}$, so that the amplitude $E(\theta)$ of the scattered field at the point $P(r,\ \theta)$ is:

$$E(\theta) = E_0\frac{\ell}{r}\sin\theta \tag{2.2}$$

where ℓ is known as **scattering length**:

$$\ell = \frac{1}{4\pi\varepsilon_0}\frac{e^2}{m_e c^2} \approx 2{,}8\cdot 10^{-12}\ \text{m} \tag{2.3}$$

2.1.2 – Scattering by a Single Atom

An atom can be schematized as a group of electrons confined in a small volume, as shown in figure 2.3. The scattering angle, that is the angle between the direction of the incident wave versor $\vec{S_0}$ and the direction of the scattered wave versor $\vec{S}$, has been set equal to 2θ.

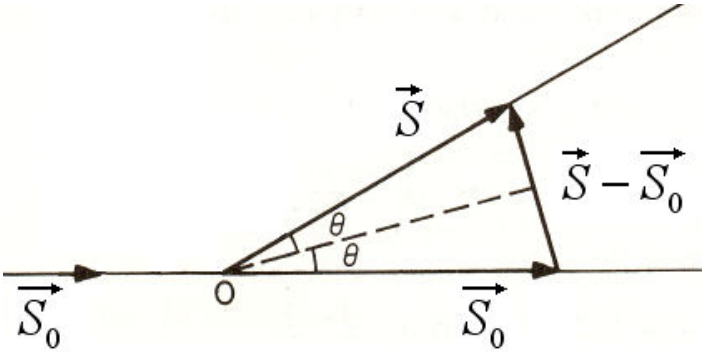

Figure 2.3 – A wave is scattered by an atom, schematized as a group of electrons confined in a small volume.

In the case of elastic scattering, the following quantity is defined as the **scattering vector**:

$$\vec{q} = \frac{2\pi}{\lambda}\left(\vec{S} - \vec{S_0}\right) \tag{2.4}$$

the magnitude of which is:

$$q = 4\pi \frac{\sin\theta}{\lambda} \tag{2.5}$$

The incident wave interacts with the electrons of the atom, which become sources of secondary waves. In a first approximation, the scattered wave is given by the superposition of these secondary waves. Successive approximations can be carried out considering the superposition of the waves resulting from the scattering of the secondary waves (multiple scattering). Assuming that the interaction between the incident wave and the centers of scattering is not very strong, multiple scattering can be neglected.

In particular, if the magnitude of the incident wave is $E_0 e^{i\vec{s_0}\vec{R}}$, then the resulting wave is:

$$E_0 e^{i\vec{s_0}\vec{R}} + \frac{E_0 b}{r} e^{i\vec{s}\vec{R}} \tag{2.6}$$

where $\vec{R}$ is the vector that ideally connects the center of scattering O and the detector, while b is a parameter that indicates the strength of interaction between the incident wave and the center of scattering .

From the theory of perturbations (*Warren, 1969*), the scattered wave is given by:

$$E_0 e^{i\vec{s_0}\vec{R}} + \frac{E_0 b e^{i\vec{s_0}\vec{R}}}{4\pi r} f\left(\vec{q}\right) \tag{2.7}$$

where $f\left(\vec{q}\right)$ is known as **atomic scattering factor** and it gives information on the strength of interaction between the electromagnetic field and the atom:

$$f\left(\vec{q}\right) = \int_V \rho(r) e^{-i\vec{q}\vec{r}} dV \tag{2.8}$$

$\rho(r)$ being the normalized charge density, given by the sum, weighted with the number of electrons, of the radial wave functions of the atom, supposed hydrogen-like.

2.1.3 – Scattering by a Group of Atoms

A group of atoms can be modelled as an object with electronic density $\rho\left(\vec{r}\right)$. In this case, the amplitude of the wave scattered by the object in a given direction $\vec{r}$ is equal, in the reciprocal space, to the Fourier transform of the electronic density $\rho\left(\vec{r}\right)$ inside the object (*Guinier and Fournet, 1955*):

$$E\left(\vec{q}\right) = \int_V \rho\left(\vec{r}\right) e^{-i\vec{q}\vec{r}} d\vec{r} \tag{2.9}$$

while the intensity is proportional to the following integral:

$$I\left(\vec{q}\right) \propto \int_V P\left(\vec{r}\right) e^{-i\vec{q}\vec{r}} d\vec{r} \tag{2.10}$$

where $P\left(\vec{r}\right)$ is known as **Patterson's Function**, which is the autocorrelation function of $\rho\left(\vec{r}\right)$:

$$P\left(\vec{r}\right) = \int_V \rho\left(\vec{r}+\vec{r'}\right)\rho\left(\vec{r'}\right) d\vec{r'} \tag{2.11}$$

In the particular case of an object with constant electronic density $\rho\left(\vec{r}\right)$, Patterson's function assumes a particular geometric meaning: it is proportional, in fact, to the overlap volume between the object and its "phantom" translated by the vector $\vec{r}$, as shown in figure 2.4.

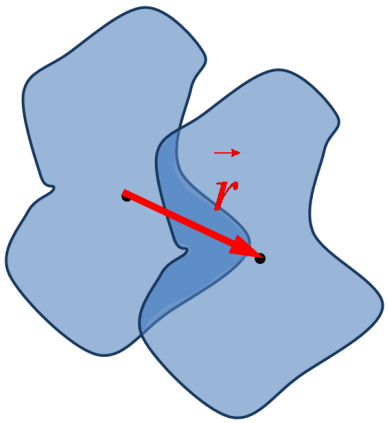

Figure 2.4 – In the case of an object with constant electronic density, Patterson's function is proportional to the overlap volume between the object and its "phantom" translated by $\vec{r}$.

2.1.4 – Systems of Identical Particles

Small-angle X-ray scattering is generally applied to systems that are statistically isotropic and do not present long-range order.
In the case of a diluted system of N identical particles of volume V, the density of which can be written as follows:

$$\rho(r) = \begin{cases} \rho & \text{inside the particle} \\ 0 & \text{outside the particle} \end{cases} \tag{2.12}$$

then the total scattered intensity is given by (*Guinier and Fournet, 1955*):

$$I(\vec{q}) = N(\rho - \rho_0)^2 V^2 \int_0^{+\infty} 4\pi r^2 \gamma(r) \frac{\sin(qr)}{qr} dr \tag{2.13}$$

where ρ_0 is the density of the medium that contains the particles, and $\gamma(r)$, which depends on the object shape, is obtained by integration of Patterson's function on the whole solid angle.

For spherical particles with constant electronic density and radius R, the equation (2.13) becomes (*Feigin and Svergun, 1987*):

$$I_{Rayleigh}(\vec{q}) = N(\rho - \rho_0)^2 V^2 9 \left[\frac{\sin(qR) - qR\cos(qR)}{(qR)^3} \right]^2 \tag{2.14}$$

which is known as **Rayleigh function**.

At variance, for two-phase systems, in which each phase has a constant electronic density and is randomly distributed, the expression (2.13) results in the so-called **Debye equation** (*Debye et al., 1957*):

$$I_{Debye}(\vec{q}) = \frac{A}{(1 + q^2 D^2)^2} \tag{2.15}$$

where A is a proportionality constant and D is the average dimension of the object of a given phase.

At last, the following integral:

$$Q = \int_0^{+\infty} q^2 I(q) dq = 2\pi^2 \rho_0^2 V \tag{2.16}$$

is called **invariant** Q. It depends only on the object volume, and not on its shape, and it is proportional to the total scattered intensity.

2.1.5 – Guinier's Approximation for Diluted Systems

If the system is diluted, the scattering contribution relative to the superposition of secondary waves of different particles is negligible, and the relation (2.13) can be approximated for small angles by a gaussian function:

$$I(q) \approx I_0 \, e^{-\frac{1}{3}R_G^2 q^2} \tag{2.17}$$

where R_G is called **Guinier's radius** or **electronic radius of gyration**.

By analogy with the radius of gyration in mechanics, Guinier's radius represents the mean square of the distances of each electron from the electronic center of mass: thus, it does not provide a complete geometric description of the particles, but it is well defined by the shape of the particles. For example, the radius R of spherical particles is given by the following relation:

$$R = \sqrt{\frac{5}{3}} R_G \tag{2.18}$$

Approximation (2.17) can be used provided that the following condition is valid:

$$qR_G < 1 \tag{2.19}$$

For this reason, Guinier's radius can be obtained by successive approximations. In the case in which the particles have the same shape but different size, lying within a limited range, Guinier's radius provides, however, an indication of the average particles size.

2.1.6 – Porod's Approximation

If the geometry of the particles is Euclidean, the part of the scattering function (2.13) at high values of q can be approximated by the following **Porod's plateau for Euclidean geometry**:

$$I_{Porod}(q) = \lim_{q \to +\infty} I(q) = \frac{Q}{\pi V} \frac{A}{q^4} \tag{2.20}$$

where Q is the invariant, defined by equation (2.16), and A is the surface area of the particles.

As q increases, the product $\left[q^4 \cdot I(q)\right]$ stabilizes at a constant value, proportional to the surface area of the particles. In addition, this asymptotic value can be reached with oscillations, which indicate the sharpness of surface, namely whether the surface is smooth or sharp.

Porod's approximation does not require that the system is diluted, but it is also valid for very close particles: the effects of scattering due to the distances among the particles, in fact, are dampened at the angles pertinent to Porod's plateau.

At variance, in the case of a **fractally** rough surface area with a dimensionality d between 2 and 3, Porod's law becomes:

$$\lim_{q \to +\infty} I(q) = \frac{Q}{\pi V} \frac{A'}{q^{6-d}} \tag{2.21}$$

2.1.7 – Decoupling Approximation for Interacting Spherical Particles

For a system of interacting spherical particles, in which there are not any long-range correlations, it is possible to separate the contribution to the scattered beam due to the shape of the particles from the one due to the correlation among the positions of the particles: this is called **decoupling approximation**. According to this approximation, the scattered intensity is proportional to the convolution of the so-called **form factor** $P(R)$, which accounts for the extension of the particles in space, with a function that identifies the lattice on which the particles are disposed, known as **structure factor** $S(R)$:

$$I(r) \propto P(r) * S(r) \tag{2.22}$$

This approximation is no longer valid if the particles are anisotropic, since in this case the structure factor depends on their mutual orientation.

In the reciprocal space the equation (2.22) is more simple, since the convolution becomes a product:

$$I(q) \propto P(q) \cdot S(q) \tag{2.23}$$

The form factor $P(q)$ is related to the Fourier transform of the electronic density of the particles, while the structure form $S(q)$ is related to the Fourier transform of the particle pair-correlation function (2.11).

The following figure shows what is the basis for the decoupling approximation.

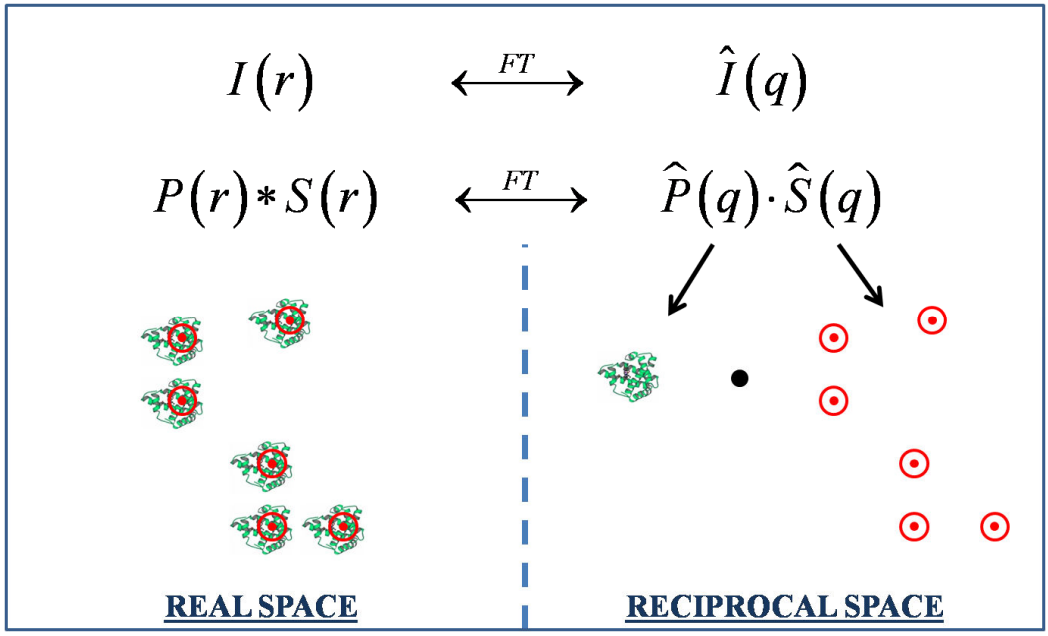

Figure 2.5 – A system of almost spherical particles disposed in a lattice, seen as a convolution in the real space (left panel) and as a product in the reciprocal Fourier space (right panel).

2.1.8 – Percus-Yevick Structure Factor for Interacting Spheres

In reference to the previous paragraph, it is of interest to consider **Percus-Yevick structure factor** (*Percus and Yevick, 1958; Brumberger, 1993*), which applies to systems of hard spheres and has been used to fit the SAXS data in this thesis:

$$I_{Percus-Yevick}(q)=\frac{1}{1-24\eta(\alpha+\beta+\gamma)} \tag{2.24}$$

with:

$$\begin{cases} \alpha=\dfrac{(1+2\eta)^2}{dq(1-\eta)^4}\left[\dfrac{\cos(dq)}{dq}-\dfrac{\sin(dq)}{(dq)^2}\right] \\ \beta=-\dfrac{6\eta(1+\eta/2)^2}{dq(1-\eta)^4}\left[\dfrac{\cos(dq)}{dq}-\dfrac{2\sin(dq)}{(dq)^2}+2\dfrac{1-\cos(dq)}{(dq)^3}\right] \\ \gamma=\dfrac{\eta(1+2\eta)^2}{2dq(1-\eta)^4}\left[\dfrac{\cos(dq)}{dq}-\dfrac{4\sin(dq)}{(dq)^2}-12\dfrac{\cos(dq)}{(dq)^3}+24\dfrac{\sin(dq)}{(dq)^4}+24\dfrac{\cos(dq)-1}{(dq)^5}\right] \end{cases} \tag{2.25}$$

where d is the average distance among the hard spheres and η is their occupied volume fraction.

Under Percus-Yevick approximation, the interparticle forces are zero except for the fact that two particles cannot interpenetrate each other. At high fractional volume there are oscillations in the pair-correlation function due to the crowding of the spheres to form a tight lattice. On the contrary, at low fractional volume the correlation function is nearly flat since the spheres are far apart and almost independent of each other. In all cases, the pair-correlation function is zero for r less than the diameter of the spheres, since the spheres are impenetrable.

2.2 – Dynamic Light Scattering

Light Scattering (LS) is a form of scattering, in which visible light is the propagating energy that is scattered. In particular, the light incident on a molecule much smaller than its wavelength induces an oscillating electric dipole:

$$\vec{\mu} = \alpha \vec{E} \tag{2.26}$$

where $\vec{E}$ is the electric field of light and α is the molecule polarizability. The light radiated by this oscillating dipole is the origin of the scattered radiation.

Fundamentally, light scattering and X-ray scattering are the same phenomenon, since they are caused by the interaction between the electromagnetic radiation and the electronic density. However, light and X-rays wavelengths differ for more than one order of magnitude: this implies great differences in the involved energies, as well as the explored scale. As regards the latter implication, it must be emphasized that light scattering treats as point-like what X-ray scattering regards as complex, since X-rays wavelength is much smaller than light wavelength.

It can be shown (*Berne and Pecora, 1976*) that the intensity I of the scattered radiation detected by a detector at a distance $\vec{r}$ is given by:

$$I = I_0 \frac{\pi^2 \alpha^2 \sin^2 \chi}{\varepsilon_0^2 \lambda^4 r^2} \tag{2.27}$$

where I_0 is the intensity of the incident light, χ is the angle between the detector line of sight and the induced dipole $\vec{\mu}$, ε_0 is the permittivity of free space, λ is the wavelength of light, and r is the distance between the sample and the detector.

It is worth emphasizing some aspects of the equation (2.27). The first one is that the solid angle of radiation sampled by a fixed slit decreases as the square of the distance r of the detector: this explains the appearance of the quantity $1/r^2$. Furthermore, the amplitude of the electric field of the light emitted depends on the amplitude of the induced dipole μ, so the scattered intensity depends on μ^2 or, equivalently, on α^2.

At last, the ability to demonstrate the $1/\lambda^4$ dependence is a good indication that Rayleigh scattering is being observed rather than absorption, Raman scattering or other effects. Nevertheless, when the sample contains molecules larger than λ, then this dependence is no longer valid. For example, very long rods will show a wavelength dependence of scattering that is closer to $1/\lambda^3$.

It is conventional, however, to rewrite the equation (2.27) in terms of the change of refractive index n with concentration, which is the experimentally determined quantity, rather than the molecular polarizability. For a gas at low pressure, that means that multiple scattering by secondary waves is negligible because the

molecules are not mutually close, the equation (2.27) can be rewritten (*Johnson and Gabriel, 1981*) as:

$$I = I_0 \frac{4\pi^2 C M_W \sin^2 \chi}{\lambda^4 r^2 N_A} \left(\frac{\partial n}{\partial C} \right)^2 \tag{2.28}$$

where C is the mass per unit volume of the gas, M_W is the molecular weight of the gas particles, and N_A is Avogadro's number.

The equation (2.28) states that the scattered intensity is directly proportional to the concentration in mass and to the molecular weight of the scattering particles. This statement is valid also for diluted solutions of scattering objects, which are smaller than the wavelength of light and larger than the solvent molecules, so that the solvent can be treated as a continuum system with uniform refractive index.

This implies that the capability of an object to be observed by light scattering not only depends on its concentration, but also on its weight or, equivalently, on its volume, since molecular weight is proportional to the third power of the radius for compact objects:

$$M \propto R^3 \tag{2.29}$$

For example, in consideration to the system shown in figure 2.6, according to equations (2.28) and (2.29) the scattered intensity of only 1 red particle of radius $10R$ is 1000 times larger than the total scattered intensity of 1000 blue particles with radius R, although concentration in mass is equal for both types of particles.

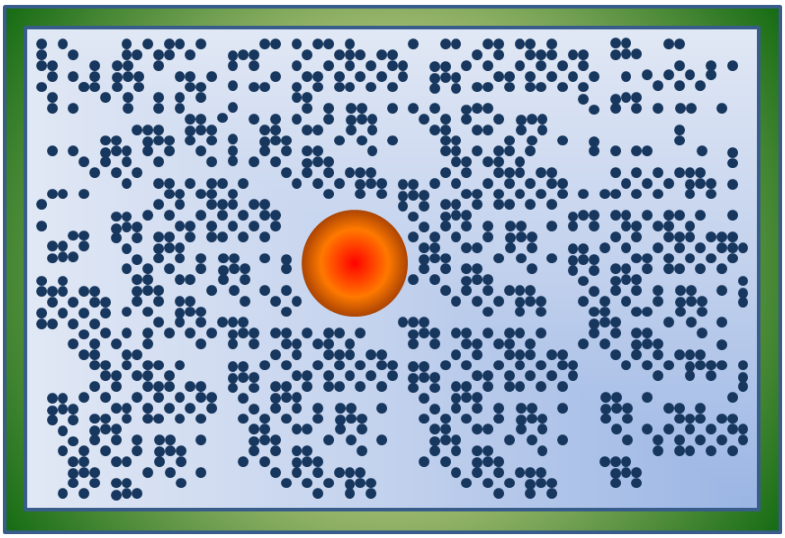

Figure 2.6 – The scattered intensity of 1000 blue particles with radius R is equal to the scattered intensity of only 1 red particle of radius $10R$.

A significant consequence of what has just been discussed is that the sample cleaning procedure, which for some other experimental techniques can be of minor importance, is a vital part of scattering measurements. Impurities in the sample, even if very few, can be enough to cover the scattering signal of interest, so **filtration** is mandatory for light scattering experiments.

2.2.1 – Time Correlation Analysis

There are several types of light scattering techniques. Among them, the technique used in this work to study protein aggregation is **dynamic light scattering (DLS)**, which detects very small line broadening of the incident beam. This scattering can arise in several ways, for example because of the Doppler shifts due to molecules in motion. Even if there is no net motion, the fluctuations in the number of scattering molecules will result in a distribution of wavelengths of scattered light. This distribution is quite narrow and an extremely monochromatic light source, such a laser, is required to study it.

There are two different approaches to obtain dynamic information from a fluctuating system, and they are entirely equivalent: the **frequency spectrum** analysis and the **time correlation** analysis. The study of protein aggregation discussed in this thesis has made use of the second method. In particular, the time autocorrelation function $G^{(1)}(\tau)$ of the scattered electric field $\vec{E}$ at a given position, sometimes called **first-order correlation function**, can be defined by:

$$G^{(1)}(\tau)=\left\langle \vec{E}(t)\vec{E}(t+\tau)\right\rangle=\frac{1}{T}\int_0^T \vec{E}(t)\vec{E}(t+\tau)\,dt \tag{2.30}$$

In practice the intensity fluctuations are measured, rather than the field fluctuations. For the intensity, which is proportional to E^2, the **second-order correlation function** is defined by:

$$G^{(2)}(\tau)=\left\langle I(t)I(t+\tau)\right\rangle \tag{2.31}$$

For systems containing a large number of independent scatterers, for which the distribution of the positions $\vec{r}(t)$ of each particle can be considered Gaussian, the intensity correlation is related to the filed correlation by (*Serdyuk et al., 2007*):

$$G^{(2)}(\tau)=1+\left|G^{(1)}(\tau)\right|^2 \tag{2.32}$$

Time correlation theory applies to **ergodic systems**, in which averaging over time is equivalent to an ensemble average.

As mentioned before, the frequency spectrum and the correlation function are equivalent descriptions of the dynamical behavior of a property of an equilibrium system, being related by the Fourier transformation:

$$I(\nu)=\frac{1}{2\pi}\int G^{(1)}(\tau)e^{-2\pi i\nu t}d\tau \tag{2.33}$$

where ν is the Hertzian frequency. Thus, if $I(\nu)$ has a Lorentzian form around zero frequency, then $G^{(1)}(\tau)$ shows a simple exponential decay with a time constant equal to the reciprocal of the Lorentzian half-width. This simple form occurs for all elementary stochastic processes.

The following figure shows the general trend and the meaning of the autocorrelation function qualitatively. In particular, it is maximum when the delay time τ is equal to zero, and it exponentially decreases to zero, as time increases, because the initial signal does not overlap the signal at great temporal distances.

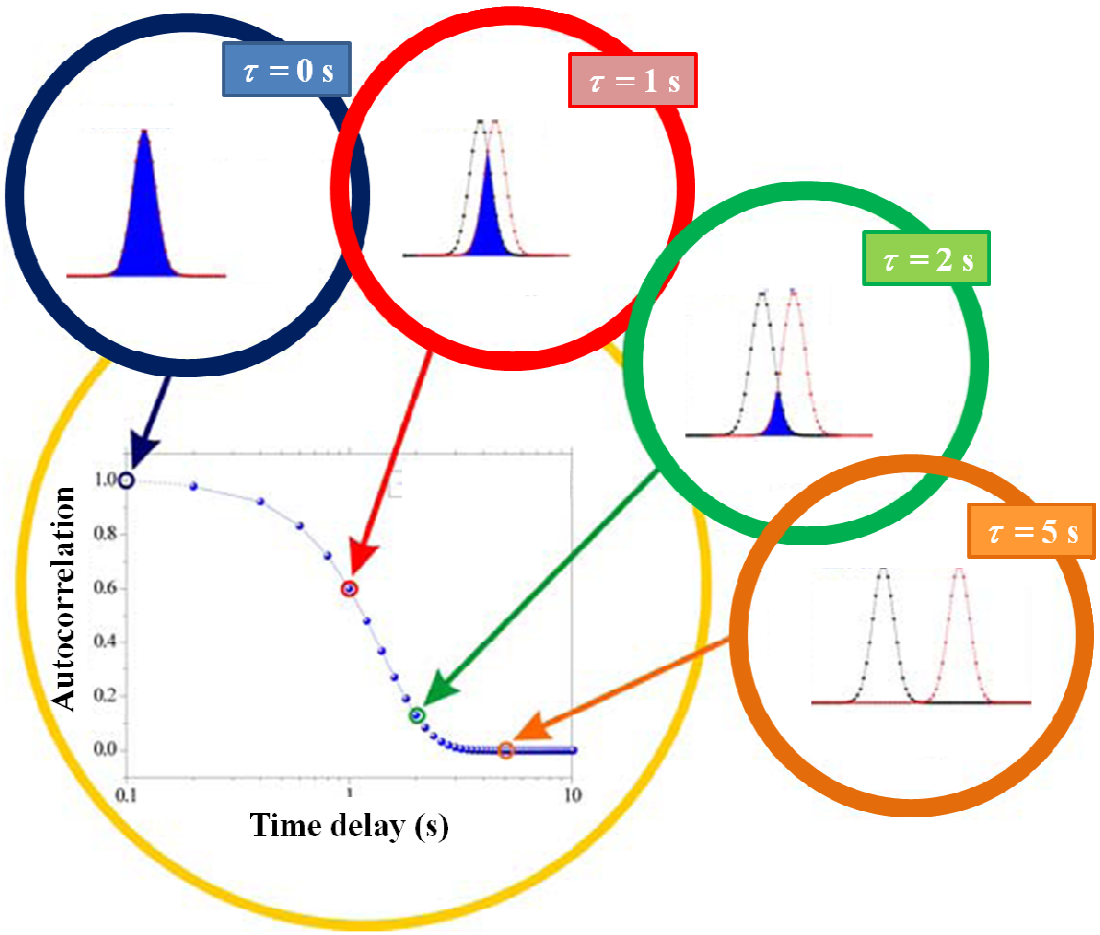

Figure 2.7 – General trend and meaning of the autocorrelation function. It represents the overlap between the initial signal and a delayed version of itself.

2.2.2 – Diffusion Coefficients from Dynamic Light Scattering

In a solution at equilibrium the molecules are subject to a disordered motion, said *Brownian motion*, undergoing collisions with the molecules of the solvent. The net force on each molecule of mass m is given by:

$$\vec{F}(t) = -b^2\vec{v}(t) + \vec{f}_{coll}(t) \tag{2.34}$$

where the first term is due to viscous friction, while the second one is an impulsive force due to collisions with other molecules. For the latter term, it is assumed that:

- its time average value is zero, because collisions do not have privileged directions: $\left\langle \vec{f}_{coll}(t) \right\rangle = 0$;
- it has zero autocorrelation, because it continually fluctuates: $\left\langle \vec{f}_{coll}(t)\vec{f}_{coll}(t+\tau) \right\rangle = \delta(\tau)$;
- it has a Gaussian trend, due to a great number of events.

From Newton's second law:

$$-b^2\vec{v}(t) + \vec{f}_{coll}(t) = m\frac{d}{dt}\vec{v}(t) \tag{2.35}$$

The autocorrelation function of the solution of equation (2.35) is:

$$\left\langle \vec{v}(0)\vec{v}(\tau) \right\rangle = \left\langle v^2(0) \right\rangle e^{-b^2 t/m} \tag{2.36}$$

The **diffusion coefficient** is defined by means of the mean square displacement of the molecule:

$$D = \frac{1}{6}\lim_{t\to+\infty}\frac{\left\langle r^2(t) \right\rangle}{t} \tag{2.37}$$

For spherical particles of radius R, diffusing in a solvent with viscosity η at temperature T, the diffusion coefficient is given by **Stokes-Einstein relation**:

$$D = \frac{k_B T}{6\pi\eta R} \tag{2.38}$$

where k_B is the Boltzmann constant.

If a gradient of the concentration $C(\vec{r},\, t)$ of the solute in solution exists, then there is a flux $\vec{J}$ of molecules that tends to uniform the concentration. If the diffusion coefficient does not depend on concentration $C(\vec{r},\, t)$, then it appears as the key parameter of **Fick's second law**:

$$\frac{d}{dt}C(\vec{r},\, t) = D\cdot\nabla^2 C(\vec{r},\, t) \tag{2.39}$$

Equation (2.39) applies also to autocorrelation $G(\tau)$, since $G(\tau)$ can be interpreted as the probability that the displacement of a particle initially at the origin O is $\vec{r}$, after a random motion in a time t.

Solution of the Fourier transform of (2.39) leads to the following expression for the autocorrelation of single monodisperse particles, small compared with the wavelength of light, which diffuse in solution:

$$G^{(2)}(\tau) = 1 + Ae^{-2Dq^2\tau} \tag{2.40}$$

From the single exponential decay of the measured autocorrelation function $G^{(2)}(\tau)$ the translational diffusion coefficient of the particle under study can be obtained.
In particular, the relation (2.38) shows that dynamic light scattering can provide a measure for the so-called **hydrodynamic radius** R_{hyd}:

$$R_{hyd} = \frac{k_B T}{6\pi\eta D} \tag{2.41}$$

When Brownian spherical particles of different radii are present, the photon correlation function can be analysed in terms of **sum of independent exponential decays** (*Koppel, 1972*) relative to each particle species if the decay times differ by a factor 3 or more.
Furthermore, if the decay times are continuously distributed, then the correlation analysis requires a different approach. This is not always easy to lead, since it involves Laplace's transformations, which are not always readily solvable.

2.2.3 – Fractal Dimension of Diffusing Species

In addition to diffusion coefficients, it is possible to obtain information on the **compactness** of the diffusing objects by dynamic light scattering measurements. The scattered intensity I of particles small compared with the wavelength of light is proportional to the average molecular weight M_W of the species in solution, as expressed by the relation (2.28).
In addition to this, the average molecular weight is proportional to (*Schärtl, 2007*):

$$M_W \propto \overline{R}_{hyd}^{\delta} \tag{2.42}$$

where $\overline{R}_{hyd}$ is the average hydrodynamic radius of the particles and δ the so-called average **fractal dimension**, so that:

$$I \propto \overline{R}_{hyd}^{\delta} \tag{2.43}$$

In a process in which $\overline{R}_{hyd}$ changes, it is possible to estimate δ by taking the logarithm of the equation (2.43): in this case the fractal dimension is given by the slope of the graph $\log I$ as a function of $\log \overline{R}_{hyd}$.
A value $\delta \sim 3$ stands for compact objects, while $\delta \sim 2$ may indicate 3D-objects with a density that is not uniform. For scattering filaments δ is almost equal to 1.
Table 2.1 reports the fractal dimension of selected topologies (*Schärtl, 2007*).

Table 2.1 – Fractal dimension of selected topologies.

	fractal dimension δ
cylinders, rods	1
ideal Gaussian coil	2
gaussian coil with excluded volume	5/3 ≈ 1.67
branched Gaussian chain	16/7 ≈ 2.29
2D-objects with smooth surfaces	2
2D-objects with fractal surfaces	1–2
3D-objects with smooth surfaces	3
3D-objects with fractal surfaces	2–3

2.3 – Electronic Absorption Spectroscopy

Absorption Spectroscopy (AS) is a technique based on the measurement of the amount of the light absorbed by a sample at a given wavelength, generally in the range from 190 nm to 1000 nm for biological systems. It is one of the most versatile and widely used experimental techniques, especially in chemistry and life sciences.

A molecule, or part of it, that can be excited by absorption is called **chromophore**. Organic chromophores, which absorb strongly in the ultraviolet or visible portions of the spectrum, usually involve aromatic rings or multiple bonds, such as $C=C$, $C=O$ or $C=N$.

The molecular electronic excitation energy can be dissipated as heat by collision of the excited molecule with another molecule or also by a process of emission of light called fluorescence, so that the intensity of the light transmitted by a collection of chromophores is less than the intensity of the incident light.

The main **applications** of absorption spectroscopy are the following:

- determination of the concentration of a substance, which is discussed in Paragraph 2.3.2 ("Beer-Lambert's Law");
- kinetic assay of chemical reactions, measuring the concentration of either the reactant or the product over time;
- study of conformational changes in the structure of a biomolecule;
- identification of materials, by determining the complete spectrum and comparing it to spectra published in the literature;
- immunoassays, to detect the presence of an *antibody* or an *antigen*.

2.3.1 – Energy States of Molecules

The excited states of a molecule are characterized by a set of discrete amounts or quanta of energy, described by the laws of quantum mechanics, called **energy levels** of the molecule. In visible and ultraviolet spectrophotometry, the major energy levels are determined primarily by the possible spatial distributions of the electrons and are called **electronic energy levels**. Superimposed on each of these states is a series of **vibrational levels** that, in turn, are subdivided into several **rotational levels**.

The wavelength, and so the energy, of absorption is determined by the difference in energy ΔE between the states of the electronic transition and is given by (*Cantor and Schimmel, 2001*):

$$\lambda = \frac{hc}{\Delta E} \tag{2.44}$$

where h is Planck's constant and c is the speed of light.

Figure 2.8 shows a section through the potential energy surfaces of the two lowest electronic states of a typical simple molecule: the ground electronic state S_0 and the first excited electronic state S_1, each subdivided into vibrational and rotational levels. The energy spacing between the lowest rotation-vibration state of S_0 and that of S_1 is typically 80 kcal/mol. This energy is much greater than the thermal energies at room temperature, so that, in absence of radiation that can excite a transition, all the molecules in a solution are in the lowest electronic state S_0. Similarly, the energy spacing between the vibrational levels is of the order of 10 kcal/mol, therefore only the lowest vibrational level of S_0 can be considered to be appreciably populated. However, rotational energy spacings are only 1 kcal/mol or less, so that many rotational levels are populated at room temperature.

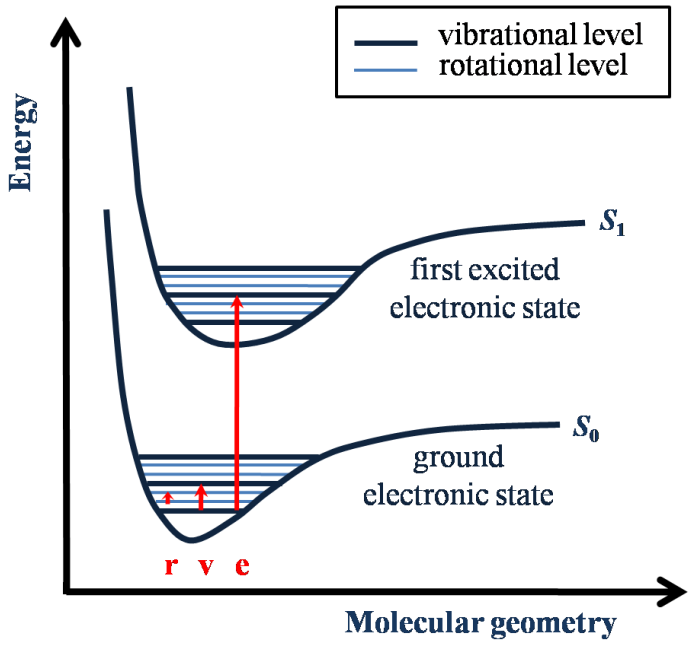

Figure 2.8 – The two lowest electronic energy levels of a small molecule, subdivided into vibrational and rotational levels. Transitions corresponding to electronic (e), vibrational (v) and rotational (r) spectra are indicated.

If all the transitions were only between the lowest vibrational levels of the ground state and the first excited state, then an absorption spectrum would consist of narrow, discrete peaks. However, the transition from one electronic level to the next electronic level can also occur among many vibrational levels. Since the energy differences between two vibrational levels are small compared to the energy differences between two electronic levels, the electronic transition consists of a cluster of very closely spaced spectral peaks. Each peak has significant width, which is comparable to the spacing between the peaks, so that they overlap so much to generate a single broad peak, called **electronic absorption band**.

2.3.2 – Beer-Lambert's Law

For a sample of molecules of molar concentration C in a layer of thickness $d\ell$, perpendicular to the direction of light propagation and sufficiently thin to consider constant the light intensity within the layer, the fraction of light absorbed $(-dI/I)$ is proportional to the number of absorbing molecules:

$$-dI/I = \varepsilon'(\lambda) C d\ell \tag{2.45}$$

where $\varepsilon'(\lambda)$ is known as **molar extinction coefficient** and depends on the cross section of the molecule, as well as the absorbed wavelength.

The integration of the equation (2.45) over a large sample results in the following expression:

$$\ln(I_0/I) = \varepsilon'(\lambda) C \ell \tag{2.46}$$

ℓ being the total geometrical path of light in the sample.

The conversion of the relation (2.46) to log base 10 leads to the so-called **Beer-Lambert's law**:

$$A(\lambda) = \varepsilon(\lambda) C \ell \tag{2.47}$$

where $\varepsilon(\lambda) = \varepsilon'(\lambda)/2.303$ and $A(\lambda)$ is the **absorbance** at a given wavelength, defined by:

$$A = log_{10}(I_0/I) \tag{2.48}$$

The most accurate measurements of A are usually obtained in the range from 0.1 to 2. Smaller values mean that only a tiny fraction of the incident light is absorbed, while larger values mean that only a small fraction of the incident light reaches the detector.

Indirect **measurements of concentration** can be obtained by measurements of absorbance, making use of Beer-Lambert's law (2.47) and of tabulated values for $\varepsilon(\lambda)$ at a given wavelength, generally where it is maximum. In order to properly determine protein concentrations in solution the measured absorbance should be minor than 1, which means that a significant part (more than 10%) of the incident beam passes through the sample.

2.4 – Circular Dichroism

Circular Dichroism (CD) is an experimental technique of investigation that takes advantage of the physical phenomenon of **optical activity**. In particular, when a beam with linear polarization passes through certain substances, said optically active, it emerges with an elliptical polarization, as shown in figure 2.9.

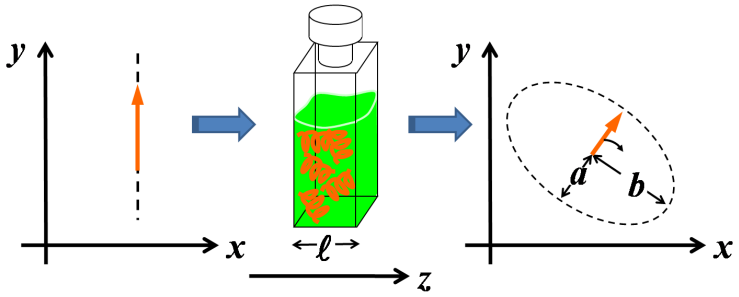

Figure 2.9 – Circular dichroism of a beam with initial linear polarization.

A quantitative measurement of this phenomenon is given by the **ellipticity angle** θ of the transmitted light, geometrically defined by (*Sletten and McLaughlin, 2005*):

$$\theta = \arctan(b/a) \tag{2.49}$$

In practice, measurements of ellipticity angles by the definition (2.49) are difficult to obtain with precision, therefore it is preferable to differently model the phenomenon just described.

In particular, a beam with linear polarization can be decomposed into the sum of two beams with circular polarization and opposite pulsations. Also in this case the transmitted beam has elliptical polarization. In fact, the two incident beams are absorbed differently by optically active substances, depending on whether they have a right-hand or a left-hand circular polarization, and this implies that they contribute to the transmitted beam with different amplitudes, as shown in the following figure.

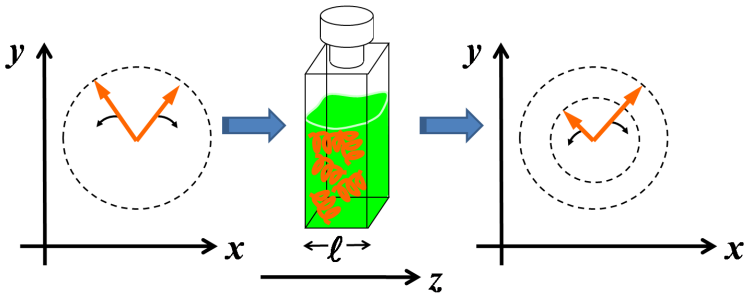

Figure 2.10 – Circular dichroism of two beams with different circular polarization.

In this case it can be shown that the ellipticity angle, expressed in degrees (°), is given by (*Cantor and Schimmel, 2001*):

$$\theta = 32.99(A_L - A_R) \tag{2.50}$$

where A_L ed A_R are the absorbances of the incident light polarized, respectively, left-hand and right-hand.

In practice, an electro-optic modulator, also called Pockels cell, switches between incident light right-hand circular polarized and left-hand circular polarized at a frequency of $50\ \text{kHz}$.
Since the signal of circular dichroism depends on both the concentration C of the optically active substance and on the geometric path ℓ of light within it, the analysis and comparison of the measurements that are based on this phenomenon are carried out through the **molar ellipticity angle** $[\theta]_{molar}$, defined by:

$$[\theta]_{molar} = \frac{100}{C\ell}\theta \tag{2.51}$$

The units of molar ellipticity $[\theta]_{molar}$ are $\text{deg}\cdot\text{cm}^2\cdot\text{dmol}^{-1}$ if θ is measured in degrees, C is the molar concentration in M and ℓ is measured in cm.

As regards the proteins, CD measurements are made in two different ultraviolet regions of the spectrum:

- **far-UV range (170-250 nm):** in this region CD signal is given by peptide bonds, so that it is possible to obtain information on the secondary structure of the protein;
- **near-UV range (250-350 nm):** in this region CD signal is mainly given by the aromatic amino acids that are sensitive to the rigidity of the protein due to the environment; their signal, in fact, is greater when they are strictly bound inside the protein, and so shielded from solvent.

For far-UV CD of proteins, the repeating unit is the peptide bond. The Mean Residue Weight MRW for the peptide bond is calculated from:

$$MRW = \frac{M}{N_{res} - 1} \tag{2.52}$$

where M is the molecular mass of the polypeptide chain (in Da) and N_{res} is the number of amino acids in the chain. For most proteins $MRW = (110 \pm 5)\ \text{Da}$.
The **mean residue ellipticity** $[\theta]_{mrw}$ is given by:

$$[\theta]_{mrw} = \frac{100 \cdot MRW}{C\ell}\theta \tag{2.53}$$

The units of molar ellipticity $[\theta]_{mrw}$ are $\text{deg}\cdot\text{cm}^2\cdot\text{dmol}^{-1}$ if MRW is measured in dalton, θ in degrees, C in g/l and ℓ in cm.
The analysis of the spectra in the far-UV range can be conducted by comparison with spectra reported in literature. In general, the spectrum of a protein can be decomposed as a weighted sum of three reference spectra, as shown in figure 2.11 .

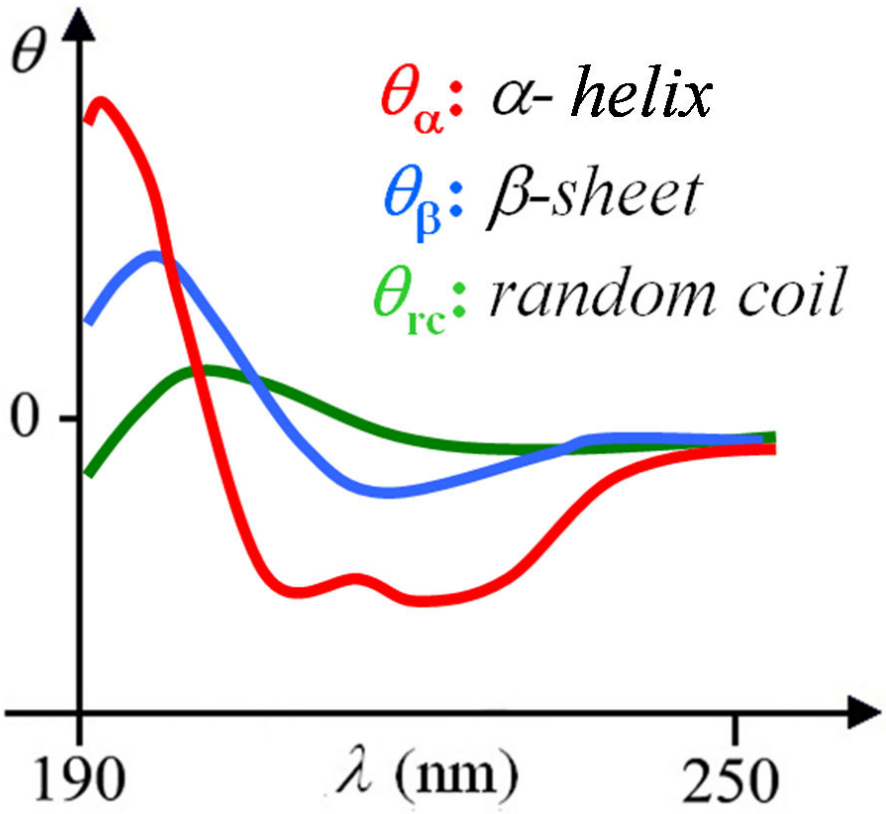

Figure 2.11 – Reference spectra for circular dichroism of protein in the far-UV range.

3 – Myoglobin Embedded in Amorphous Saccharide Matrices

In this chapter Small-Angle X-Ray Scattering (SAXS) measurements performed on samples of myoglobin embedded in low hydrated saccharide matrices are reported. The study has been carried out on two types of myoglobin, namely metmyoglobin and carboxymioglobin, and four different sugars: trehalose, sucrose, maltose and lactose. The data confirm the occurrence, already reported for trehalose samples, of inhomogeneities in sucrose, maltose and lactose, which depend on the sample hydration and on the presence of sodium dithionite.
Furthermore, the results show that the previously proposed mechanism for trehalose bioprotection (*Cesàro et al., 2006; Kilburn et al., 2006; Longo et al., 2010*) based on water-buffering action, that would contrast moisture variations, can be extended to other sugars, and it is likely to be a general behaviour.

The work here discussed has been published as an article[4] on the European Physical Journal:
S. Giuffrida, M. Panzica, F. M. Giordano, A. Longo, "*SAXS Study on Myoglobin Embedded in Amorphous Saccharide Matrices*", Eur. Phys. J. E 34: 87, 2011. DOI: 10.1140/epje/i2011-11087-6

3.1 – Myoglobin

Myoglobin is a globular protein formed by 153 amino acids, which are arranged in a single chain constituted by 8 alpha-helices connected by loops. These helices form an internal hydrophobic pocket, in which a **heme** prosthetic group is bound to the protein by non-covalent bonds (*Kendrew, 1958*), as shown in figure 3.1.

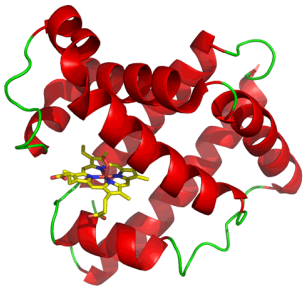

Figure 3.1 – Ribbon structure of myoglobin.

[4] The contribution to the published paper by the author of this thesis concerns the sample preparation and the data analysis.

The only polar residues in the internal hydrophobic pocket are two histidines, one on either side of the heme. Heme is made up of an iron atom and a protoporphyrin IX molecule, that has four heterocyclic pyrrole rings, joined at their corners by methylene bridges. The four nitrogen atoms N of the pyrrole groups bind the iron atom, which can be either ferrous Fe^{2+} or ferric Fe^{3+}. Depending on the molecule bound to the iron (*Antonini and Brunori, 1971*), the protein is called:

- **oxymyoglobin MbO**, with O_2 bound to Fe^{2+};
- **carboxymyoglobin MbCO**, with CO bound to Fe^{2+};
- **metmyoglobin metMb**, with H_2O bound to Fe^{3+};
- **deoxymyoglobin**, with no molecule bond to Fe^{2+}.

Iron can form two additional bonds on either side of the plane of the heme and these additional bonds are important not only in the association of the heme with myoglobin, but also for the binding of O_2. In particular, on the side of the porphyrin where the oxygen is bond, there is the histidine-64, called distal, which acts as trap for the protons that otherwise could catalyze the oxidation of the iron.
Figure 3.2 shows the heme group and the structure around it.

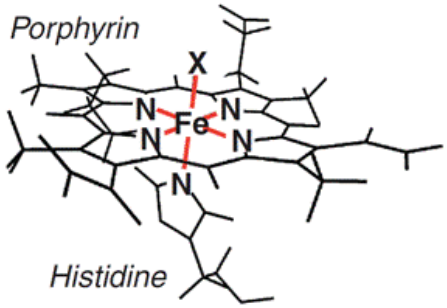

Figure 3.2 – Heme prosthetic group. X denotes O_2, CO, H_2O or a vacancy.

Myoglobin is found primarily in cardiac and red skeletal muscles. Its main function is to **store oxygen** for muscle contraction, but it also facilitates the transport of oxygen to the mitochondria for oxidative phosphorylation (*Kendrew, 1958*). Diving mammals, such as whales, seals and dolphins, are able to remain submerged for long periods due to the storage of oxygen in their muscles, which are so rich in myoglobin to be brown (*Antonini and Brunori, 1971*).
The following table reports the main physical-chemical properties of myoglobin.

Table 3.1 – Main physical-chemical properties of myoglobin.

number of amino acids	153
dimensions of associated ellipsoid	$33 \times 25 \times 4$ Å^3
molecular weight	17 800 Da
λ_P of the absorption peak	279 nm
molar extincion coefficient at λ_P	$\varepsilon_{279\ \mathrm{nm}} = 13\,980\ \mathrm{M^{-1}cm^{-1}}$
isoelectric point in water at 25 °C	7.1

3.2 – Myoglobin Coupling with Amorphous Saccharide Matrices

Recent studies on the role played by amorphous, sugar-containing matrices on the dynamics and structure of embedded proteins have suggested the formation of **hydrogen bond networks** that anchor the protein surface to the surrounding matrix, the stiffness of which increases by lowering the sample water content. The topic is discussed in more detail in the following paragraphs.

3.2.1 – Myoglobin Coupling with Trehalose-Water Matrix

Molecular dynamics simulations in the nanosecond timescale (*Cottone et al., 2002*) and **infrared spectroscopy** measurements (*Giuffrida et al., 2003*) showed that, in samples of trehalose-coated carboxymyoglobin (MbCO), the protein surface is connected to the water–sugar medium by a hydrogen bond network, which couples the internal degrees of freedom of the protein to the degrees of freedom of the external matrix. Such coupling has been experimentally detected in samples of different content of residual water, in which the thermally induced structural rearrangements (20–300 K) of both protein and external matrix were increasingly hindered by lowering the water content (*Giuffrida et al., 2003*). The whole set of data led to conclude that the strength of the anchoring hydrogen bond network is modulated by the residual water content.

In particular, the infrared spectroscopy study is based on the strict correlation observed between the thermal evolution, from 300 K to 20 K, of the **stretching band of the *CO*** bound to the myoglobin heme group and the thermal evolution of the so-called **water association band (WAB)**, which is attributed to a combination of the bending mode of water molecules with intermolecular vibrational modes involving either water or non-water *–OH* groups (*Giuffrida et al., 2003*). While the first band accounts for the protein behaviour, the latter one is assumed to reflect the thermal rearrangements of the solvent matrix because of its intermolecular origins.

The following figure shows the *CO* stretching band, in the range 1900-2000 cm^{-1}, and the water association band, in the range 2000-2400 cm^{-1}, for a sample consisting of trehalose-coated carboxymyoglobin.

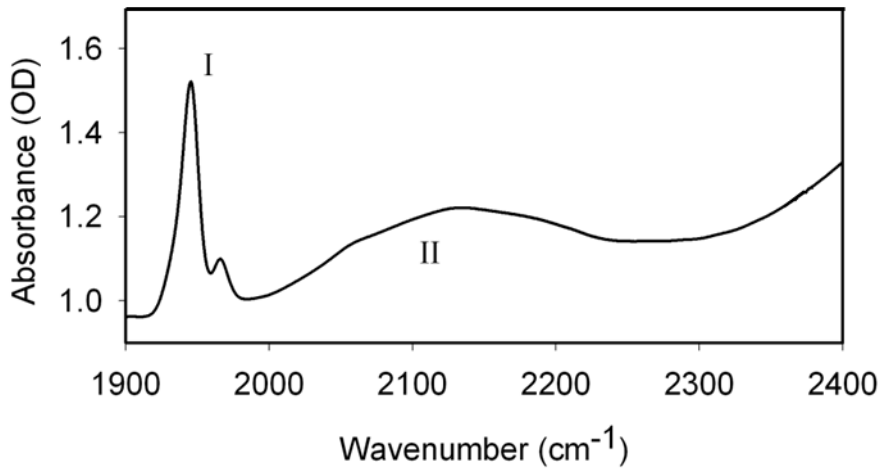

Figure 3.3 – The *CO* stretching band (I, 1900-2000 cm^{-1}) and the water association band (II, 2000-2400 cm^{-1}) in trehalose-coated carboxymyoglobin (*Giuffrida et al., 2003*).

The above conclusions were further supported by **flash photolysis** measurements at room temperature on samples with MbCO embedded in trehalose water matrices of different content of residual water (*Librizzi, 2002*). Such measurements showed that the hydrogen bond network regulates the diffusion of the flashed off CO within the protein.
Furthermore, **Raman and neutron scattering** experiments (*Magazù et al., 2004; Lerbret et al., 2005*) confirmed later on that trehalose orders water molecules in its neighbours, disrupting the tetrahedral network of the bulk water and avoiding ice formation, acting as kosmotrope co-solvent.
All the studies discussed above lead to the so-called **water network perturbation hypothesis** for the explanation of the bioprotective effect of trehalose discussed in paragraph 1.4.1 ("*The Peculiar Effect of Trehalose*"). Accordingly, when strong, extended HB network is formed, as in amorphous trehalose-water-protein systems, the large energy required for the rearrangements of the matrix, which accompany large-scale protein internal motions, sizably increases, thus preserving biostructures against denaturation (*Francia et al., 2008*).

3.2.2 – Myoglobin Coupling with Other Disaccharide Matrices

Analogue studies to those regarding myoglobin-trehalose-water systems were carried out for other sugars. In particular, **molecular dynamic simulations** (*Cottone et al., 2005, Cottone, 2007*) and **infrared spectroscopy** measurements (*Giuffrida et al., 2006*) compared amorphous systems composed by different disaccharides and showed that at low water content MbCO is less coupled to sucrose and maltose matrices than in trehalose matrix.
Figure 3.4 shows the water association band of amorphous dried samples containing small traces of water and trehalose (left panel) or sucrose (right panel). The gray curves in each panel refers to the additional presence of myoglobin in the sample. The greater spectral alteration induced by the presence of the protein in the trehalose-water system, with respect to the one in the sucrose-water system, reflects the higher capability of trehalose to perturb the hydrogen bond network.

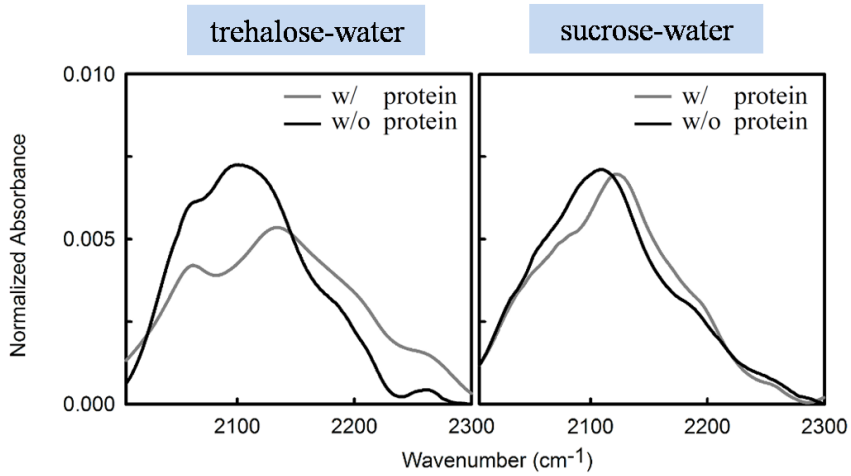

Figure 3.4 – The water association band of amorphous dried samples containing small traces of water and trehalose (left panel) or sucrose (right panel). The gray curves refers to the additional presence of myoglobin in the sample.

In respect of this, simulations on binary disaccharide-water systems showed that, at variance with trehalose, sucrose performs intra-molecular hydrogen bonds already at relatively low sugar concentration (about 0.1 M), and that the hydration number in the range 10%-90% sugar/water w/w is about two units lower for sucrose than for trehalose. This suggests that at low hydration, when the components of the system compete for binding the residual water, there are more internal hydrogen bonds and a lower disruption of the tetrahedral network of water molecules in sucrose than in trehalose.

3.2.3 – Myoglobin-Solvent Coupling in Liquid Aqueous Solutions

Based on the previous discussion, the slaving process, which is the influence of the solvent on the protein internal dynamics (*Frauenfelder et al., 2002*), in aqueous solutions can be thought to result from the attempts to match the protein structure with the rapidly evolving structure of the water dipole networks. However, there is a significant conceptual difference between the slaving by a liquid matrix and the one by a non-liquid matrix. In fact, the time scale of the structural relaxation of the liquid matrix is much faster than that of the protein dynamics. Accordingly, the energy of interaction for a given conformation between the protein and its surrounding will rapidly flicker among a large number of values, so that the actual interaction energy assumes the role of a free energy because of the required thermodynamic averaging over fast variables (*San Biagio et al., 1998*). The configurational landscape, introduced in paragraph 1.2.2 ("*Protein Folding and Configurational Landscape*"), contains therefore entropic and enthalpic contributions from both the protein and the solvent and its minima represent hence the global system. This implies the intrinsic coupling between the dynamics of the solute and that of the solvent. The above argumentation helps to rationalize, at a molecular level, how the addition of organic co-solvents to the solution medium affects the structural properties of macromolecular solutions and modifies the protein conformational equilibrium and function (*Von Hippel et al., 1965; Cordone et al., 1981*), by perturbing the hydrogen bond network surrounding the protein.

3.3 – Water-Dependent Domains in Myoglobin-Sugar-Water Glasses

Recent results of Small-angle X-ray scattering measurements (*Longo et al., 2010*) on carboxymyoglobin (MbCO) embedded in amorphous saccharide matrices, shown in figure 3.5, suggest that, at low hydration level, the protein influences the structural properties of trehalose matrices, but it has a limited effect in sucrose matrices. In fact, structures of the order of about 150 Å have been observed in protein-trehalose systems. These large structures are absent in protein-sucrose systems and in absence of protein.
Furthermore, it is worth noticing that the shape and the size of the protein do not appear to be affected by the presence of sugars in both cases.
In addition, nanocrystals are observed in dry binary sucrose-water systems, since the most stable crystalline form of this saccharide is anhydrous (*Mathlouthi and Genotelle, 1998*). This agrees with infrared spectroscopy results on binary sugar-water samples (*Giuffrida et al., 2004*), which show that the residual water content after exhaustive drying is lower in sucrose than in trehalose.

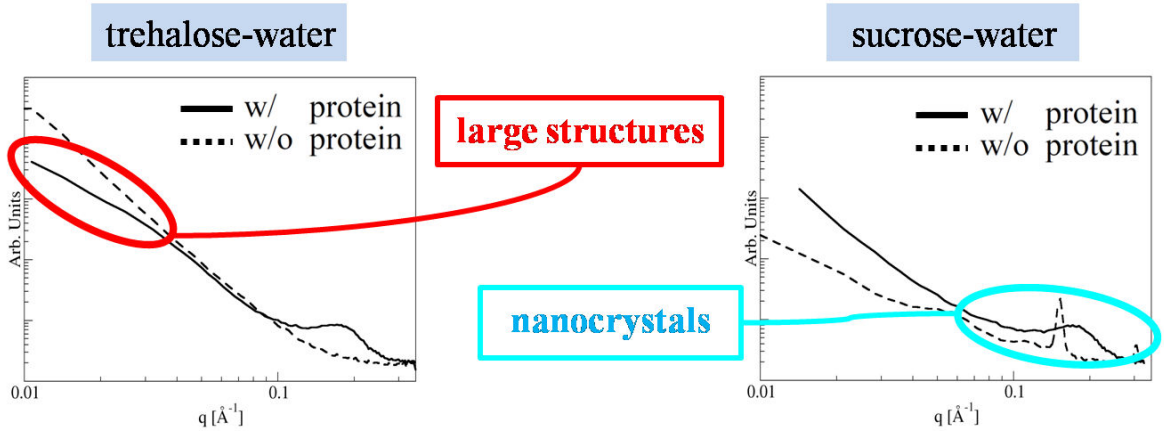

Figure 3.5 – SAXS data on amorphous samples containing trehalose (left panel) or sucrose (right panel), in absence/presence of carboxymyioglobin. The dotted lines refer to the absence of protein.

The large structures observed in myoglobin-trehalose-water systems, but not in myoglobin-sucrose-water systems, have been supposed to be **protein-poor regions** in a protein-rich background. Besides, some measurements on hydrated samples showed that the dimension of these structures increases with the sample hydration, as well as the average distance among the protein molecule.
The large inhomogeneities observed in myoglobin-trehalose-water systems, but not in myoglobin-sucrose-systems, agree with the higher trehalose capability, compared to sucrose, to perturb the hydrogen bond network around the protein in dry conditions, as suggested by infrared spectroscopy measurements (*Giuffrida et al., 2004*).
The following figure gives a pictorial view of the model above described.

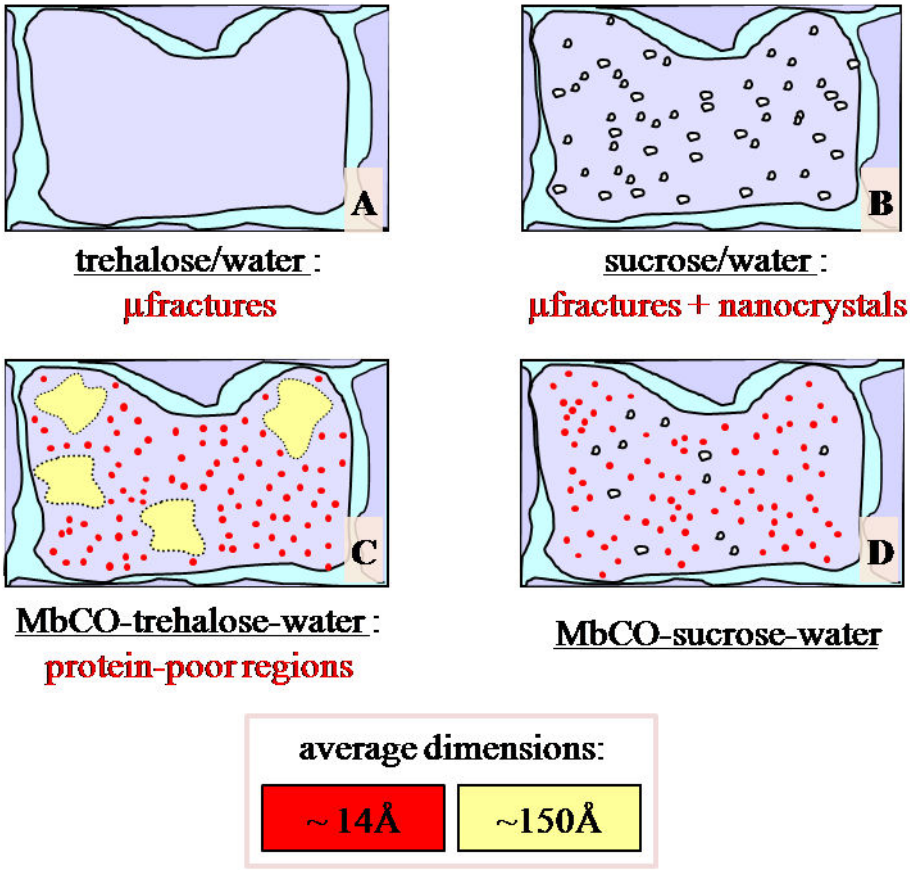

Figure 3.6 – Pictorial view of carboxymyoglobin-sugar-water samples from SAXS results. (A) Trehalose-water: homogeneous domains are sketched in violet. (B) Sucrose-water: small nanocrystals are sketched in white. (C) Protein-trehalose-water and (D) Sucrose-protein-water: proteins are sketched in red, protein-poor trehalose-water domains are sketched in yellow and sucrose nanocrystals are sketched in white.

According to the proposed model, water-rich domains might play an important role in the anhydrobiosis state of some organisms, discussed in paragraph 1.4 ("*Biopreservation by Sugars*"), thanks to their buffer effect that would organize the restoration of the cellular activity, when the atmospheric humidity changes, thus preventing the damages caused by a random, sudden hydration. In fact, in the absence of these domains rehydration would imply a random distribution of the incoming water, and so a random restarting of the biological functions in the various compartments of the cell. On the contrary, the buffer effect of the protein-poor domains would lead to the diffusion of the water only when it is sufficient to spread throughout the cell, thus restoring the vegetative cycles.

3.4 – Materials and Methods

This section gives a detailed account of the procedure that has been followed to carry out the study of amorphous saccharide systems containing myoglobin.
First, the sample preparation protocol is described. Afterward the experimental setup is illustrated. The final part deals with the analysis of the data.

3.4.1 – Sample Preparation

The samples studied by X-Ray Scattering were prepared with the chemical products listed in table 3.2.

Table 3.2 – Main chemical products used to prepare the samples.

	product
myoglobin	Sigma M0630 (lot.: 064K7006)
trehalose	Hayashibara TREHA
sucrose	Fluka 84097
maltose	Sigma M9171
lactose	Galeno Lattosio Monoidrato
sodium dithionite	Sigma 71699

Trehalose (from Hayashibara Shoji inc., Okayama, Japan) and lactose (from Galeno srl, Comeana, Italy) have been used after recrystallization from aqueous solutions. Sucrose (from Fluka GmbH, Buchs, Switzerland) and the other products (from Sigma, St. Louis, MO, USA), have been used without further purification.
For the **samples containing protein**, ferric myoglobin ($5\ \text{mM}$) was dissolved in a phosphate buffer ($\text{pH}\ 7, 20\ \text{mM}$), then the disaccharide ($200\ \text{mM}$) was added to the solution. For the preparation of the samples with carboxymyoglobin (MbCO), the solutions were equilibrated with CO and Fe^{3+} of myoglobin heme was reduced to Fe^{2+} by anaerobic addition of $100\ \text{mM}$ sodium dithionite ($Na_2S_2O_4$).
The **samples without protein**, used as references, were prepared from $400\ \text{mM}$ disaccharide solutions with the same buffer used for the samples with protein. The difference in the saccharide concentration between the solution without protein and that with protein is aimed at giving roughly the same mass, and so a similar thickness, to the resulting solid samples. Besides, the reference samples were prepared both with and without sodium dithionite, in order to preserve ionic strength and cosolute composition among the samples.
The final amorphous samples were obtained through the following procedure. First, the above solutions were deposited in the sample holder, that was a stainless steel stick with thickness of $1.5\ \text{mm}$ and with truncated cone holes, each having an average diameter of $2.5\ \text{mm}$, as shown in figure 3.7. In particular, small drops of $30\ \mu\text{L}$ were poured into the holes, hanging at the bottom of the stick thanks to the surface tension of the solution. Then the whole sample holder, containing several samples, was initially dried for 8 h in a silica gel desiccator, under either CO atmosphere, for the samples with MbCO, or N_2 atmosphere, for the other types of

samples. The samples were further dried under vacuum for 15 h at 80 °C. This high temperature treatment avoids microcrystallization, although small nanocrystals might form even under such conditions, as already observed in some sucrose samples without protein (*Longo, 2010*). Finally, the sample holder was transferred to the measurement chamber, where it was left under vacuum at room temperature for a couple of hours.
The figure 3.7 gives a pictorial view of the samples and the sample holder before and after desiccation.

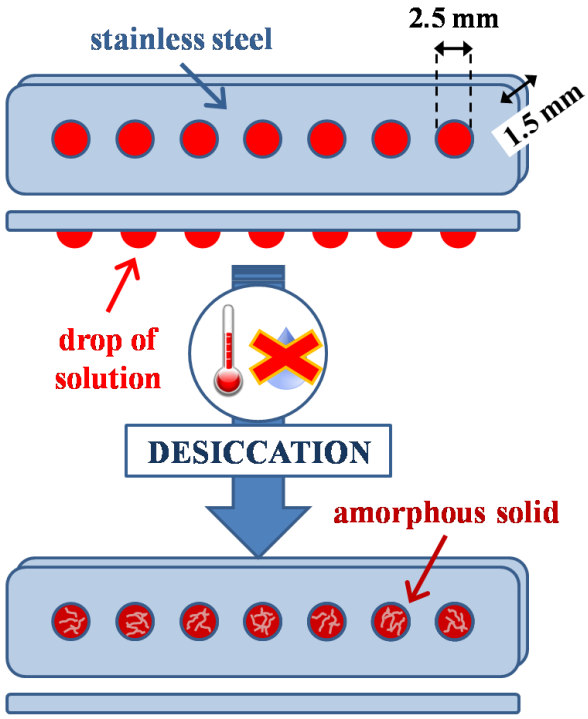

Figure 3.7 – Pictorial view of the SAXS samples and sample holder before and after desiccation.

The final amount of water in the final amorphous solids was evaluated by measuring the weight of analogously prepared samples at the end of the drying procedure. The amount of water measured for all the different samples was comparable, with no sizable difference due to the content of dithionite or the type of sugar. As already shown (*Giuffrida et al., 2006*), the water contents in different sugar matrices are not strictly the same, even if a fixed preparation protocol is used. However, comparisons of experimental results at strict equal water content would be meaningless because of the different water binding properties of the saccharides.

3.4.2 – Experimental Setup

The SAXS measurements were performed at room temperature by means of an X-ray diffractometer (Bruker Nanostar C), equipped with a graphite monochromator using $Cu\ K_\alpha$ radiation and a point collimation geometry with a bidimensional detector (HighStar Multiwire Detector). The wavelenght produced by the X-ray source was $\lambda = 1.54$ Å, characteristic of the Cu target. Dynamic vacuum was maintained in the sample chamber during all the measurements.

A preliminary scan was performed for each sample, in order to optimize the X-ray transmission because of the small dimension of the beam, namely $0{,}1\ mm^2$, and the non-homogeneity of the samples. SAXS data were then recorded in the q range $0.015 - 0.3$ Å. For each system 4 samples were analyzed, and the results were averaged.

The experimental setup for SAXS measurements is shown in the following figure.

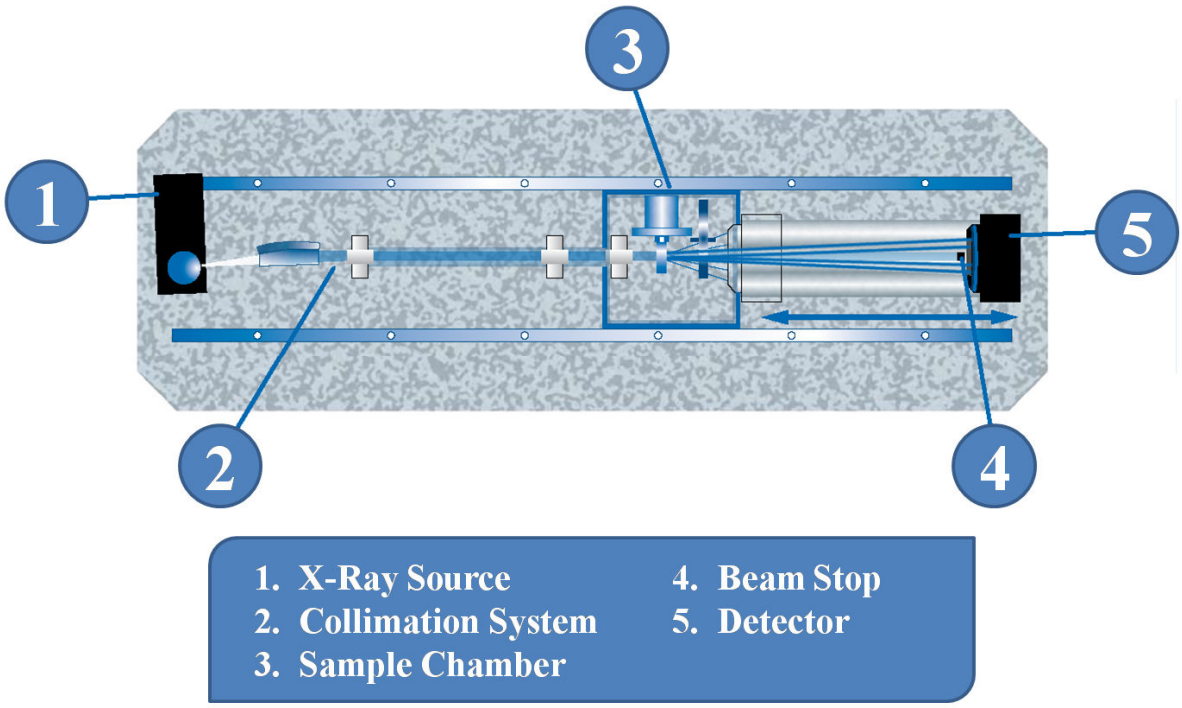

Figure 3.8 – Experimental setup for SAXS measurements.

3.4.3 – Data Analysis

The scattering curves of all the protein-sugar-water samples were fitted assuming additivity of the single contributions from the different structures in the samples to the total scattering signal.

The contribution to the scattered intensity due to the protein molecules has been determined by making use of the decoupling approximation (2.23) in the reciprocal Fourier space:

$$I(q) \propto P(q) \cdot S(q) \tag{2.23}$$

where the form factor $P(q)$ accounts for the extension of particles in space, and the structure factor $S(q)$ identifies the lattice on which the particles are disposed.

The protein molecules have been supposed to be hard spherical particles, so as to consider Rayleigh's form factor (2.14) $I_{Rayleigh}(q)$ and Percus-Yevick's structure factor (2.24) $I_{Percus-Yevick}(q)$.

In addition to this, there is another contribution to the total scattered intensity because of the microscopic cracking of the samples during desiccation, which gave rise to large fractures with a size larger than 500 Å. In the range of interest, where $q > 0.01$ Å^{-1}, the behaviour of the scattered intensity due to the fractures follows Porod's law (2.20), according to which $I(q) \propto q^{-4}$.

Therefore, the samples with metmyoglobin, which do not contain sodium dithionite, have been analyzed according to the following fitting function:

$$I(q) = I_{Rayleigh}(q) \cdot I_{Percus-Yevick}(q) + I_{Porod}(q) + k \tag{3.1}$$

where k is a background constant.

The following figure shows a typical scattering curve of a metmyoglobin-sugar-water sample with the fitting curve and the single contributions to it.

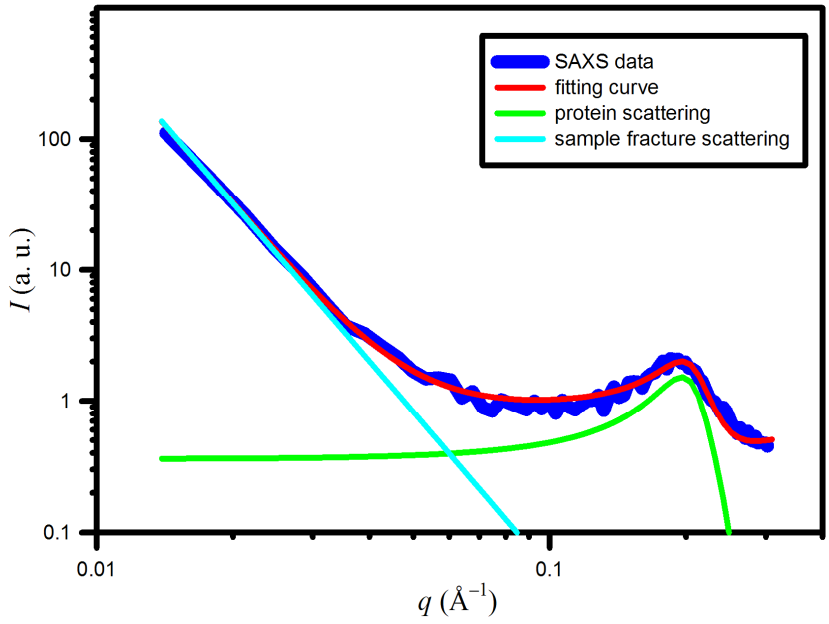

Figure 3.9 – SAXS data (blue line) of a metmyoglobin-trehalose-water glass, fitting curve (red line) and the single contributions to it: the protein scattering (green line) and the sample fracture scattering (cyan line).

As regard to the samples with carboxymyoglobin, which also contained sodium dithionite, the occurrence of a broad feature in the scattered curves made it necessary to add a third term in the previous fitting function, because the curves do not obey to Porod's law (2.20) in the q range $0.01-0.1$ Å^{-1}:

$$I'(q) = I_{Rayleigh}(q) \cdot I_{Percus-Yevick}(q) + I_{Porod}(q) + I_{Debye}(q) + k \qquad (3.2)$$

where $I_{Debye}(q)$ is Debye's function (2.15), which refers to domains randomly distributed on a background with a different electronic density. The presence of this large inhomogeneities will be discussed in the next paragraph.

Figure 3.10 shows a typical scattering curve of a carboxymyoglobin-sugar-water sample with the fitting curve and the single contributions to it.

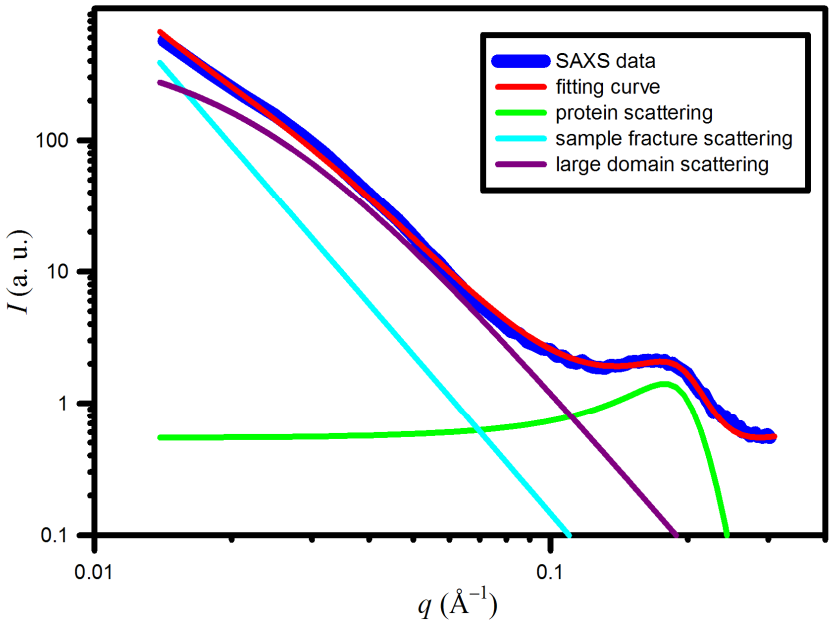

Figure 3.10 – SAXS data (blue line) of a carboxymyoglobin-trehalose-water glass, fitting curve (red line) and the single contributions to it: the protein scattering (green line), the sample fracture scattering (cyan line) and the large domain scattering (purple line).

3.5 – Results and Discussion

SAXS measurements were performed on sugar-water glasses, used as references, and on myoglobin-sugar-water glasses. The samples were prepared as reported in paragraph 3.4.1 ("*Sample Preparation*"). The glasses with carboxymyoglobin and the corresponding references without protein contained also sodium dithionite ($Na_2S_2O_4$), that was essential for the first ones in order to properly bind the CO to the heme prosthetic group of the protein.

The scattering curves of all the samples containing myoglobin show a peak in the q range $0.1-0.3$ Å due to the scattering of the protein. The data analysis, performed as described in the previous paragraph, provided an estimation for the gyration radius of myoglobin, which resulted:

$$R_{gyr,Mb} = (14{,}5 \pm 1{,}5) \text{ Å}$$

for all the different type of samples, in agreement with the value reported in literature (*Ibel and Stuhrmann, 1975*).

3.5.1 – Sugar-Water Glasses

Preliminary measurements were performed on sugar-water glasses, so to be used as references. The samples were prepared both with and without sodium dithionite ($Na_2S_2O_4$), which was also present in the samples containing carboxymioglobin in order to properly prepare the samples, as to preserve ionic strength and cosolute composition among the samples.

The scattering of the sugar glasses, shown in figure 3.11 (non-reducing disaccharides) and in figure 3.12 (reducing disaccharides), seems not to be affected by the presence of sodium dithionite. The salt is likely to be homogenously distributed in the sugar matrix, so that there are not structures to be revealed. Furthermore, the double logarithm plots of $I(q)$ versus q exhibit a q^{-4} trend for all the different type of samples. According to Porod's law (2.20), this trend is due to the presence of domains with homogeneous electronic density, the size of which is larger than 500 Å. Such domains are supposed to originate from the microscopic cracking of the samples during desiccation in the preparation procedure.

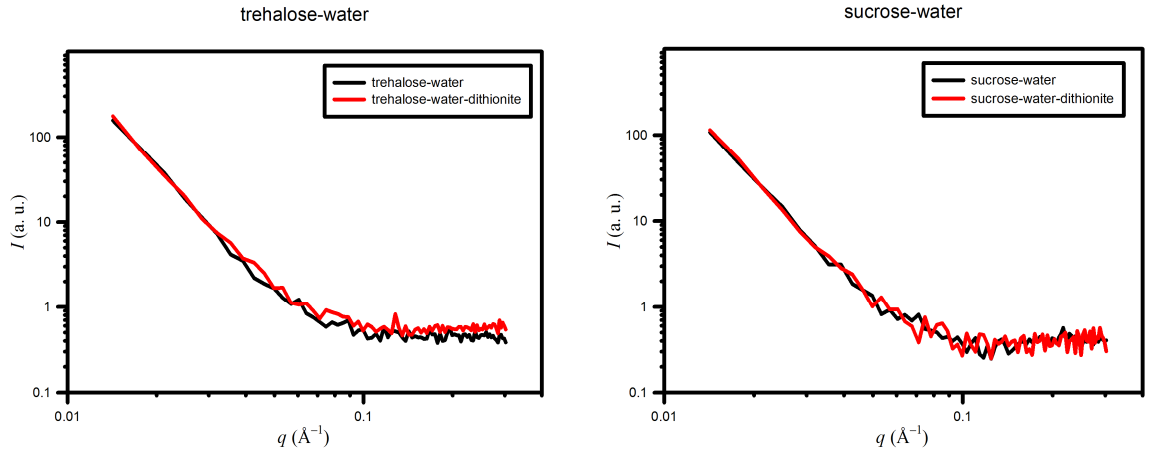

Figure 3.11 – SAXS data of sugar-water glasses for the non-reducing disaccharides, trehalose and sucrose, without (black line) and with (red line) sodium dithionite.

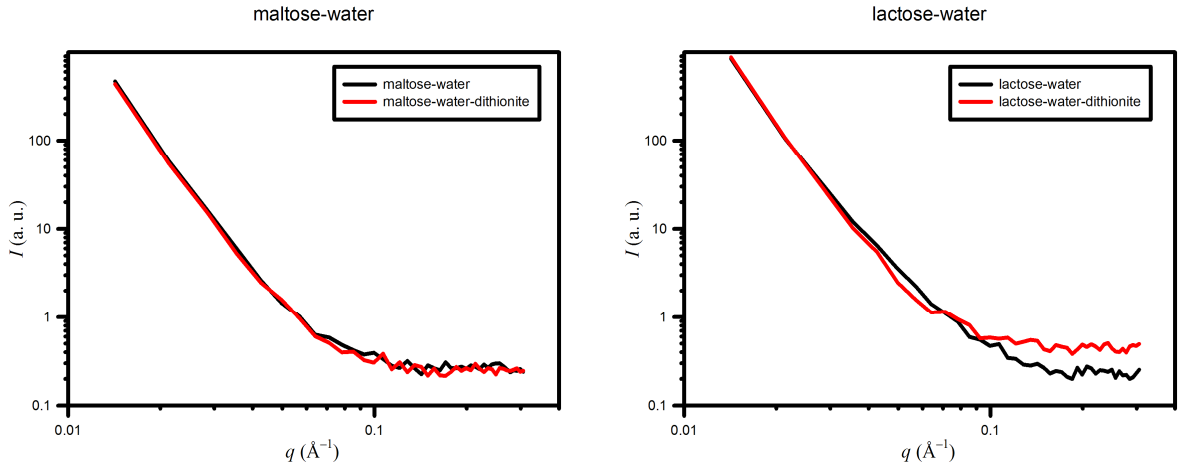

Figure 3.12 – SAXS data of sugar-water glasses for the reducing disaccharides, maltose and lactose, without (black line) and with (red line) sodium dithionite.

The plot of the scattered intensity of some sucrose glasses, one of which is reported in figure 3.13, shows a small crystallographic peak at $q \approx 0.15$ Å^{-1}. According to what has been previously reported (*Longo et al., 2010*), this peak has been attributed to the formation of nanocrystals in the samples, the size of which is about 35 Å. In fact, nanocrystallization is expected in sucrose glasses after desiccation to extreme dryness, since the most stable crystalline form of this saccharide is anhydrous (*Mathlouthi and Genotelle, 1998*). Furthermore, this agrees with infrared spectroscopy results (*Giuffrida et al., 2004*), which show that the residual water content after exhaustive drying is lower in sucrose glasses than in glasses composed by other sugars.

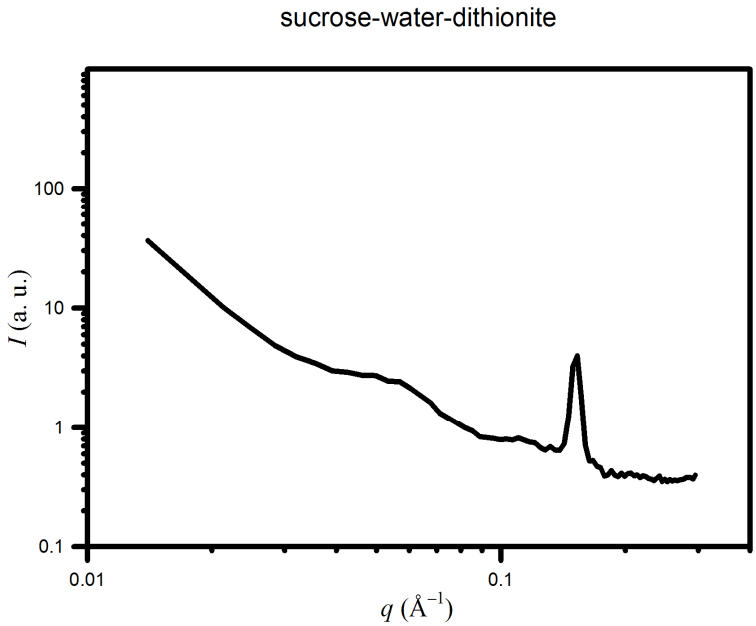

Figure 3.13 – SAXS data of a sucrose-water-dithionite glass extremely dehydrated. A crystallographic peak is present at $q \approx 0.15$ Å^{-1}, suggesting the local nanocrystallization of the samples.

3.5.2 – Metmyoglobin-Sugar-Water Glasses

The scattering curves of metmyoglobin embedded in different saccharide matrices are reported in figure 3.14, as well as the reference curves of the related amorphous systems without the protein.

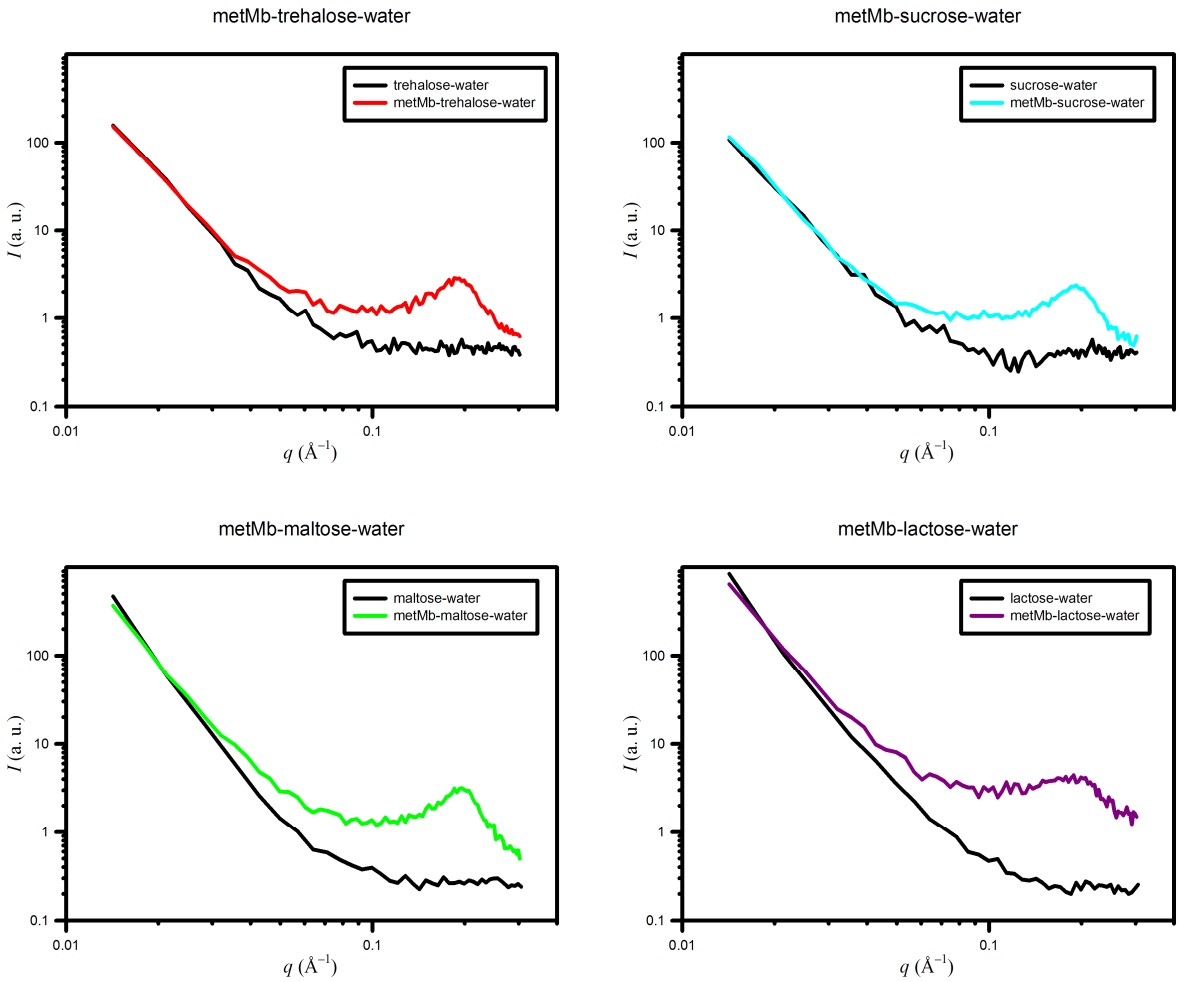

Figure 3.14 – SAXS data of metmyoglobin embedded in different saccharide matrices: trehalose (red), sucrose (cyan), maltose (green) and lactose (purple). The reference curves (black lines) of the saccharide amorphous systems without the protein are also plotted.

The scattering curves containing metmyoglobin were fitted by means of function (3.1), as discussed in paragraph 3.4.3 ("*Data Analysis*"):

$$I(q) = I_{Rayleigh}(q) \cdot I_{Percus-Yevick}(q) + I_{Porod}(q) + k \qquad (3.1)$$

In table 3.3 the average distance among the myoglobin molecules d and their occupied volume fraction η obtained from the data fitting are reported.

Table 3.3 – Average distance among the met-myoglobin molecules d and their occupied volume fraction η obtained from the data fitting.

	Mb –	trehalose	sucrose	maltose	lactose
***d* (Å)**	**metMb**	30.5±0.2	30.7±0.2	30.3±0.2	29.1±0.3
η	**metMb**	0.386±0.009	0.378±0.010	0.383±0.012	0.313±0.018

The **protein-protein average distance** d is slightly affected by the type of sugar matrix, except for the lactose matrix, for which d is remarkably lower. This can be explained with the occurrence of a partial phase separation of lactose, as already reported in literature (*Lam et al., 2002*), which would reduce the available sugar interacting with the protein and, consequently, the protein-protein separation.

As regards the observed **protein volume fractions** η, it must be pointed out that they are strictly affected by the protein conformation, since they represent the volume fraction of the supposedly spherical molecules of myoglobin in the Percus-Yevick approximation. The lower η value observed for metmyoglobin embedded in lactose matrices, compared to those observed in the other type of sugar matrices, could be due to the presence of denaturated myoglobin in the sample. In fact, denaturated proteins generally unfold, therefore ceasing to contribute to the scattering structure factor as hard spherical particles. This agrees with the partial phase separation supposed to happen in metmyoglobin-lactose samples, which would reduce the amount of sugar available per protein, thus weakening the lactose protective effect against protein denaturation.

The connection between the observed η values and the protein conformation has been confirmed by measuring some samples of carboxymyoglobin embedded in trehalose matrices, prepared by heating the initial solution at 80 °C before the desiccation procedure. Trehalose is not able to totally prevent the protein denaturation in solution, hence the samples obtained with this procedure contained denatured myoglobin. The data fitting provided very low η values, from 0.15 to 0, for all the samples with denaturated protein.

The scattering curves of one sample containing denaturated myoglobin is shown in figure 3.15 (grey line), as well as the scattering curve (red line) of a sample containing the same material, but with myoglobin in a folded state. The unfolded protein peak at $q \approx 0.18$ Å^{-1} is considerably flattener than the folded protein peak.

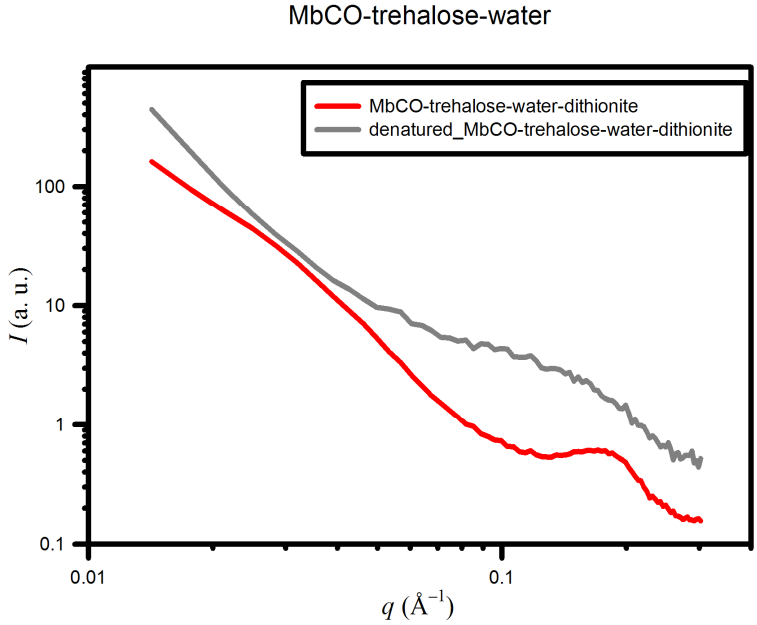

Figure 3.15 – Scattering curves of folded carboxymyoglobin (red line) and unfolded carboxymyoglobin (grey line), embedded in trehalose glass.

3.5.3 – Carboxymyoglobin-Sugar-Water Glasses

In addition to metmyoglobin-sugar-water amorphous samples, SAXS studies were also carried out on carboxymyoglobin embedded in sugar glasses. These latter differ from the former for the molecule bound to the myoglobin heme group, which is CO instead of H_2O, and for the presence of sodium dithionite in the matrix, which was essential for binding the CO to the protein heme group.
The reference samples for carboxymyoglobin-sugar-water glasses contained sodium dithionite, unlike those for metmyoglobin-sugar-water, as to preserve ionic strength and cosolute composition.
The scattering curves of carboxymyoglobin embedded in different saccharide matrices are reported in figure 3.16, as well as the reference curves of the related amorphous systems without the protein.

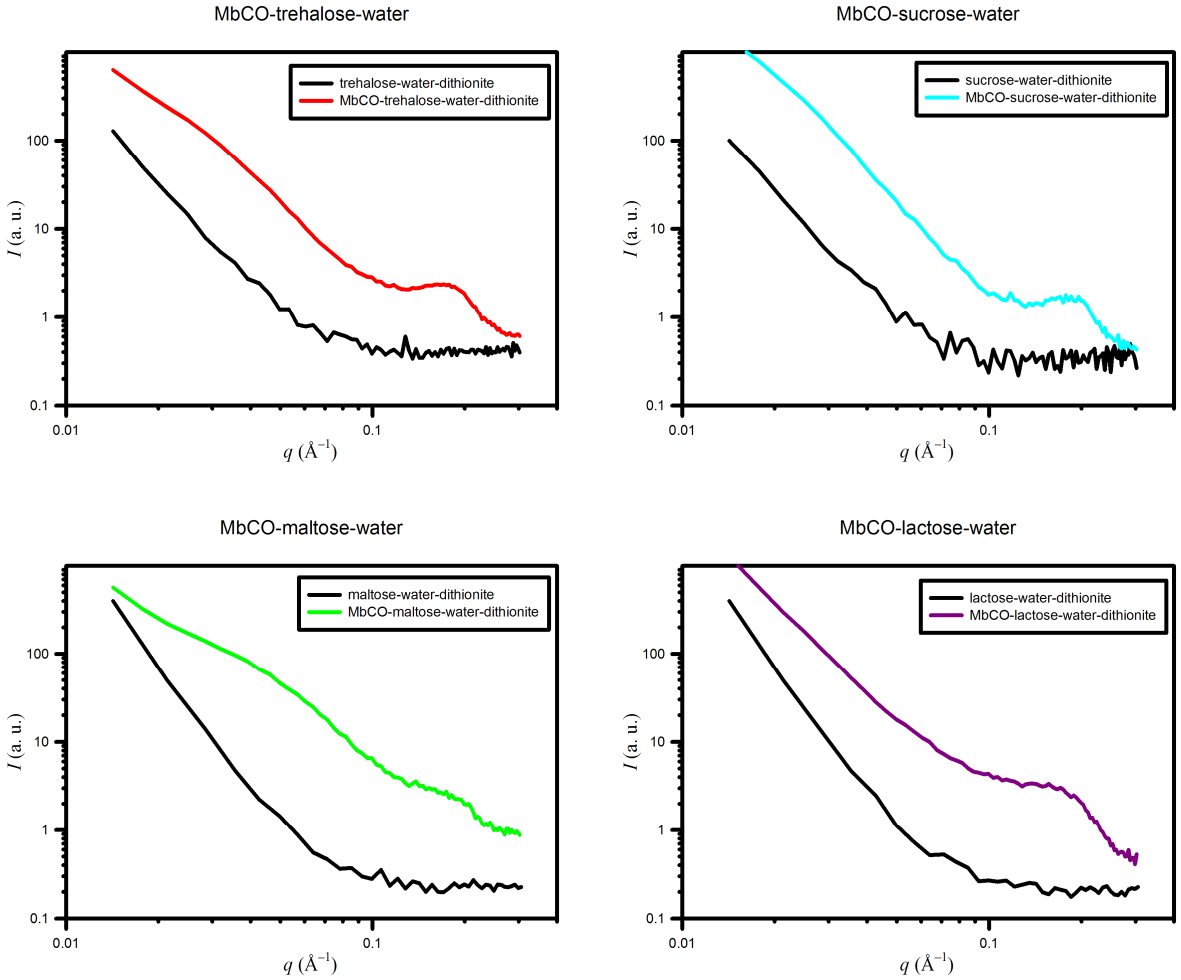

Figure 3.16 – SAXS data of carboxymyoglobin embedded in different saccharide matrices: trehalose (red), sucrose (cyan), maltose (green) and lactose (purple). The reference curves (black lines) of the saccharide amorphous systems without the protein are also plotted.

The scattering curves containing carboxymyoglobin were fitted by means of function (3.2), as discussed in paragraph 3.4.3 ("*Data Analysis*"):

$$I'(q) = I_{Rayleigh}(q) \cdot I_{Percus-Yevick}(q) + I_{Porod}(q) + I_{Debye}(q) + k \qquad (3.2)$$

In the following table the average distance among the carboxy-myoglobin molecules d and their occupied volume fraction η obtained from the data fitting are reported. The table reports also d and η values for the samples containing metmyoglobin, which has been previously shown and discussed, for a comparison.

Table 3.4 – Average distance among the carboxy-myoglobin molecules d and their occupied volume fraction η obtained from the data fitting. Data of met-myoglobin are also reported for comparison.

	Mb –	trehalose	sucrose	maltose	lactose
d (Å)	metMb	30.5 ± 0.2	30.7 ± 0.2	30.3 ± 0.2	29.1 ± 0.3
	MbCO	31.4 ± 0.4	30.9 ± 0.4	31.2 ± 0.6	29.4 ± 0.2
η	metMb	0.386 ± 0.009	0.378 ± 0.010	0.383 ± 0.012	0.313 ± 0.018
	MbCO	0.337 ± 0.012	0.307 ± 0.009	0.270 ± 0.018	0.201 ± 0.016

* In some sugar-containing samples was not possible to determine any large inhomogeneity in the range of $0.01 - 0.1$ Å^{-1}, because Porod's law was enough to fit the data in that range.

Although the **protein-protein average distances** d are slightly smaller for metMb samples than for MbCO ones, the difference is too small to draw a conclusion on the protein behaviour. As it happens for the metMb samples, the protein molecules seem to be closer to each other in lactose matrix than in other saccharide matrices, and this can be explained with the occurrence of a partial phase separation of lactose, as already reported in literature (*Lam et al., 2002*).
Concerning the **protein volume fraction** η, a significant difference exists between MbCO samples and metMb samples. In particular, η values of the former are consistently lower than the latter and they strictly depend on the type of sugar. This difference has been attributed to the presence of sodium dithionite in the MbCO samples. In fact, sodium dithionite is a chemically active substance, both oxidizing and reducing, that can alter or interfere with the protein. Taking into account that η values determined by means of Percus-Yevick approximation reflect the protein folding state, as previously discussed, the observation of lower η values in matrices with sodium dithionite can therefore be interpreted as a partial degradation of myoglobin. The comparison of the protein volume fraction in the different saccharide matrices puts the sugars in the following order in respect to their capability of preserve the biological matter:

trehalose > sucrose > maltose > lactose

thus confirming that trehalose is the most efficient bio-preserver (*Crowe, 2007; Jain et al., 2008*). At variance, maltose and lactose have a lower protective effect, as already reported in literature (*Giuffrida et al., 2006; Bellavia et al., 2009*), probably because they are reducing sugars and, for this reason, they can undergo Maillard's reaction with the protein, as discussed in paragraph 1.3.4 ("*Maillard's*

Reaction"). As regard to lactose matrices, another explanation for the low protein volume fraction is the possible phase separation, also occourring in metMb-lactose samples, due to the specific sugar, which would reduce the amount of sugar available per protein, thus weakening the lactose protective effect against protein denaturation.

It must be pointed out that the effects on η are due only to the presence ofsodium dithionite, and not to the different binding state of myoglobin. As a confirm of this attribution, the analysis of the scattering curves of samples containing metmyoglobin and sodium dithionite gave results very similar to those of MbCO samples. The following figure shows the scattering curve of two myoglobin samples containing trehalose and sodium dithionite, but with myoglobin in a different binding state, namely with H_2O (blue line) and with CO (red line) bound to the heme group.

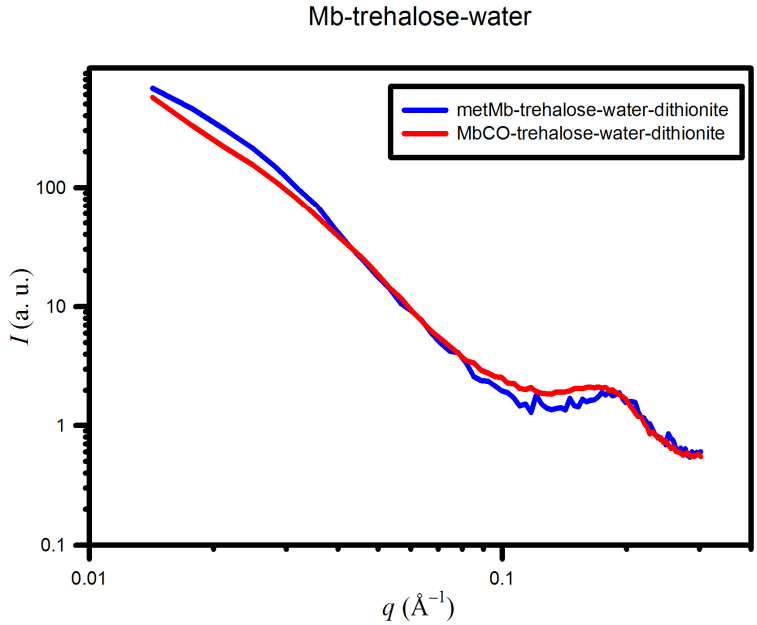

Figure 3.17 – SAXS data of two myoglobin samples containing trehalose and sodium dithionite, but with myoglobin in a different binding state, namely with H_2O (blue line) and with CO (red line) bound to the heme group.

In addition to the protein signal and to the scattering of the fractures of the samples, the scattering curves of MbCO samples show a further signal in the q range $0.01-0.1$ Å^{-1}. This explains the third term in the fitting function (3.2), namely Debye's function (2.15), which accounts for a random distribution of **inhomogeneities** of average dimension D on a background with different electronic density. This domains have not been observed in metMb samples, since in this case Porod's law (2.20) was enough to fit the data in the q range $0.01-0.1$ Å^{-1}.

Table 3.5 reports the average dimension D of the inhomogeneities observed in MbCO samples, which seems to strictly depend on the specific saccharide matrix. Some sucrose-containing samples did not show any inhomogeneity, so that they

have not been taken into consideration when averaging. The error associated to the dimension of the domains is quite large, probably because of the intrinsic uncertainty of the water content in the samples.

Table 3.5 – Average dimension D of large inhomogeneities obtained from the data fitting.

	Mb –	**trehalose**	**sucrose**	**maltose**	**lactose**
***D* (Å)**	**MbCO**	150 ± 10	$180 \pm 20^{*}$	60 ± 10	120 ± 20

* In some sucrose-containing samples was not possible to determine any large inhomogeneity in the range of $0.01 - 0.1$ Å^{-1}, because Porod's law was enough to fit the data in that range.

These data support the belief that the occurrence of inhomogeneities in highly concentrated protein-saccharide dry systems is a general phenomenon. In particular, the different behaviour of the four disaccharides can be related to the different strength of interaction with water, hence their solubility in water, although with some discrepancies (*Lammert et al., 1998*).
Following what previously reported (*Longo et al., 2010*), these inhomogeneities have been attributed to local differences in the protein/sugar ratio. In particular, because of the high protein concentration in the samples, protein-rich regions constitute the SAXS background, on which protein-poor domains are observable. These latter would be mainly constituted by sugar and water connected by extensive hydrogen bond networks, the bonds of which would be stronger than the weak ones involving the protein. This model agrees with the observed water dependence of the domains, specifically domain size increasing with water content (*Longo et al., 2010*), and with the absence of features in the scattering curves, which could indicate crystallization or aggregation.
The absence of the low-q signal in the scattering curves related to the presence of protein-poor regions for the metMb samples, which do not contain sodium dithionite, can be explained by making use of the above model. The protein-poor domains are more polar than the background, due to the higher concentration of saccharide molecules, so water seems to be preferentially bound in this regions. The same argumentation may apply to ionic molecules and salts, such as sodium dithionite: they should preferentially concentrate in the most polar regions of the sample, namely in the protein-poor inhomogeneities. This would result in the increase of the electronic density contrast with the background, because of the presence of sulphur atoms in the salt, leading to the signal magnification of the inhomogeneities, which would not be otherwise detectable. An alternative explanation could be that the high salt concentration promotes the nucleation of inhomogeneities, thus stabilizing the protein-poor areas. Presently, it is not possible to solve this issue on the basis of the current data. Additional measurements of samples containing different salts or small cosolutes would give valuable hints on the nature of this protein-poor domains.
As regard to the different average dimension of the protein-poor domains for the different saccharides, this difference might originate from variations in the composition of the domains. The inhomogeneities observed in MbCO-maltose

glasses are the smallest ones, with an average size of just twice the protein size. Experimental (*Giuffrida et al., 2006*) and simulative (*Lerbret et al., 2005*) studies on analogous maltose systems at molecular scale support the belief that maltose-water systems are less homogeneous than trehalose-water and sucrose-water systems, because of the greater tendency of maltose molecules to form clusters, favouring more sugar-sugar bonds than the other disaccharides, thus with a lower capability to perturb the hydrogen bond water network.

At variance, the case of sucrose glasses, in which the inhomogeneities appear to be the largest, is more complex. In some samples it is not possible to identify any inhomogeneity, while in others they are clearly present with an average dimension of 180 Å, which is very close to the resolution limit of the instrument. This could suggest that inhomogeneities are always present in MbCO-sucrose glasses, but if they are much larger than 180 Å they cannot be detected, as their contribution to the scattered intensity falls out of the range of measurement. Taking into account that the size of these domains increases with the water content, as already observed (*Longo et al., 2010*), larger domains correspond to more hydrated samples. As a result of this, the observation of inhomogeneities also in MbCO-sucrose systems, which has not been previously reported in literature, could be therefore due to the specific sample preparation. In fact, the water content of a glass obtained by desiccating a drop of solution placed into a hole is lower than that of a glass obtained from a drop placed on a kapton sheet, as in the first case the sample can lose water by means of two free surfaces.

Moreover, the amplitude of Debye's function obtained from the fitting of the MbCO-sucrose data, $A_S = 1700$, is much lower than the value obtained from MbCO-trehalose data, $A_T = 2900$. It can be therefore suggested that either the concentration of inhomogeneities is low or there is little contrast with the background. This contributes to the difficulty in the identification of the inhomogeneities in MbCO-sucrose systems.

Lastly, the dimensions of the inhomogeneities in MbCO-trehalose and in MbCO-lactose systems lay between the dimensions of the other two protein-saccharide systems.

Therefore, the occurrence and the nature of the observed inhomogeneities lie on the different hydrogen bonding properties of the four disaccharides.

3.5.4 – Conclusions

Small-Angle X-Ray Scattering measurements have been performed on samples of myoglobin embedded in low hydrated saccharide matrices. The study has been carried out on four different sugars: trehalose, sucrose, maltose and lactose. The protein has been studied both in the oxidized metMb form and in the reduced MbCO form. In the systems containing the protein in the latter form, sodium dithionite was added to keep the protein in the reduced state.

The results indicate that the protein embedded in the saccharide matrices maintains approximately the same properties in all the sugars but in lactose, the protective effect of which is reduced by the occurrence of a phase separation.

The comparison of the protein volume fractions in the different saccharide matrices, which reflect the protein folding state, confirms the best protective effect of trehalose against protein damaging and, conversely, the poor performance of the reducing disaccharides, maltose and lactose.

Local inhomogeneities have been detected in all the samples containing sodium dithionite. The size and the composition of these inhomogeneities depend on the specific sugar matrix. In particular, their dimensions range from almost sugar-only clusters in maltose to large low-contrasted regions in sucrose.

In conclusion, the results show that the previously proposed mechanism for trehalose bioprotection, which is based on the water-buffering action (*Cesàro et al., 2006; Kilburn et al., 2006; Longo et al., 2010*) that would contrast moisture variations, can be extended to other sugars, and it is likely to be a general behaviour.

4 – Thermal Aggregation of Bovine Serum Albumin in Sugar Solutions

This chapter deals with thermal aggregation of bovine serum albumin (BSA) in trehalose and sucrose solutions. Static and dynamic light scattering measurements have been performed in order to study the effects of the two disaccharides on the first steps of the thermal aggregation of BSA in aqueous solutions at two protein concentrations (1 mg/ml and 30 mg/ml) at increasing sugar/water ratio. The results show that sugars modify the early stages of protein aggregation mainly via thermodynamic changes of solvent without any direct, specific sugar-protein interactions. This agrees with current hypotheses on sugar action in protein solutions (*Timasheff, 1998; Timasheff, 2002; Shimizu and Matubayasi, 2006*). Furthermore, these findings are strengthen by the linear correlation observed between the characteristic temperature of the aggregation process and the glass transition temperature of the water-sugar solvent.

The work here discussed has been submitted as an article to the Journal of Physical Chemistry:
M. Panzica, A. Emanuele, L. Cordone, "*Thermal Aggregation of Bovine Serum Albumin in Trehalose and Sucrose Solutions*", submitted to J. Phys. Chem. B

4.1 – Bovine Serum Albumin

Bovine serum albumin (BSA) is a bovine blood protein, formed by 585 amino acids and having a molecular weight of about 67 kDa (*Brown, 1975).*
As the most abundant protein in the circulatory system of bovines, with typical blood concentration of 50 mg/ml, it carries a large number of substances, thanks to 6 specific binding sites (*Carter and Ho, 1994*), and chiefly contributes to blood pH and colloid osmotic pressure (*Figge et al., 1991*). Because of their availability, low cost, stability and unusual ligand-binding properties, serum albumins are among the most extensively studied and applied proteins in biochemistry.
The secondary **structure** of bovine serum albumin at pH 7.0 is mainly constituted by alpha-helices (67%) and random coils (30%) (*Takeda et al., 1989*). As regard to its tertiary structure, hydrodynamics measurements suggest an ellipsoidal shape (*Squire et al., 1968*), while X-Ray diffraction measurements show a more compact, heart-like shape (*Carter et al., 1989*). In particular, at room temperature 17 disulphide bonds ensure some rigidity within each sub-domain, but allow significant modification in the shape and size of the protein under different external conditions. Moreover, at neutral pH the disulphide bridges are buried and not exposed to the solvent (*Katchalski et al., 1957*). In addition to it, a unique free

cystein (Cys-34) and two tryptophans (Trp-134 and Trp-214) are present within hydrophobic pockets in different parts of the protein (*Moriyama et al., 1996*). The structure of the normal shape of BSA is shown in figure 4.1.

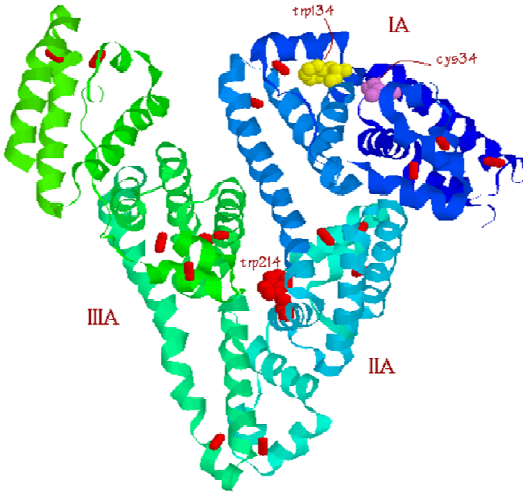

Figure 4.1 – Ribbon structure of the normal form of bovine serum albumin.

Serum albumins undergo reversible conformational isomerization with changes in pH (*Bendedouch and Chen, 1983*), as shown in the following table.

Table 4.1 – Influence of pH on the conformation of serum albumins.

BSA form	E Expanded	F Fast	N Normal	B Basic	A Aged
% α-helix	35	45	55	48	48
pH of transition	2.7 ↔	4.3 ↔	8.0 ↔	10.0	

In the following figure two different ribbon diagrams of serum albumin, namely its N-form and its proposed F-form (*Carter and Ho, 1994*), are shown.

F-form **N-form**

Figure 4.2 – Ribbon diagrams of the F-form and the N-form of serum albumin.

The N–F transition involves the unfolding of domain III (*Kahn, 1986*). The F-form is characterized by a dramatic increase in viscosity, much lower solubility and a significant loss in the helical content (*Foster, 1960*). At pH values lower than 4 albumin undergoes another expansion with a loss of the intra-domain helices. This

expanded form is known as the E-form, which is characterized by an increased intrinsic viscosity and a rise in the hydrodynamic axial ratio from 4 to 9 (*Harrington et al., 1956*). At pH 9 albumin changes conformation to the basic form B. If solutions of albumin are maintained at pH 9 and low ionic strength at 3°C for about 3 days, another isomerization occurs, known as the A-form.
Structural and conformational changes of the native structure as a function of pH can be ascribed also to variations in the **net charge** of the protein, which corresponds to the number of charges accessible to binding and can have therefore implications on the electrostatic interactions among the different domains. As a consequence, it can be responsible of sovramolecular assemblies or complexes between the protein and its ligand (*Bendedouch and Chen, 1983*).
The following table reports the net charge of BSA at some pH values, where e is the elementary charge. It is worth to notice that above the isoelectric point, which is 4.7, the net charge is negative.

Table 4.2 – Net charge of BSA at some pH values in terms of the elementary charge e.

pH	net charge
2.4	$+65 \cdot e$
5.1	$-1 \cdot e$
5.4	$-9 \cdot e$
7.0	$-18 \cdot e$
7.4	$-20 \cdot e$
10.5	$-39 \cdot e$

The following table reports the main physical-chemical properties of bovine serum albumin.

Table 4.3 – Main physical-chemical properties of bovine serum albumin.

number of amino acids	585
dimensions of associated ellipsoid	$140 \times 40 \times 40$ Å^3
molecular weight	66 800 Da
λ_P **of the absorption peak**	279 nm
molar extincion coefficient at λ_P	$\varepsilon_{279\ \mathrm{nm}} = 43\ 820\ \mathrm{M^{-1}cm^{-1}}$
isoelectric point in water at 25 °C	4.7

4.2 – Thermal Aggregation of Bovine Serum Albumin

A strong interest is currently focused on protein self-association and deposit, usually consequent to conformational protein changes. It can occur even at low protein concentrations and is responsible for severe pathologies, such as systemic amyloidosis, Alzheimer's and Prion diseases and other neurodegenerative pathologies. Readily available proteins, such as bovine serum albumin, exhibiting at low concentration self-association properties related to conformational changes, offer very convenient model systems capable of providing insight into this class of problems.

Recent studies showed that high temperatures strongly affect secondary and tertiary structure of bovine serum albumin. As temperature increases, some molecular regions become accessible to new intermolecular interactions, producing soluble aggregates through disulphide and non-covalent bonds (*Honda et al., 2000*). Sometimes irreversible oligomeric structures are also formed (*Wetzel et al., 1980; San Biagio et al., 1996; Vaiana et al., 2004; Militello et al., 2004*).

It is well known that thermal aggregation of BSA in neutral to low acidic pH is the result of many intertwining processes (*San Biagio et al., 1996; San Biagio et al., 1999*): conformational and structural changes, protein-protein crosslinking and phase separation, as shown in figure 4.3.

These different mechanisms, due to both direct and solvent-induced forces (*Vaiana et al., 2001*), interact with multiple feedbacks, governed by the external conditions. In respect of this, the aggregation pathways depend on protein concentration, solvent pH, salt concentration and other variables (*Barone et al., 1995; Giancola et al., 1997; Veerman et al., 2003*).

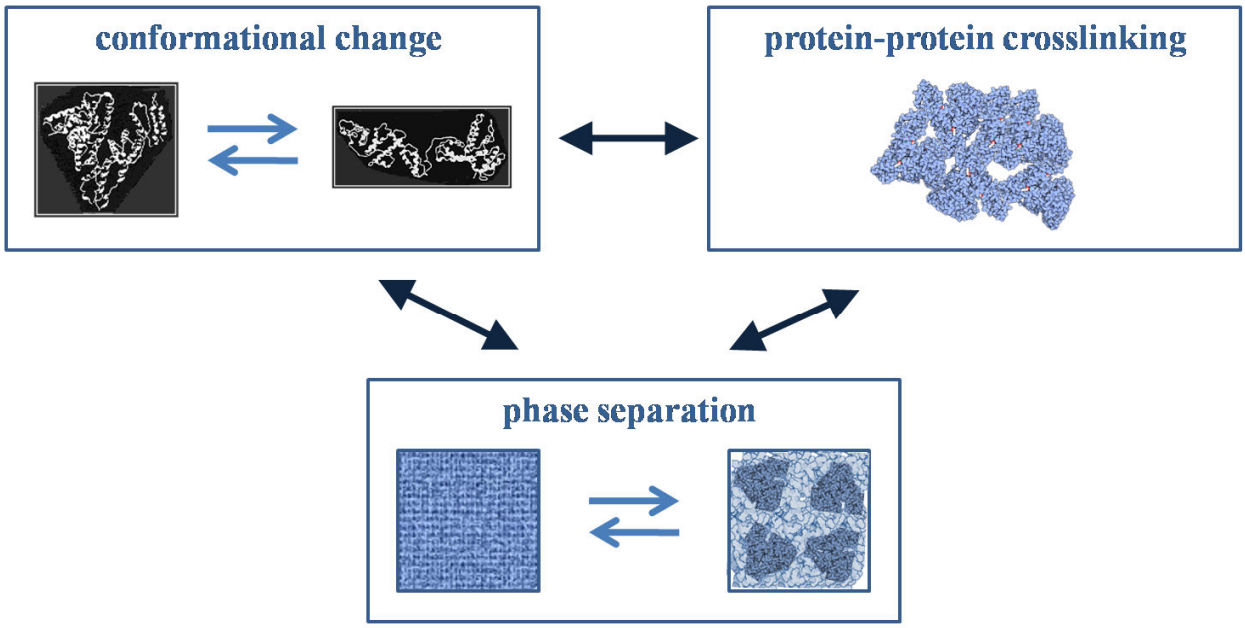

Figure 4.3 – Different mechanisms involved in the thermal aggregation process of bovine serum albumin: conformational change, protein-protein crosslinking and phase separation. These mechanisms are strictly interconnected and strongly affected by the external conditions.

Thermal aggregation of BSA at low concentrations is known to have conformational and structural changes as first and necessary step (*Vaiana et al., 2004*), which is followed by protein-protein crosslinking. On one hand, conformational changes imply the decrease of the alpha-helix and random coil contents in favor of beta-aggregate structures (*Militello et al., 2004, Barreca et al., 2010*).

On the other hand, protein-protein crosslinking is directly related to the solvent exposure of the free sulphydryl residue, Cys-34. In fact, it has been shown that blocking residue Cys-34 by binding it to other molecules, such as iodoacetamide, cysteine or glutathione, prevents the occurrence of albumin dimers (*Peters, 1985; Militello et al., 2004*).

It has also been found that BSA aggregation is reduced by the addition of sugars (*Barreca et al., 2010*), which stabilize BSA native structure. In fact, sugar addition in high concentrated BSA solution appears to increase protein stability against thermal denaturation (*Hédoux et al., 2009*), mainly altering the water around the protein. More generally, recent studies (*Timasheff, 1998; Timasheff, 2002; Shimizu and Matubayasi, 2006*) have shown that the stabilization of proteins by sugars is mainly due to solvent modifications, and not to direct, specific sugar-protein interactions. In particular, sugar molecules are preferentially excluded from the protein domain and entrap the residual water at the interface by glass formation, thus preserving the native solvation. Charged sites of the protein with high binding energy are essentially occupied only by water molecules, so that sugars can weakly bind the protein in low-energy sites.

4.3 – Thermal Denaturation of Bovine Serum Albumin in Sugar Matrices

The role of aqueous solvent as a global matrix in dried sample of protein solution has lately received new insights. Recent calorimetric studies on ternary systems of protein, water and sugar, aimed to investigate the effects of confinement and electrostatic interactions on the protein-matrix coupling, have been performed with several proteins differing in volume, surface and charge properties (*Bellavia et al., 2009; Bellavia et al., 2011*).

It has been shown that, at high to intermediate hydration, high protein concentrations increase the glass transition temperature T_{glass} of the encapsulating matrix, while no sizable effects are detected for low protein concentrations. This effect, which is larger for high molecular weight proteins and does not depend appreciably on the protein charge, has been attributed to the confinement experienced by the solvent.

On the contrary, at a very low hydration level, the lack of water leads to increasing protein-matrix interactions, which weaken the confinement effect. In this case, the sugar matrix would be coupled to the softer protein component through relatively weak hydrogen bonds, so depressing the glass transition temperature.

In addition to it, a linear correlation between the denaturation temperature T_{den} of the embedded protein and the glass transition temperature T_{glass} of the matrix is found, specific for each protein, at least in non-reducing disaccharides (trehalose and sucrose). In reducing disaccharide matrices (maltose and lactose) proteins undergo Maillard's reaction before thermal denaturation. The observed linear correlation indicates that the collective properties of the matrix, which regulate the glass transition, are linearly correlated to local properties that determine the denaturation of the protein.

4.4 – Materials and Methods

This section gives an account of the procedure that has been followed to carry out the study of the thermal denaturation of bovine serum albumin in saccharide solutions. Only non-reducing sugar solutions have been studied, to avoid Maillard's reaction with protein at high temperatures, that would occur in presence of reducing saccharides. First, the sample preparation protocol and the experimental setup are described. The final part deals with the analysis of the data.

4.4.1 – Sample Preparation

The samples studied by Light Scattering were prepared with the chemical products listed in table 4.4.

Table 4.4 – Main chemical products used to prepare the samples.

	product
serum bovine albumin (BSA)	Sigma A0281 (lots.: 100K7415, 020M7400V)
trehalose	Hayashibara TREHA
sucrose	Fluka 84097

BSA, purchased from Sigma, was used without further treatments. Aqueous solutions of 1 mg/ml (0.1% wt/wt, 0.073% vol/vol) were prepared in a phosphate buffer (pH 6.2, 100 mM) and filtered through 0.22 µm filters. The protein concentration was determined measuring the absorption intensity at 279 nm. To ensure the full dissolution of the lyophilized protein, addition of sugars was done using the following procedure. Solutions of protein in buffer were prepared at appropriate concentration values.
Sugar were added in due amounts to obtain the required protein and sugar concentration values. Solutions were gently stirred for 30 minutes to assure complete dissolution of sugar. The samples with sugar were first filtered through 0.8 µm filters, then through 0.22 µm filters, in order to avoid the obstruction of the finest filters due to the presence of large objects. Finally, the protein concentration was spectroscopically checked. Sugar has been added to the samples substituting approximately 20 molecules of water with 1 of sugar, in order to alter only the solvent part of the solution; so doing, the ratio of the protein mass over total sample mass remained unaltered. This choice appears to be in agreement with previous results (*Timasheff, 1998; Timasheff, 2002; Shimizu and Matubayasi, 2006*), showing that the protein stabilization by sugars is mainly due to solvent modifications, and not to direct, specific sugar-protein interactions. In particular, sugar molecules are preferentially excluded from the protein domain and entrap the residual water at the interface by glass formation, thus preserving the native solvation. Charged sites of the protein with high binding energy are essentially occupied only by water molecules, so that sugars can weakly bind the protein in low-energy sites. Other consequences of keeping the protein mass fraction constant will be discussed in the Results and Discussion section.

4.4.2 – Experimental Setup and Data Analysis

Light scattering experiments were performed on a Brookhaven BI-SM200 goniometer, at fixed 90° scattering angle, using a duplicated Nd-doped solid state laser, $\lambda = 532$ nm. The intensity of the scattered light (SLS) was measured using an APD detector (Perkin Elmer Optoelectronics SPCMAQR-14), while the intensity autocorrelation function (DLS) was obtained by using a 1024 channels correlator (Correlator.com Flex-01D). The time resolution of the experimental setup is 100 ns.

The analysis of correlation functions were performed as a sum of single exponential decays. In fact, in the simple case of scattering by a monodisperse spherical specie of Brownian diffusing particles, the intensity correlation function has the mathematical form of a single exponential decay, as already discussed in paragraph 2.2.2 ("*Diffusion Coefficients from Dynamic Light Scattering*"):

$$G^{(2)}(\tau) = 1 + Ae^{-2Dq^2\tau} \tag{2.40}$$

where D represents the diffusion coefficient of the particles and q the scattering vector.

Fitting of correlation functions by means of (2.40) provides the correlation time:

$$\tau_S = \frac{1}{Dq^2} \tag{4.1}$$

By using Stokes-Einstein's relation, the hydrodynamic radius R_{hyd} of such particles can be obtained by means of equation (2.41):

$$R_{hyd} = \frac{k_B T}{6\pi\eta D} \tag{2.41}$$

where k_B is the Boltzmann constant, and η is the viscosity of the solvent at the absolute temperature T.

When Brownian spherical particles of different radii are present, the photon correlation function can be analyzed in terms of sum of independent exponential decays relative to each particle species, as discussed in paragraph 2.2.2 ("*Diffusion Coefficients from Dynamic Light Scattering*"). Intensity of scattered light depends on the product of particle mass and mass concentration of the scattering particles. Thus it allows to monitor the amount of species diffusing in the sample. The fraction of intensity scattered by each species can be determined by the analysis of intensity correlation functions. For this reasons, for solutions with added sugar the analysis of light scattering data were performed by using three exponential decays: two were chosen as in the analysis of the sample without sugar, while the third one was added to take into account the diffusion of the sugar molecules and its variations with temperature. It is worth noticing that with this choice only amplitudes of two exponentials and the size of only one of the diffusion coefficients were free in fitting procedure.

In addition to it, the compactness of the diffusing objects has been determined by using the radius estimation R from DLS, as described in paragraph 2.2.3 ("*Fractal Dimension of Diffusing Species*"). In particular, in a process in which R changes, it

is possible to estimate the fractal dimension δ by the slope of the graph $\log I$ as a function of $\log R$ (*Schärtl, 2007*).

Circular dichroism measurements were performed on a Jasco J-715 Spectropolarimeter, equipped with a Jasco PTC-348WI peltier type temperature control system.

Temperature scans were done at 1.3 °C/h for light scattering experiment and at 2.0 °C/h for circular dichroism measurements; it was not possible to perform similar temperature scans with the two different experimental techniques, because of the experimental setup, which did not allow this.

4.5 – Results and Discussion

Thermal aggregation of bovine serum albumin (BSA) in saccharide solutions has been studied by means of static and dynamic light scattering measurements. Only non-reducing sugars (trehalose and sucrose) have been taken into account, because at high temperatures BSA undergoes Maillard's reaction in presence of reducing sugars. Additional Circular Dichroism (CD) measurements were performed, in order to further confirm the proposed model. The samples were prepared as reported in paragraph 4.4.1 ("*Sample Preparation*").
Preliminarily, experiments on BSA solutions without sugar were performed during temperature scans. In these experiments the time autocorrelation function of the scattered intensity was analyzed as a sum of two exponential decays, one of which with a large fixed radius to account for dust, as discussed in paragraph 4.4.2 ("*Experimental Setup and Data Analysis*").
In Figure 4.4 typical results are reported. In the left panel the scattered intensity of the species with free time decay is reported as a function of temperature, normalized with respect to its initial value. In the right panel the corresponding radius is reported.

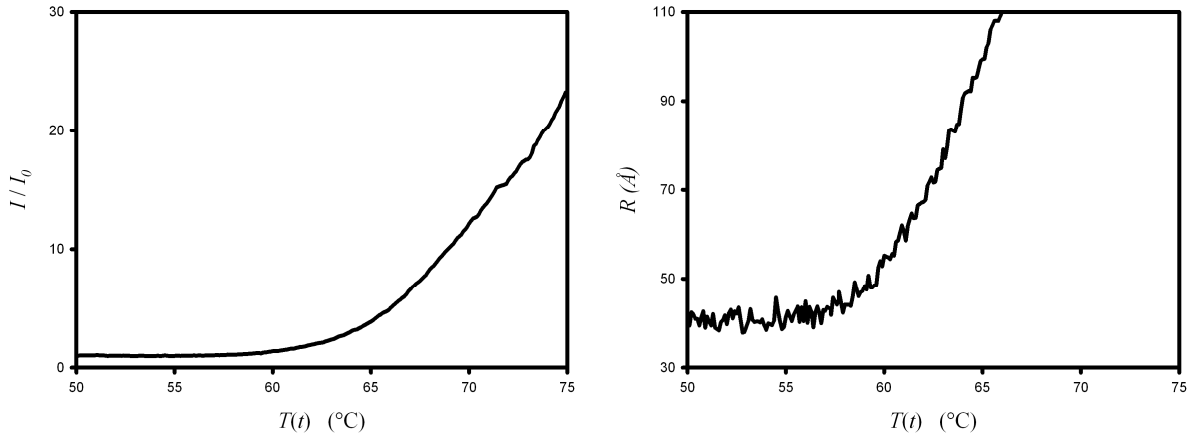

Figure 4.4 – Scattering intensity (left panel), normalized with respects to its initial value, and hydrodynamic radius (right panel) of BSA in solutions at 0.1% w/w concentration in absence of sugar.

Figure 4.4 shows an increase of the scattering intensity starting around 58 °C and an increase of the corresponding radius of a diffusing object having the initial value of its radius equal to the protein size as measured at 20°C. Thus, such simultaneous increase of radius and intensity has been ascribed to the progressive formation of protein aggregates, as already reported in literature (*Vaiana et al., 2004*). At the end of the experiments samples appeared macroscopically liquid.

4.5.1 – Light Scattering on 0.1% BSA in Sugar Solutions

Static and dynamic light scattering measurements during temperature scans were performed on BSA solution containing sugar at various saccharide concentrations, namely from 10 to 40% w/w. As previously specified, only non-reducing sugars (trehalose and sucrose) have been taken into account, since at high temperatures the protein undergoes Maillard's reaction in the presence of reducing sugars.
For solutions with added sugar, the analysis of light scattering data were performed by using three exponential decays: two were chosen as in the analysis of the sample without sugar, while the third one was added to take into account the diffusion of the sugar molecules and its variations with temperature. It is worth noticing that with this choice only amplitudes of two exponentials and the size of only one of the decay times were free in fitting procedure.
Figure 4.5 shows the normalized intensity scattered by the species with free diffusion coefficient in trehalose (left panel) and in sucrose (right panel) solutions, as well as the data relative to BSA solution without sugar for comparison. The shown data are limited up to a value of 5, because the aim of the experiment is focused only in the initial stages of the aggregation process, which it is well known to depend on conformational changes of the protein (*Vaiana et al., 2004*).

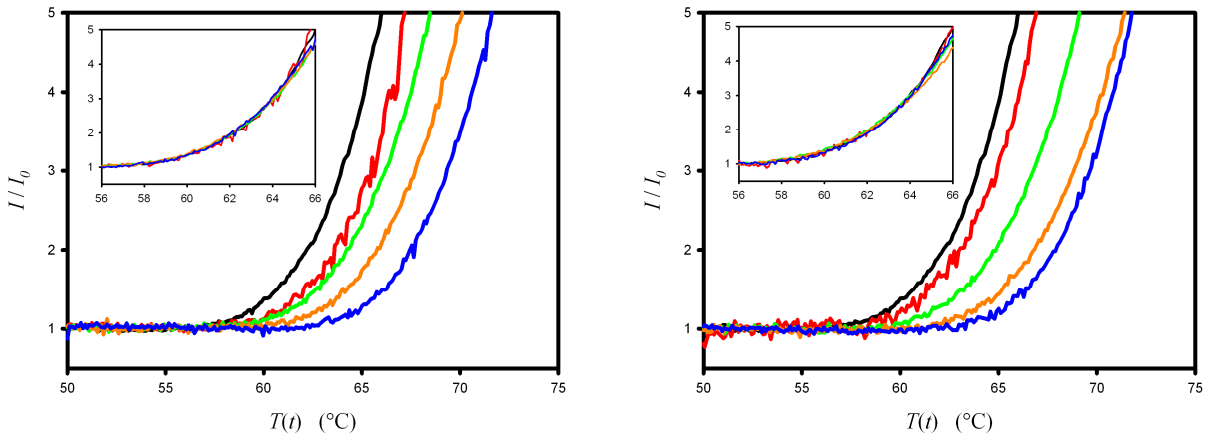

Figure 4.5 – Scattering intensity, normalized with respect to its initial value, of BSA in solutions at 0.1% w/w concentration in trehalose (left panel) and sucrose (right panel). The total sugar w/w percent in solution is: 0% (black lines), 10% (red lines), 20% (green lines), 30% (orange lines) and 40 % (blue lines). In the inset temperature-shifted curves are reported, showing a good superposition.

All the curves appear of identical shape, but shifted towards higher temperatures as the saccharide concentration is increased, with different shifts for the two saccharides. Shifted curves are shown in the inset of each panel. They evidence a coincidence over a temperature interval of about 10 °C, a relevant interval for changes to occur. It is worth noticing that the scattered intensity due to the aggregating species, reported in Figure 4.5, is the most relevant contribution to the total intensity of scattered light.
As stated in paragraph 4.2 ("*Thermal Aggregation of Bovine Serum Albumin*"), it is thought that the sugar influence on the protein thermal aggregation depends only

on the solvent modifications induced by the saccharide, and not on direct, specific sugar-protein interactions (*Timasheff, 1998; Timasheff, 2002; Shimizu and Matubayasi, 2006*). As reported in literature (*Vaiana et al., 2004*), the first steps of BSA aggregation at low protein concentrations are (a) conformational and structural changes of protein followed by (b) protein-protein crosslinking, in which Cys-34 plays a key role (*Peters, 1985; Militello et al., 2004*). The (a) step depends on general protein-solvent interactions, which may be affected by the presence of sugars. However the initial crosslinking, step (b), in absence of a direct sugar-protein interaction, should not be modified by sugar addition. Results showed in figure 4.5 are in agreement with these hypotheses, that is, the shape of intensity curves does not change by the addition of sugar.

As an additional check, measurements have been performed, in which rather than the weighted protein concentration the molar protein concentration has been kept constant. At 40% w/w of sugar concentration, the measured protein molar concentration corresponds to 0.12 w/w protein concentration in sample without sugar. Results, reported in figure 4.6, show scattering curves of BSA in buffer at 0.1% w/w (black line) and 0.12% w/w (red line) concentration, which are not superimposable by means of simple translations, even at early stages of aggregation. This confirms the hypothesis that initial protein crosslinking process, namely the second step of BSA aggregation, depends on the protein mass content of the solution.

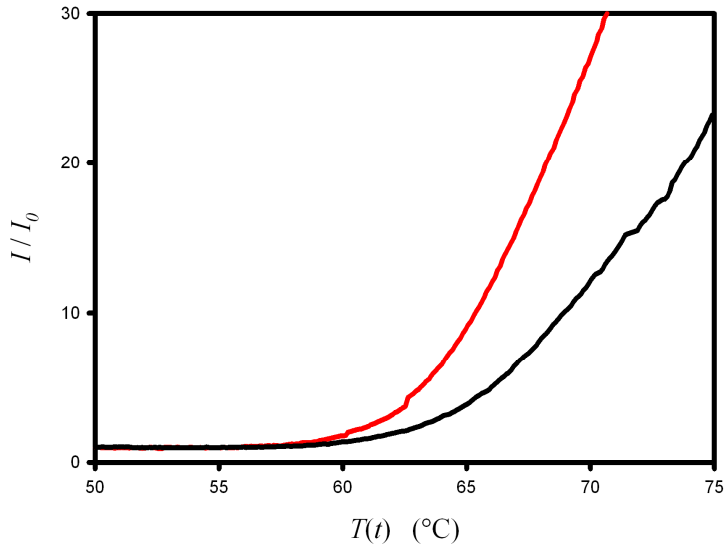

Figure 4.6 – Scattering intensity, normalized with respect to its initial value, of BSA in buffer at 0.1% w/w (black line) and 0.12% w/w (red line) concentration.

However, subsequent growth of aggregates is the result of an intertwining of crosslinking, conformational/structural changes and demixing of the solution (*San Biagio et al., 1996; San Biagio et al., 1999*). In this respect, superposition of curves of figure 4.5 is not obtained for higher temperatures and later times.

Figure 4.7 shows the temperature dependence of the hydrodynamic radii of aggregating specie obtained using Stokes-Einstein's relation (2.38). Data are plotted with the same colour code as in Figure 4.5.

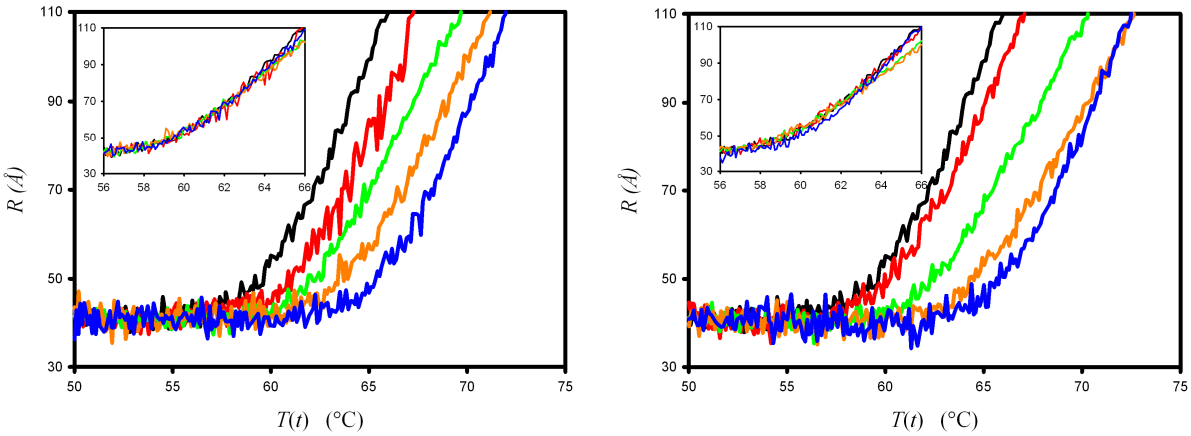

Figure 4.7 – Hydrodynamic radius of BSA in solutions at 0.1% w/w concentration in trehalose (left panel) and sucrose (right panel). The total sugar w/w percent in solution is: 0% (black lines), 10% (red lines), 20% (green lines), 30% (orange lines) and 40 % (blue lines). In the inset temperature-shifted curves are reported, showing a good superposition.

All the radii have an initial value that corresponds to the hydrodynamic radius of the native protein and their values increase with temperature $T(t)$. This behaviour can be attributed to the initial free diffusion of protein in its monomeric state, followed by progressive formation of aggregates. This is confirmed by observing that the scattered intensity of this growing species is the main contribution to the total scattering intensity during all the temperature scans showed in figure 4.7. Values of radii appear to be shifted towards higher temperatures as the content in sugar increases. Shifted curves are shown in the inset of each panel. Temperature shifts are slightly larger than those used in figure 4.5.
The following table reports all the temperature shift values.

Table 4.5 – Temperature shifts for 0.1% BSA samples at a given sugar content. The error associated to each value is ±0.25 °C.

	BSA 0.1%			
% sugar (w/w)	**ΔT trehalose (°C)**		**ΔT sucrose (°C)**	
	(from *I*)	**(from *R*)**	**(from *I*)**	**(from *R*)**
10 %	1.40	1.40	0.90	0.90
20 %	2.10	2.80	2.80	3.20
30 %	3.70	4.40	4.70	5.40
40 %	5.40	5.90	5.60	6.50

The temperature shifts at low sugar concentration depend significantly on the sugar type. As mentioned above, there is no evidence of direct protein-sugar interactions, thus the observed behaviour should be due to solvent mediated sugar action. Indeed at low protein content conformational and structural changes precede and promote aggregation (*San Biagio et al., 1999; Vaiana et al., 2004*).

4.5.2 – Effects of Protein Concentration on Temperature Shifts

The results of measurements performed on 0.1% BSA solutions were in agreement with previous suggested hypotheses, according which in absence of direct protein-sugar interactions the observed behaviour should be due to solvent mediated sugar action. As already reported in literature (*San Biagio et al., 1999; Vaiana et al., 2004*), at low protein content conformational and structural changes precede and promote aggregation. In this respect, even if the overall aggregation process depends on solvent mediated protein-protein interactions, as suggested by Palma and co-workers (*Pullara et al., 2007*), it can be expected that at higher protein concentration temperature shifts should not significantly change. In order to investigate the effects of protein concentration, samples with BSA concentration of 3% w/w have been studied. This value is sufficiently high to evidence any significant effects of protein concentration on temperature shifts, but sufficiently low to deal with initially liquid solutions. Also, macroscopically self-supporting gels are formed in all solvent (water or water+sugar) environments at the end of the temperature scan.

Experimental results show that addition of sugar to protein solutions of 3% BSA causes temperature shifts similar to the ones observed at 0.1%. In figure 4.8 the normalized light scattering intensities of 3% BSA samples are reported with the same colour code as in Figure 4.7 and 4.5 and with suitable temperature shifts.

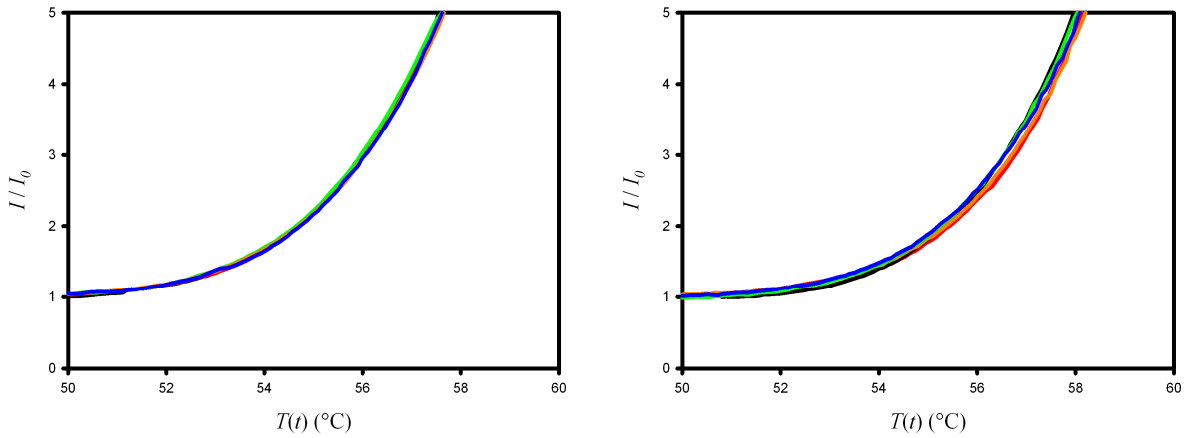

Figure 4.8 – Temperature-shifted scattering intensities, normalized with respects to their initial value, of BSA in solutions at 3% w/w concentration in trehalose (left panel) and sucrose (right panel). The total sugar w/w percent in solution is: 0% (black lines), 10% (red lines), 20% (green lines), 30% (orange lines) and 40 % (blue lines).

At variance with data at 0.1% of BSA, the same temperature shifts used for the intensity curves make also the hydrodynamic radii to overlap. The observed temperature shift values are reported in table 4.6, which also shows the temperature shifts for 0.1% BSA samples for comparison.

Table 4.6 – Temperature shifts for 0.1% BSA samples and for 3% BSA samples at a given sugar content. The error associated to each value is ±0.25 °C.

	BSA 0.1%				**BSA 3%**	
% sugar (w/w)	**Δ*T* trehalose (°C)**		**Δ*T* sucrose (°C)**		**Δ*T* trehalose (°C)**	**Δ*T* sucrose (°C)**
	(from *I*)	**(from *R*)**	**(from *I*)**	**(from *R*)**		
10 %	1.40	1.40	0.90	0.90	1.25	1.40
20 %	2.10	2.80	2.80	3.20	2.50	1.80
30 %	3.70	4.40	4.70	5.40	3.75	3.10
40 %	5.40	5.90	5.60	6.50	5.10	5.10

It is worth noting that the shape and position of the plotted curves are different from the corresponding ones at lower concentration (inset of figure 4.5). Also, at the end of the experiment and at variance with 0.1% BSA concentration, samples appeared macroscopically as translucent gels. This is in agreement with the expected dependence of aggregation on protein concentration. In fact, it is known that at low concentration (0.1% or less) only small free floating aggregates are formed, while firm self-supporting gel results from aggregation at higher concentration (*San Biagio et al., 1996*).

No significant dependence of temperature shifts on protein concentration have been observed in the case of trehalose, while smaller ones have been observed in the case of sucrose.

The different behavior between the two saccharides can be rationalized with reference to molecular dynamic simulations (*Cottone et al., 2005, Cottone, 2007*), which showed that two intramolecular hydrogen bonds can be formed in sucrose, at difference with trehalose, where a single intramolecular hydrogen bond can take place. This makes sucrose, on the average, more rigid than trehalose and less disposable to hydrogen bonding to its surroundings under conditions of low water. Accordingly, when the various components of the solution start competing for hydrogen bonding to residual water, the formation of internal hydrogen bonds may, in sucrose, break the continuity of the water sugar network, thus making the hydrogen bonds network in the protein surroundings softer than in trehalose and allowing aggregation to take place with different temperature shifts at different protein concentrations, as the competition for water of the protein and the sugar is changing. The formation of internal bonds in sucrose has also been invoked by Venturoli and coworkers (*Francia et al., 2008*) for rationalizing the sizable difference between trehalose and sucrose in hindering, under low water conditions, the internal dynamics of the reaction center of *Rhodobacter Sfaeroides*.

The above argument confirms that, at least in the initial stages of aggregation, the effects of sugar addition can be ascribed to alterations of thermodynamic properties of water-mediated interactions, namely to the different behaviour of the sugar-water solvent.

4.5.3 – Compactness of Aggregates

Aggregates resulted isotropic particles, as checked by measuring the depolarized scattering intensity. Also, as specified in paragraph 4.4.2 ("*Experimental Setup and Data Analysis*"), the packing of aggregates was evaluated by plotting the scattered intensity versus the corresponding radius in a log-log scale. In fact, the slopes of such plots can be related to the so-called fractal dimension of the scattering objects (*Schärtl, 2007*). In Figure 4.9 data for BSA solution without sugar are reported.

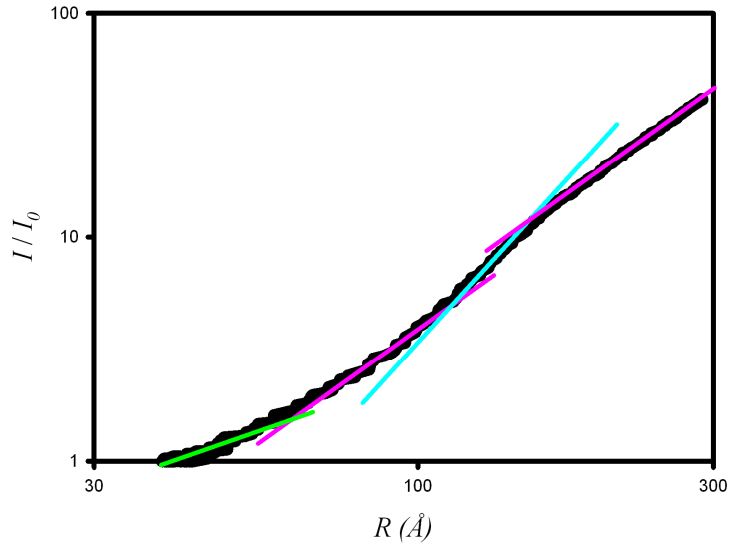

Figure 4.9 – Normalized scattering intensity as a function of the hydrodynamic radius of BSA (0.1 % w/w) in log-log scale for a sample, which does not contain any sugar. The slope of the curves can be related to the fractal-dimension of the BSA: 1.5 (green line), 2 (pink line) and 3 (cyan line).

Essentially, aggregate growth shows four distinct regions. An initial growth with very low compactness ($\delta \approx 1.5$) is followed by gaussian-coil like growth ($\delta \approx 2$). After this growth, a narrow interval of very compact growth ($\delta \approx 3$) precedes another gaussian-coil like growth. All this fractal dimension values but the initial one reveal the formation of relatively compact objects. This is in agreement with previous studies (*San Biagio et al., 1999; Militello et al., 2004*), evidencing a complex mechanism for the aggregation of BSA. The low value of fractal dimension of initial growth is compatible with the partial reversibility at the onset of protein aggregation, as observed in literature (*Vaiana et al., 2004*). Aggregates formed at higher concentration appear definitely less compact than those formed at low protein concentration. This agrees with the formation of a large network, typical of physical gels.
Figure 4.10 shows the normalized scattered intensity as a function of the mean hydrodynamic radius on a log-log scale for samples with and without sugar.

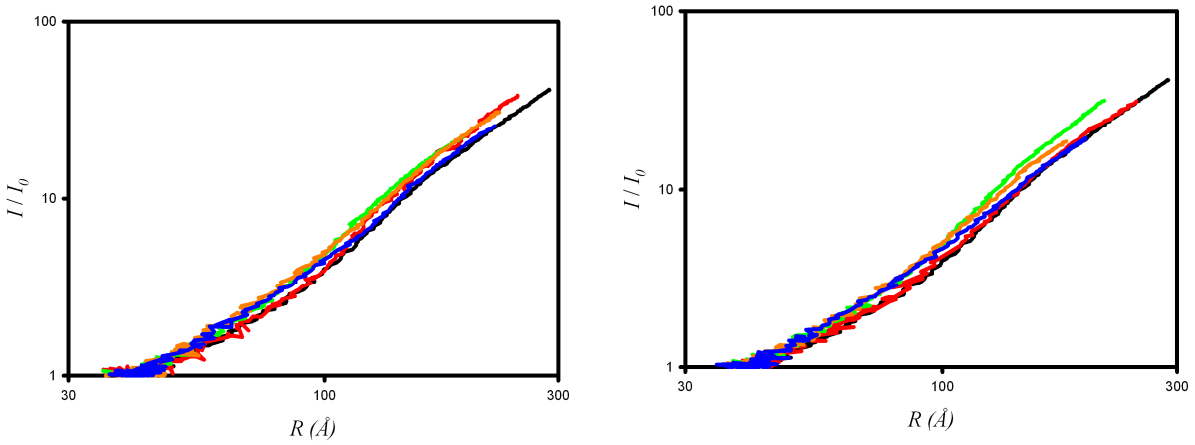

Figure 4.10 – Normalized scattering intensity as a function of the hydrodynamic radius of BSA (0.1 % w/w) in log-log scale for samples containing trehalose (left panel) and sucrose (right panel). The slope of the curves can be related to the fractal-dimension of the BSA aggregates. The total sugar w/w percent in solution is: 0% (black lines), 10% (red lines), 20% (green lines), 30% (orange lines) and 40 % (blue lines).

All the curves have similar shapes. The small differences in the normalized intensity, at fixed radius value, indicate a different concentration of scatterers. This data also confirm that sugar influences protein crosslinking through general solvent effects, and do not bind to protein, in line with the suggestion by Timasheff and coworkers (*Timasheff, 1998; Timasheff, 2002*), according which sugar molecules are preferentially excluded from the protein domain.

4.5.4 – Thermal Aggregation and Matrix Glass Transition

As mentioned in paragraph 4.3 ("*Thermal Denaturation of Bovine Serum Albumin in Sugar Matrices*"), a calorimetric study of ternary systems of protein, water and sugar has shown that at low water content (high protein concentration values) a linear correlation between the protein denaturation temperature T_{den} and the glass transition temperature T_{glass} of the same ternary protein solutions exists(*Bellavia et al., 2009; Bellavia et al., 2011*). This suggested that the change of stability of the protein (denaturation temperature) can be put in relation with a property of the solution (glass transition temperature), which is directly related to the statistical thermodynamics of the solution. Because the observed effects on BSA aggregation appear to depend on sugar addition only via the conformational and structural changes of the protein, it has been thought to compare the temperature shifts, reported in the previous paragraph of this thesis to the corresponding shifts of the glass transition temperature T_{glass} of the solvent.

The glass transition temperature depends on hydration according to Gordon-Taylor's expression (*Gordon and Taylor, 1952*):

$$T_{glass}(f) = \frac{T_{glass}(0) + k\, f \frac{M_{water}}{M_{sugar}} T_{glass}(+\infty)}{1 + k\, f \frac{M_{water}}{M_{sugar}}} \qquad (4.2)$$

where $T_{glass}(0)$ and $T_{glass}(+\infty)$ are, respectively, the glass transition temperatures of the system in the absence of water and of disaccharide, k is a parameter depending on the whole system, M_{water} and M_{sugar} are, respectively, the water and disaccharide molecular weights and f is the water/disaccharide molar ratio.

In the present work the protein concentrations are sufficiently low to justify the use, for comparison, of the T_{glass} values obtained by extrapolation of Gordon-Taylor expression with the parameters for binary water-sugar solutions calculated by Bellavia et al. (*Bellavia et al., 2009*) and reported in the following table.

Table 4.7 – Parameters of Gordon-Taylor expression for binary water-sugar systems, obtained from literature (*Bellavia et al., 2009*).

Sugar	$T_{glass}(0)$	$T_{glass}(+\infty)$	k
Trehalose	373 K	(297 ± 13) K	$4,9 \pm 0,4$
Sucrose	335 K	(283 ± 16) K	$4,6 \pm 0,3$

This choice appears also confirmed by the low dependence of T_{glass} on the protein concentration in our concentration range, as evidenced by the data of those Authors. Use of extrapolated data are needed because T_{glass} cannot be determined experimentally for solutions with water to sugar ratios as low as the ones used in

this work. In figure 4.11 the temperature shifts in table 4.6 are reported as a function of the glass transition temperature T_{glass}.

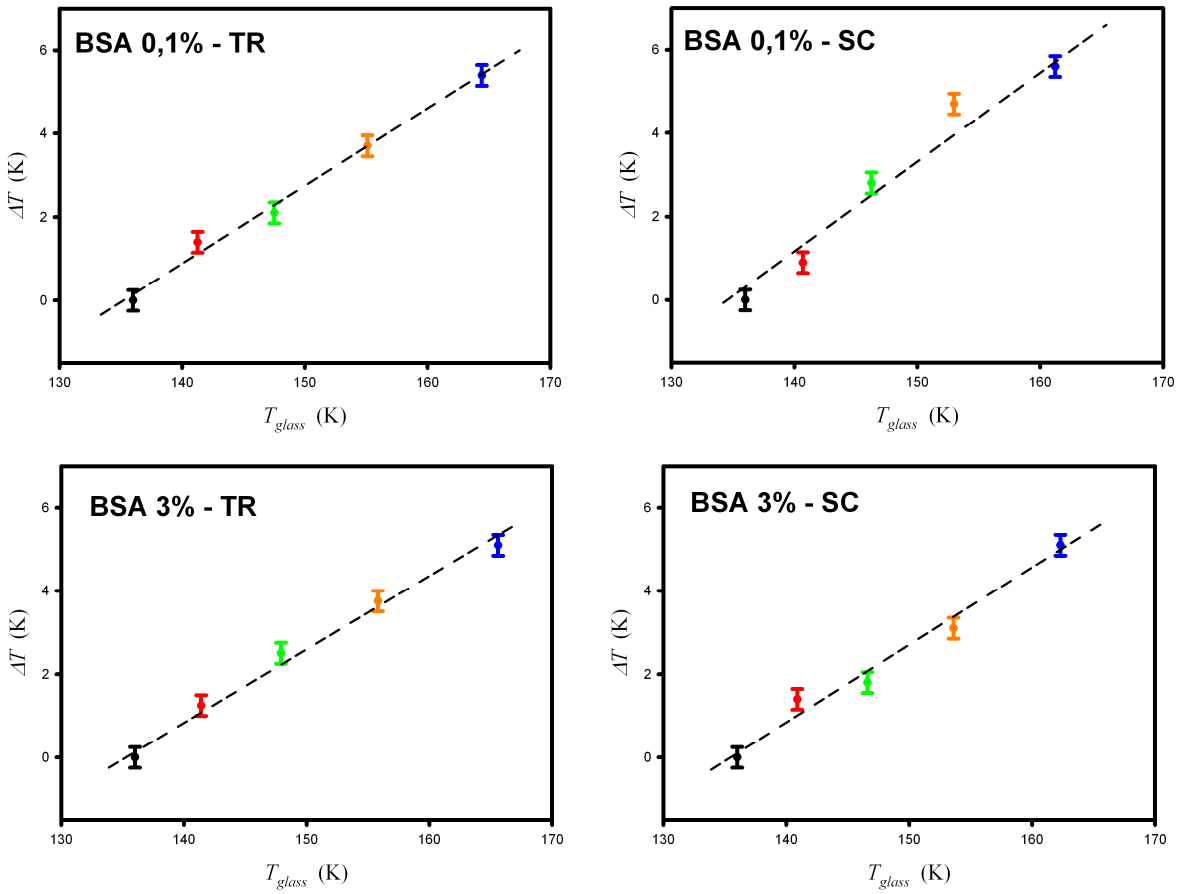

Figure 4.11 – Temperature shifts of scattering curves induced by trehalose (left panels) and sucrose (right panels) as a function of the glass transition temperature of the system. The protein is present in the samples at 0.1% w/w (upper panels) and at 3% w/w(lower panels), while the total sugar w/w percent in solution is: 0% (black), 10% (red), 20% (green), 30% (orange) and 40 % (blue). The black dashed lines shows qualitatively a linear correlation among the temperature shifts and the glass transition temperatures in trehalose, while larger departures from linearity are observed in sucrose.

A linear correlation among the temperature shifts and T_{glass} values is observed for samples containing trehalose. Larger departures from linearity are, instead, observed for samples containing sucrose.

4.5.5 – Circular Dichroism Measurements

As it is well known (*San Biagio et al., 1999; Vaiana et al., 2004*) the protein aggregation process is preceded by conformational changes in the protein structure. In order to confirm the suggestion of Barreca et al. (*Barreca et al., 2010*), according which the addition of sugar in solution stabilizes BSA native structure, circular dichroism measurements have been performed at 222 nm on 0.1% BSA solutions with sugar during temperature scan. The temperature shifts observed in the measured curves for samples with sugar concentration from 0% to 40%, here not shown, accounts for the strict correlation between protein conformational changes and aggregation.
In figure 4.12 circular dichroism data on 0.1% BSA solutions with no sugar (black line), 10% trehalose (red line) and 10% sucrose (green line) are shown.

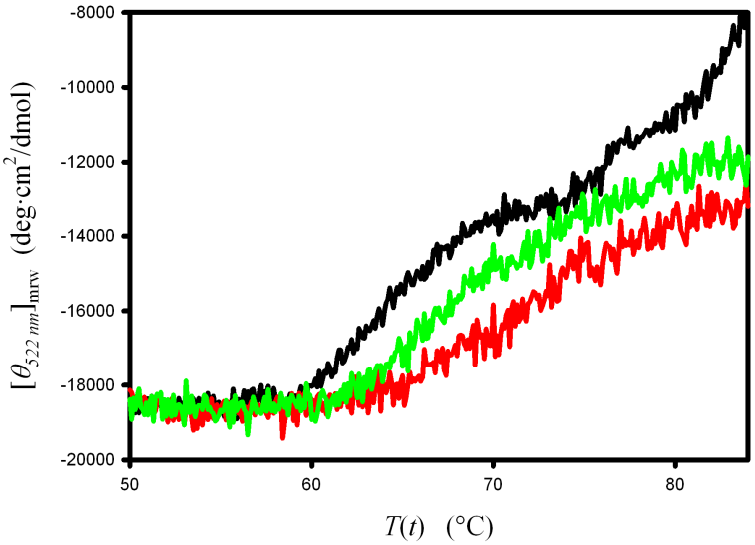

Figure 4.12 – Circular dichroism data on 0.1% BSA solutions with no sugar (black line), 10% trehalose (red line) and 10% sucrose (green line).

The small differences between 10% trehalose and 10% sucrose may explain the differences observed by light scattering, reported in table 4.5.
Moreover, at the end of each temperature scan systems were taken back to the initial temperature of 50 °C and the CD signal was measured for comparison with the initial one. Results showed that the CD signal at 222 nm is restored by 68% when no sugar is present in solution, while is restored by 92% when trehalose or sucrose were present at 40% w/w in solution. This confirms the ability of sugars to protect biomolecules against damages induced by external factors, such as increasing temperatures. Aggregation, as measured by light scattering, was not reversible. This agrees with the current understanding of BSA aggregation process, as crosslinking is a direct protein-protein mechanism and sugars do not interact directly to protein molecules.

4.5.6 – Conclusions

In this part of the thesis, static and dynamic light scattering measurements performed on bovine serum albumin (BSA) in saccharide (trehalose or sucrose) aqueous solutions at increasing sugar/water ratio are reported. In particular, the effects of each of the two disaccharides on the first steps of thermal aggregation of BSA have been studied at two protein concentrations (1 mg/ml and 30 mg/ml) during temperature scan, at increasing sugar/water ratio.

The analysis of the plots of the scattered intensity and of the hydrodynamic radius of the protein aggregates as a function of temperature showed that such curves appear of identical shape at each protein concentration value, but shifted towards higher temperatures when increasing the amount of sugar, with shifts depending on sugar type.

Furthermore, the evaluation of the packing of aggregates by means of their fractal dimension evidences that the growth mechanisms are not affected by the presence of sugar. In particular, aggregates at 0.1% BSA concentration show an initial growth with very low compactness ($\delta \approx 1.5$), followed by mainly gaussian-coil like growth ($\delta \approx 2$). The former is compatible with partial reversibility of initial aggregates as observed in literature (*Vaiana et al., 2004*), while the latter reveals the formation of irreversible compact objects. This is in agreement with previous studies on BSA aggregation (*San Biagio et al., 1999; Militello et al., 2004*), evidencing such complex mechanism of aggregation. The first conclusion of this work is that sugar addition does not alter protein crosslinking via a direct, specific sugar-protein interactions, in agreement with the current literature (*Timasheff, 1998; Timasheff, 2002; Shimizu and Matubayasi, 2006*). Large reversibility of structural changes observed in CD measurements enforces this conclusion.

It is well known that aggregation depends also on protein concentration. The results of measurements on samples with BSA concentration of 3% w/w confirm this evidence. However, addition of sugar to protein solutions of 3% BSA causes temperature shifts similar to the ones observed at 0.1%, although significant differences have been observed in the shift values for sucrose samples. This enforces the conclusion on the indirect effect of sugar and, at the same time, allows to ascertain that the addition of sugar acts only via global changes of the solvent. Differences between trehalose and sucrose are to be linked to the different structure of their aqueous solutions, as proposed by various authors (*Lerbret et al., 2005; Francia et al., 2008*). Specifically, trehalose and sucrose have a different ability to form intra-molecular hydrogen bonds.

The second conclusion of this work is that the properties and behaviour of an aggregating protein solution depends on the statistical mechanics of the whole solution. In particular, the observed temperature shifts depend mainly on the interactions and overwhelming configurations of the solvent matrix.

Consequently, the measured temperature shifts of the aggregation process have been put into relation to the corresponding shifts of the glass transition temperature T_{glass} of the solvent. A linear correlation among these temperature shifts and T_{glass} values is observed for samples containing trehalose, while departures from

linearity are observed for samples containing sucrose. In trehalose samples the observed linear correlation could illustrate that overwhelming configurations of the solvent in the liquid state are the same, which dictate the low temperature behaviour of the same solvent. This is not the case for sucrose samples, as probably due to the temperature dependence of intra-molecular hydrogen bonding of sucrose. However, this question deserves further scrutiny.

5 – Conclusions

The work presented in this thesis was aimed to take a step forward in understanding how the external matrix influences the protein structure and dynamics in conditions that remind those occurring in living organisms. Such conditions, which are far from thermodynamical ideality, as already discussed in the Introduction, are mimicked in vitro by studying the behaviour of proteins in saccharide matrices. Actually, saccharide matrices have been chosen because living organisms are very rich in saccharides, especially in the extra-cellular medium (*Karp, 2004*). In addition to this, sugars have been of large interest in the last decades, because of their bioprotective properties (*Crowe and Clegg, 1973; Crowe et al., 1984*).

The studied systems are composed by objects of different size (water molecules, sugars, proteins), so that dynamics at different temporal scales were simultaneously present. Small-Angle X-ray Scattering (SAXS) has been used to study structural properties of amorphous systems, where the glass formation arrests faster motions, thus allowing to study the systems in a slower time scale dictated by the proteins dynamics. Static and dynamic light scattering have been used to study protein aggregation in crowded saccharide solutions, where the effects of the solvent matrix on proteins are thought to be the average of its dynamics up to the protein time scale.

SAXS results, obtained on samples of myoglobin embedded in low hydrated amorphous matrices of saccharide (trehalose, sucrose, maltose and lactose), indicated that the protein maintains approximately the same properties in all the sugars but in lactose. The protective effect of the last is reduced by the occurrence of a phase separation. Moreover, the best protective effect of trehalose against protein damaging and, conversely, the poor performance of the reducing disaccharides, maltose and lactose has been confirmed by comparing the protein volume fractions in the different saccharide matrices, which reflect the protein folding state. Besides, local inhomogeneities have been detected in all the samples containing sodium dithionite, with size and composition depending on the specific sugar matrix. In addition, the previously proposed mechanism for trehalose bioprotection, which is based on the water-buffering action (*Cesàro et al., 2006; Kilburn et al., 2006; Longo et al., 2010*) that would contrast moisture variations, has been extended to other sugars, turning out to be a general behaviour.

The study of protein aggregation was performed on bovine serum albumin in trehalose and sucrose solutions. The analyses of the scattered intensity and of the hydrodynamic radius of protein aggregates as a function of temperature showed that such curves appear of identical shape at each protein concentration value, but shifted towards higher temperatures if the amount of sugar is increased, with shifts depending on sugar type. Furthermore, the evaluation of the packing of aggregates by means of their fractal dimension evidenced that the growth mechanisms of the

aggregates are not affected by the presence of sugar. In particular, the addition of sugar does not alter the protein crosslinking via a direct, specific sugar-protein interactions, in agreement with the current literature (*Timasheff, 1998; Timasheff, 2002; Shimizu and Matubayasi, 2006*). Also, as revealed by far-UV CD results, large reversibility of protein structural changes of otherwise irreversible aggregates confirms that the sugar effect occurs only via solvent matrix changes. This conclusion has been strengthened by results of measurements on samples with BSA concentration of 3% w/w, showing that protein aggregation also depends on protein concentration. In fact, addition of trehalose to protein solutions of 3% BSA causes temperature shifts similar to the ones observed at 0.1%, but significant differences have been observed in the shift values for sucrose samples. This allows to ascertain that effects of the addition of sugar occur only via global changes of the solvent. Differences between trehalose and sucrose are to be linked to the different structure of their aqueous solutions, as proposed by various authors (*Lerbret et al., 2005; Francia et al., 2008*). Specifically, trehalose and sucrose have a different ability to form intra-molecular hydrogen bonds.

Results on protein aggregation can be put in a unifying view by noting that the observed temperature shifts depend mainly on the overwhelming configurations of the solvent matrix and its interactions with proteins. Statistical thermodynamics of the whole protein solution is the key to understand the observed behaviour, including the phase separation in lactose samples. Thus, the measured temperature shifts of the aggregation process have been put into relation to the corresponding shifts of the glass transition temperature T_{glass} of the solvent. A linear correlation among these temperature shifts and T_{glass} values has been found for samples containing trehalose, while departures from linearity are found for samples containing sucrose. In trehalose samples the observed linear correlation could illustrate that overwhelming configurations of the solution, which dictate the thermodynamics of aggregation in the liquid state, are also responsible for the low temperature behaviour of the solvent. This is not the case for sucrose samples, as probably due to the temperature dependence of intra-molecular hydrogen bonding of sucrose. However, this question deserves further scrutiny.

In conclusion, both works on protein-sugar-water systems showed how the structure and dynamics of the protein are strictly affected by the external matrix and, in particular, by the sugar molecules through indirect, solvent-mediated interactions. Differences observed among different sugars are in agreement with current literature on the behaviour of sugar systems without (*Magazù et al., 2004; Lerbret et al., 2005*) and with (*Giuffrida et al., 2006; Francia et al., 2008*) proteins.

Appendix – PhD Activity

PUBLICATIONS

- M. Collini, L. D'Alfonso, M. Caccia, L. Sironi, **M. Panzica**, G. Chirico, I. Rivolta, B. Lettiero, G. Miserocchi, "*In Vitro–in Vivo Fluctuation Spectroscopies*", Optical Fluorescence Microscopy, 165-181, DOI 10.1007/978-3-642-15175-0_10, ISBN 978-3-642-15174-3, Springer-Verlag Berlin Heidelberg, 2011
- S. Giuffrida, **M. Panzica**, F. M. Giordano, A. Longo, "*SAXS Study on Myoglobin Embedded in Amorphous Saccharide Matrices*", Eur. Phys. J. E 34: 87, 2011. DOI: 10.1140/epje/i2011-11087-6
- **M. Panzica**, A. Emanuele, L. Cordone, "*Thermal Aggregation of Bovine Serum Albumin in Trehalose and Sucrose Solutions*", submitted to J. Phys. Chem. B

COMMUNICATIONS TO CONGRESSES – POSTERS

- A. Longo, S. Giuffrida, **M. Panzica**, G. Cottone, L. Cordone, "*SAXS and FTIR Study on MbCO-Saccharide Amorphous Systems*", XIII European Conference on the Spectroscopy of Biological Molecules (Università degli Studi di Palermo, 2009)
- A. Longo, S. Giuffrida, **M. Panzica**, G. Cottone, L. Cordone, "*SAXS and FTIR Study on MbCO-Saccharide Amorphous Systems*", 6th International Discussion Meeting on Relaxations in Complex Systems" (IDMRCS) (Università Sapienza di Roma, 2009)
- **M. Panzica**, A. Emanuele, L. Cordone, "*BSA Aggregation in Trehalose-Water Systems*", Frontiers in Water Biophysics (Università degli Studi di Trieste, 2010)

ATTENDED COURSES

COURSE	PROFESSOR	A. Y.	MARK
Statistical Mechanics	G. M. Palma	2008/2009	A
Interaction of Radiation with Matter	R. Passante	2008/2009	A
Optics Laboratory	M. Cannas	2008/2009	A
Raman Spectroscopy Applied to Amorphous Systems Applicata a Sistemi Amorfi	M. Leone	2009/2010	A

ATTENDED INTERNATIONAL SCHOOLS

SCHOOL	ORGANIZATION	TIME
International School of Biological Magnetic Resonance: "*9th Course – Biophysics and Structure to Counter Threats and Challenges*"	University of Stanford, with courses at "Ettore Majorana Center for Scientific Culture" in Erice (Italy)	from 2009/06/22 to 2009/07/02
31st Berlin School on Neutron Scattering	Helmholtz-Zentrum Berlin für Materialien und Energie, Berlin (Germany)	from 2010/03/11 to 2010/03/19

OTHER ACTIVITIES

- Development of a software in Microsoft Visual C++ .NET for reading the .pdb file of a macromolecule and simulating its X-ray structure factor.
- **Scientific Animator** in the project "School Adopts an Experiment", during the XIX Week of Scientific and Technologic Culture, from 2009/03/23 to 2009/03/29 at the Department of Physics of University of Palermo.
- **Scientific Animator** for the Department of Physics of University of Palermo in the Scientific Event "*PalermoScienza Esperienza inSegna 2010*", from 2010/02/18 to 2010/02/25.
- **Academic Tutor** for "*Mathematics and Physics*" subject of study at University of Palermo in A.Y. 2009/2010 and in A.Y. 2010/2011.

Bibliography

M. Akke, S. Forsén, "*Protein Stability and Electrostatic Interactions between Solvent Exposed Charged Side Chains.*", Prot. Struct. Func. and Gen. 8: 1-23, 1990.

M. Amadori, "*Condensation Products of Glucose with p-Toluidine*", Atti R. Accad. Naz. Lincei Mem. Cl. Sci. Fis. Mat. Nat. 13: 72-73, 1931.

C. Anfinsen, "*The Formation and Stabilization of Protein Structure*", Biochem. J. 128 (4): 737–49, 1972.

E. Antonini, M. Brunori, "*Hemoglobin and Myoglobin in their Reactions with Ligands*", American Elsevier Publishing Company, 1971.

P. W. Atkins, J. De Paula, "*Chimica Fisica*", Zanichelli, 2004.

G. Barone, S. Capasso, P. Del Vecchio, C. De Sena, D. Fessas, C. Giancola, G. Graziano, P. Tramonri, "*Thermal Denaturation of Bovine Serum Albumin and its Oligomers and Derivatives pH Depedence*", J. Thermal Analysis 45: 1255-1264, 1995.

D. Barreca, G. Laganà, S. Ficarra, E. Tellone, U. Leuzzi, S. Magazù, A. Galtieri, E. Bellocco, "*Anti-aggregation Properties of Trehalose on Heat-induced Secondary Structure and Conformation Changes of Bovine Serum Albumin*", Biophys. Chem. 147: 146-152, 2010.

G. Batta, K.E. Kövér, "*Heteronuclear Coupling Constants of Hydroxyl Protons in a Water Solution of Oligosaccharides: Trehalose and Sucrose*", Carbohydr. Res. 320: 267-272, 1999.

G. Bellavia, G. Cottone, S. Giuffrida, A. Cupane, L. Cordone, "*Thermal Denaturation of Myoglobin in Water-Disaccharide Matrixes: Relation with the Glass Transition of the System*", J. Phys. Chem. B 113: 11543–11549, 2009.

G. Bellavia, S. Giuffrida, G. Cottone, A. Cupane, L. Cordone, "*Protein Thermal Denaturation and Matrix Glass Transition in Different Protein-Trehalose-Water Systems*", J. Phys. Chem. B 115: 6340-6346, 2011.

D. Bendedouch, S. H. Chen, "*Structure and Interparticle Interactions of Bovine Serum Albumin in Solution Studied by Small-Angle Neutron Scattering*", J. Phys. Chem. 87: 1473-1477, 1983.

B. J. Berne, R. Pecora, "*Dynamic Light Scattering*", Wiley, 1976.

G. Bianchi, A. Gamba, C. Murellie, F. Salamini, D. Bartels, "*Novel Carbohydrate Metabolism in the Resurrection Plant Craterostigma Plantagineum*", Plant. J. 1: 355-359, 1991.

G. Bianchi, A. Gamba, R. Limiroli, N. Pozzi, R. Ester, F. Salami, D. Bartels, "*The Unusual Sugar Composition in Leaves of the Resurrection Plant*", Physiol. Plantarum 87: 223–226, 1993.

A. Borgia, P. M. Williams, J. Clarke, "*Single-Molecule Studies of Protein Folding*", Annu. Rev. Biochem. 77: 101-125, 2008.

E. H. C. Bromley, M. R. H. Krebs, A. M. Donald, "*Aggregation across the Length Scales in beta-lactoglobulin*", Faraday Discussions 128: 13-27, 2005.

G. M. Brown, D. C. Rohrer, B. Berking, C. A. Beevers, R. O. Gould, R. Simpson, "*The Crystal Structure of $\alpha\alpha$,-Trehalose Dihydrate from Three Independent X-ray Determinations*", Acta Cryst. B 28: 3145-3158, 1972.

J. R. Brown, "*Structure of Bovine Serum Albumin*", Fed. Proc. 34: 591, 1975.

H. Brumberger, "*Modern Aspect of Small-Angle Scattering*", Kluwer Academic Publishers, Dordrecht, 1993.

D. Bulone, M. B. Palma-Vittorelli, M. U. Palma, "*Enthalpic and Entropic Contributions of Water Molecules to the Functional T-R Transition of Human Hemoglobin in Solution*", Int. J. Quant. Chem. 42: 1427-1437, 1992.

D. Bulone, P. L. San Biagio, M. B. Palma-Vittorelli, M. U. Palma, "*The Role of Water in Hemoglobin Function and Stability*", Science 259: 1335-1336, 1993.

D. Bulone, A. Emanuele, P. L. San Biagio, "*Effects of Solvent Perturbation on Gelation Driven by Spinodal Demixing*", Biophysical Chemistry 77: 1-8, 1999.

C. R. Cantor, P. R. Schimmel, "*Biophysical Chemistry*", W. H. Freeman and Company, 2001.

P. Cappelli, V. Vannucchi, "*Chimica degli Alimenti*", Zanichelli, 1998.

J.F. Carpenter, J.H. Crowe, "*An Infrared Spectroscopic Study of the Interactions of Carbohydrates with Dried Proteins*", Biochemistry 28 (9): 3916-3922, 1989.

C. D. Carter, X. M. He, S. H. Munson, P. D. Twigg, K. M. Gernert, M. B. Broom, T. Y. Miller, "*Three-Dimensional Structure of Human Serum Albumin*", Science 244: 1195-1198, 1989.

D. C. Carter, J. X. Ho, "*Structure of Serum Albumin*", Adv. Protein Chem. 45: 153-203, 1994.

A. Cesàro, "*Carbohydrates: All Dried up!*", Nature Materials 5: 593-594, 2006.

A. Cesàro, O. De Giacomo, F. Sussich, "*Water Interplay in Trehalose Polymorphism*", Food Chem. 106: 1318–1328, 2008.

F. Chiti, C. M. Dobson, "*Protein Misfolding, Functional Amyloid, and Human Disease*", Annu. Rev. Biochem. 75, 333–366, 2006.

J. S. Clegg, "*Metabolic Studies of Encysted Dormant Embryos of Artemia Salina*", Comp. Biochem. Physiol. 20: 801–809, 1967.

L. Cordone, A. Cupane, P. L. San Biagio, E. Vitrano, "*Effect of Some Monohydric Alcohols on the Oxygen Affinity of Hemoglobin: Relevance of Solvent Dielectric Constant and Hydrophobicity*", Biopolymers 18: 1975-1988, 1979.

L. Cordone, A. Cupane, P. L. San Biagio, E. Vitrano, "*Effects of Some Organic Cosolvents on the Reaction of Hemoglobin with Oxygen*", Biopolymers 20: 39– 51, 1981.

L. Cordone, A. Cupane, E. Vitrano, "*Conformational and Functional Properties of Hemoglobin in Perturbed Solvent: Relevance of Electrostatic and Hydrophobic Interactions*", J. Mol. Liq. 42: 213-229, 1989.

L. Cordone, G. Cottone, S. Giuffrida, G. Palazzo, G. Venturoli, C. Viappiani, "*Internal Dynamics and Protein-Matrix Coupling in Trehalose-Coated Proteins*", Biochimica et Biophysica Acta 1749: 252-281, 2005.

G. Cottone, L. Cordone, G. Ciccotti, "*Molecular Dynamics Simulation of Carboxy-Myoglobin Embedded in a Trehalose-Water Matrix*", Biophysical J. 80: 931-938, 2001.

G. Cottone, G. Ciccotti, L. Cordone, "*Protein–Trehalose–Water-Structures in Trehalose Coated Carboxy-Myoglobin*", J. Chem. Phys. 117: 9862– 9866, 2002.

G. Cottone, S. Giuffrida, G. Ciccotti, L. Cordone, "*Molecular Dynamics Simulation of Sucrose- and Trehalose-Coated Carboxy-Myoglobin*", Proteins 59 (2): 291-302, 2005.

G. Cottone, "*A comparative study of carboxy myoglobin in saccharide/water systems by Molecular Dynamics Simulation*", J. Phys. Chem B 111: 3569, 2007.

J. H. Crowe , J. S. Clegg, "*Anhydrobiosis*", Dowden, Hutchinson and Ross, Stroudsburg: 141-147, 1973.

J. H. Crowe, K. A. C. Madin, "*Anhydrobiosis in Nematodes: Evaporative Water Loss Survival*", J. Exp. Zool. 193: 323–334, 1975.

J. H. Crowe, L. M. Crowe, D. Chapman, "*Preservation of Membranes in Anhydrobiotic Organisms: the Role of Trehalose*", Science 223: 701-703, 1984.

J. H. Crowe, "*Trehalose as a 'Chemical Chaperone': Fact and Fantasy.*", Adv. Exp. Med. Biol. 594: 143-158, 2007.

P. Debye, H.R. Anderson, H. Brumberger, "*Scattering by an Inhomogeneous Solid. The Correlation Function and Its Application*", J. Appl. Phys. 28, 679 (1957).

K. A. Dill, "*Dominant Forces in Protein Folding*", Biochem. 29: 7133-7155, 1990.

K. A. Dill, H. S. Chan, "*From Levinthal to Pathways to Funnels*", Nat. Struct. Biol. 4, 10-19, 1997.

T. Eichner, A. P. Kalverda, G. S. Thompson, S. W. Homans, S. E. Radford, "*Conformational conversion during amyloid formation at atomic resolution*", Mol. Cell 41, 161–172, 2011.

L.A. Feigin, D.I. Svergun, "*Structure Analysis by Small Angle X-Ray and Neutron Scattering*", Plenum Press, New York, 1987.

J. Figge, T. H. Rossing, V. Fencl, "*The Role of Serum Proteins in Acid-Base Equilibria*", J. Lab. Clin. Med. 117 (6): 453–467, 1991.

S. Focardi, I. Massa, A. Uguzzoni, "*Fisica Generale – Elettromagnetismo*", Casa Editrice Ambrosiana, 2005.

J. F. Foster, "*Plasma Albumin*", The Plasma Proteins 1: 179-239, 1960.

F. Francia, M. Dezi, A. Mallardi, G. Palazzo, L. Cordone, G. Venturoli, "*Protein-Matrix Coupling/Uncoupling in 'Dry' Systems of Photosynthetic Reaction Centre*

Embedded in Trehalose/Sucrose: The Origin of Trehalose Peculiarity", J. Am. Chem. Soc. 130 (31): 10240-10246, 2008.

H. Frauenfelder, P. W. Fenimore, B. H. McMahon, "*Hydration, Slaving and Protein Function*", Biophys. Chem. 98: 35–48, 2002.

C. Giancola, C. De Sena, D. Fessas, G. Graziano, G. Barone, "*DSC Studies on Bovine Serum Albumin Denaturation. Effects of Ionic Strength and SDS Concentration*", Int. J. Biol. Macromol. 20: 193-204, 1997.

S. Giuffrida, G. Cottone, F. Librizzi, L. Cordone, "*Coupling between the Thermal Evolution of the Heme Pocket and the External Matrix Structure in Trehalose Coated Carboxymyoglobin*", J. Phys. Chem. B 107: 13211– 13217, 2003.

S. Giuffrida, G. Cottone, L. Cordone, "*Structure-Dynamics Coupling between Protein and External Matrix in Sucrose-Coated and in Trehalose-Coated MbCO: An FTIR Study*", J. Phys. Chem. B 108: 15415–15421, 2004.

S. Giuffrida, G. Cottone, L. Cordone, "*Role of Solvent on Protein-Matrix Coupling in MbCO Embedded in Water-Saccharide Systems: A Fourier Transform Infrared Spectroscopy Study*", Biophysical Journal 91: 968-980, 2006.

M. Gordon, J. S. Taylor, "*Ideal Copolymers and the Second-Order Transitions of Synthetic Rubbers. I. Non-Crystalline Copolymers*", J. Appl. Chem. 2: 493-500, 1952.

G. R. Grimsley, K. L. Shaw, L. R. Fee, R. W. Alston, B. M. Huyghues-Despointes, R. L. Thurlkill, J. M. Scholtz, C. N. Pace, "*Increasing Protein Stability by Altering Long-Range Coulombic Interactions*", Prot. Sci. 8: 1843-1849, 1999.

A. Guinier, G. Fournet, "*Small-Angle Scattering of X-Rays*", Chapman & Hall, 1955.

W. F. Harrington, P. Johnson, R. H. Ottewill "*Bovine Serum Albumin and its Behaviour in Acid Solution*", Biochem. J. 62: 569–582, 1956.

A. Hédoux, J. Willart, L. Paccou, Y. Guinet, F. Affouard, A. Lerbret, M. Deschamps, "*Thermostabilization Mechanism of Bovine Serum Albumin by Trehalose*", J. Phys. Chem. B 113: 6119-6126, 2009.

T. T. Herskovits, N. J. Solli, "*Studies of the Conformation of Apomyoglobin in Aqueous Solutions and Denaturing Organic Solvents*", Biopolymers 14: 319-344, 1975.

C. Honda, H. Kamizono, T. Samejima, K. Endo, "*Studies o Thermal Aggregation of Bovine Serum Albumin as a Drug Carrier*", Chem. Pharm. Bull. 48: 464-466, 2000.

D. D. Horikawa, T. Kunieda, W. Abe, M. Watanabe, Y. Nakahara, T. Sakashita, N. Hamada, S. Wada, T. Funayama, Y. Kobayashi, C. Katagiri, S. Higashi, T. Okuda, "*Establishment of a Rearing System of the Extremotolerant Tardigrade Ramazzottius Varieornatus: a New Model Animal for Astrobiology*", Astrobiology 8: 549-556, 2008.

K. Ibel, H. B. Stuhrmann, *"Comparison of Neutron and X-Ray Scattering of Dilute Myoglobin Solutions*", J. Mol. Biol. 93: 255-265, 1975.

N. K. Jain, I. Roy, "*Role of Trehalose in Moisture-Induced Aggregation of Bovine Serum Albumin.*", Eur. J. Pharm. Biopharm. 69: 824-834, 2008.

C. S. Johnson, A. Gabriel, "*Laser Light Scattering*", Dover, 1981.

M. Y. Kahn, "*Direct Evidence for the Involvement of Domain III in the N-F Transition of Bovine Serum Albumin*", Biochem. J. 236: 307-310, 1986.

G. Karp, "*Biologia Cellulare e Molecolare*", EdiSES, 2004.

E. Katchalski, G. S. Benjamin, V. Gross, "*The Availability of the Disulfide Bonds of Human and Bovine Serum Albumin and of Bovine γ-Globulin to Reduction by Thioglycolic Acid*", J. Am. Chem. Soc. 79: 4096–4099, 1957.

D. Keilin, "*The Problem of Anabiosis or Latent Life: History and Current Concept*", Proc. R. Soc. Lond. B 150: 149–191, 1959.

J. C. Kendrew, G. Bodo, H. M. Dintzis, R. G. Parrish, H. W. Wyckoff, D. C. Phillips, "*A Three-Dimensional Model of the Myoglobin Molecule Obtained by X-Ray Analysis*", Nature 181: 622-626, 1958.

D. Kilburn, S. Townrow, V. Meunier, R. Richardson, A. Alam, J. Ubbink, "*Organization and Mobility of Water in Amorphous and Crystalline Trehalose*", Nature Materials 5(8): 632-635, 2006.

D. E. Koppel, "*Analysis of Macromolecular Polydispersity in Intensity Correlation Spectroscopy: The Method of Cumulants*", J. Chem. Phys. 57: 4814-4820, 1972.

Y. H. Lam, R. Bustami, T. Phan, H. K. Chan, F. Separovic, "*A Solid-State NMR Study of Protein Mobility in Lyophilized Protein-Sugar Powders*", J. Pharm. Sci. 91: 943-951, 2002.

A. M. Lammert, S. J. Schmidt, G. A. Day, "*Water Activity and Solubility of Trehalose*", Food Chem. 61: 139-144, 1998.

A. Lerbret, P. Bordat, F. Affouard, M. Descamps, F. Migliardo, "*How Homogeneous are the Trehalose, Maltose, and Sucrose Water Solutions? An Insight from Molecular Dynamics Simulations.*", J. Phys. Chem. B 109: 11046-11057, 2005.

C. Levinthal, "*Are There Pathways for Protein Folding?*", J. Chim. Phys. 65: 44–45, 1968.

F. Librizzi, C. Viappiani, S. Abbruzzetti, L. Cordone, "*Residual Water Modulates Dynamics of the Protein and of the External Matrix in 'trehalose-coated' MbCO: An Infrared and Flash-Photolysis Study*", J. Chem. Phys. 116: 1193-1200, 2002.

H. Lodish, A. Berk , C. A. Kaiser, M. Krieger, M. P. Scott, A. Bretscher, H. Ploegh, P. Matsudaira, "*Biologia Molecolare della Cellula*", Zanichelli, 2009.

A. Longo, S. Giuffrida, G. Cottone, L. Cordone, "*Myoglobin Embedded in Saccharide Amorphous Matrices: Water-Dependent Domains Evidenced by Small Angle X-Ray Scattering*", Phys. Chem. Chem. Phys. 12: 6852–6858, 2010.

S. Magazù, G. Maisano, F. Migliardo, C. Mondelli, "*Mean Square Displacement Relationship in Bioprotectant Systems by Elastic Neutron Scattering*", Biophys. J., 86: 3241-3249, 2004.

L. C. Maillard, "*Action des Acides Amines sur les Sucres: Formation des Melanoidines par Voie Methodique*", C. R. Acad. Sci. Gen. 154: 66-68, 1912.

M. Manno, P. L. San Biagio, M. U. Palma, "*The Role of pH on Instability and Aggregation of Sickle Hemoglobin Solutions*", Proteins 55: 169-176, 2004.

M. Mathlouthi, J. Genotelle, "*Role of Water in Sucrose Crystallization*", Carbohydrate Polymers 37: 335–342, 1998.

V. Militello, C. Casarino, A. Emanuele, A. Giostra, F. Pullara, M. Leone, "*Aggregation Kinetics of Bovine Serum Albumin Studied by FTIR Spectroscopy and Light Scattering*", Biophys. Chem. 107: 175-187, 2004.

Y. Moriyama, D. Ohta, K. Hachiya, Y. Mitsui, and K. Takeda, "*Fluorescence Behavior of Tryptophan Residues of Bovine and Human Serum Albumins in Ionic Surfactant Solutions: A Comparative Study of the Two and One Tryptophan(s) of Bovine and Human Albumins*", J. Protein Chem. 15: 265-272, 1996.

C. Pace, B. Shirley, M. McNutt, K. Gajiwala, "*Forces Contributing to the Conformational Stability of Proteins*", FASEB J. 10 (1): 75–83, 1996.

J. K. Percus, G. J. Yevick, "*Analysis of Classical Statistical Mechanics by Means of Collective Coordinates*", Phys. Rev. 110: 1-13, 1958.

C. Pereira, R. D. Lins, I. Chandrasekhar, L. C. G. Freitas, P. H. Hunenberger, "*Interaction of the Disaccharide Trehalose with a Phospholipid bilayer: a Molecular Dynamics Study*", Biophys. J. 86: 2273-2285, 2004.

T. J. Peters, "*Serum Albumin*", Advances in Protein Chemistry 37: 161-245, 1985.

P. Picotti, G. De Franceschi, E. Frare, B. Spolaore, M. Zambonin, F. Chiti, P. Polverino De Laureto, A. Fontana, "*Amyloid Fibril Formation and Disaggregation of Fragment 1-29 of Apomyoglobin: Insights into the Effect of pH on Protein Fibrillogenesis*", J. Mol. Biol. 367: 1237-1245, 2007.

F. Pullara, A. Emanuele, M. B. Palma-Vittorelli, M. U. Palma, "*Protein Aggregation/Crystallization and Minor Structural Changes: Universal Versus Specific Aspects*", Biophysical Journal 93: 3271-3278, 2007.

F. Pullara, A. Emanuele, M. B. Palma-Vittorelli, M. U. Palma, "*Protein Crystallization: Universal Thermodynamic VS. Specific Effects of PEG*", Faraday Discuss. 139: 299-308, 2008.

G. Rose, P. Fleming, J. Banavar, A. Maritan, "*A Backbone-Based Theory of Protein Folding*", Proc. Natl. Acad. Sci. U.S.A. 103 (45): 16623–33, 2006.

J. G. Sampedro, S. Uribe, "*Trehalose-Enzyme Interactions Result in Structure Stabilization and Activity Inhibition. The Role of Viscosity*", Mol. Cell. Biochem. 256: 319-327, 2004.

P. L. San Biagio, D. Bulone, A. Emanuele, M. U. Palma, "*Self-Assembly of Biopolymeric Structures Below the Threshold of Random Cross-Link Percolation*", Biophys. J. 70: 494-499, 1996.

P. L. San Biagio, D. Bulone, V. Martorana, M. B. Palma-Vittorelli, M. U. Palma, "*Physics and Biophysics of Solvent Induced Forces: Hydrophobic Interactions and Context-Dependent Hydration*", Eur. Biophys. J. 27: 183-196, 1998.

P. L. San Biagio, V. Martorana, A. Emanuele, S. M. Vaiana, M. Manno, D. Bulone, M. B. Palma-Vittorelli, M. U. Palma, "*Interacting Processes in Protein Coagulation*", Prot. 37: 116-120, 1999.

W. Schärtl, "*Light Scattering from Polymer Solutions and Nanoparticle Dispersions*", Springer, 2007.

I. N. Serdyuk, N. R. Zaccai, J. Zaccai, "*Methods in Molecular Biophysics*", Cambridge University Press, 2007.

S. Shimizu, N. Matubayasi, "*Preferential Hydration of Proteins: A Kirkwood-Buff Approach*", Chemical Physics Letters 420: 518-522, 2006.

A. Sletten and D. J. McLaughlin, "*Radar Polarimetry*", in K. Chang ed., Encyclopedia of RF and Microwave Engineering, John Wiley & Sons, 2005.

P. G. Squire, P. Moser, C. T. O'Konski, "*The hydrodynamic Properties of Bovine Serum Albumin Monomer and Dimer*", Biochem. 7: 4261-4272, 1968.

A. K. Sum, R. Faller, J. J. de Pablo, "*Molecular Simulation Study of Phospholipid Bilayers and Insights of the Interactions with Disaccharides*", Biophys. J. 85: 2830-2844, 2003.

F. Sussich, R. Urbani, F. Princivalle, A. Cesàro, "*Polymorphic Amorphous and Crystalline Forms of Trehalose*", J. Am. Chem. Soc. 120: 7893-7899, 1998.

K. Takeda, A. Wada, K. Yamamoto, Y. Moriyama, K. Aoki, "*Conformational Change of Bovine Serum Albumin by Heat Treatment*", J. Prot. Chem. 8: 653-659, 1989.

C. Tanford, "*Protein Denaturation*", Adv. Protein Chem. 23: 121-282, 1968.

S. N. Timasheff, "*Control of Protein Stability and Reactions by Weakly Interacting Cosolvents: The Simplicity of the Complicated*", Adv. Prot. Chem. 51: 355-432, 1998.

S. N. Timasheff, "*Protein Hydration, Thermodynamic Binding, and Preferential Hydration*", Biochemistry 41 (46): 13473–13482, 2002.

D. Tomos, "*Life without Water*", Curr. Biol. 2: 594–596, 1992.

S. M. Vaiana, M. Manno, A. Emanuele, M. B. Palma-Vittorelli, M. U. Palma, "*The Role of Solvent in Protein Folding and in Aggregation*", J. Bio. Phys. 27: 133-145, 2001.

S. M. Vaiana, A. Emanuele, M. B. Palma-Vittorelli, M. U. Palma, "*Irreversible Formation of Intermediate BSA Oligomers Requires and Induces Conformational Changes*", Prot. 55: 1053-1062, 2004.

S. M. Vaiana, M. A. Rotter, A. Emanuele, F. A. Ferrone, M. B. Palma-Vittorelli, "*Effect of T-R Conformational Change on Sickle-Cell Hemoglobin Interactions and Aggregation*", Prot. 58: 426-438, 2005.

B. Van den Berg, R. Wain, C. M. Dobson, R. J. Ellis, "*Macromolecular Crowding Perturbs Protein Refolding Kinetics: Implications for Folding Inside the Cell*", EMBO J. 19 (15): 3870–5, 2000.

C. Veerman, L. M. C. Sagie, J. Heck, E. Van Der Linden, "*Mesostructure of fibrillar Bovine Serum Albumin Gels*", Int. J. Biol. Macromol. 31: 139-146, 2003.

V. Vetri, C. Canale, A. Relini, F. Librizzi, V. Militello, A. Ghiozzi, M. Leone, "*Amyloid Fibrils Formation and Amorphous Aggregation in Concanavalin A*", Biophys. Chem. 125: 184-190, 2006.

P. H. Von Hippel, K.Y. Wong, "*On the Conformational Stability of Globular Proteins*", J. Biol. Chem. 940: 3909– 3923, 1965.

B. E. Warren, "*X-Ray Diffraction*", Dover, 1969.

R. Wetzel, M. Becker, J. Behlke, H. Billwitz, S. Bohm, B. Ebert, H. Hamann, J. Krumbiegel, G. Lasmann, "*Temperature Behaviour of Human Serum Albumin*", Eur. J. Biochem. 104: 469-478, 1980.

J. C. Wright, "*Cryptobiosis 300 Years on from Van Leeuwenhoek: What Have We Learned About Tardigrades?*", Zool. Anz. 240: 563–582, 2001.